MONASH University

East Australian spring rainfall during strong El Niño events

Peter Andrew Joseph van Rensch

BSc. (Hons), The University of Melbourne (2008)

A thesis submitted for the degree of *Doctor of Philosophy* at

Monash University in 2020

Faculty of Science, Earth, Atmosphere and Environment

Copyright notice

Abstract

This thesis examines the physical mechanisms associated with the teleconnection between east Australian rainfall and the El Niño–Southern Oscillation (ENSO) during the austral spring (September–November, SON). In east Australia, El Niño is typically associated with less than average rainfall during SON. However, the rainfall response during the three strongest El Niño events of the satellite era, 1982-1983, 1997-1998 and 2015-2016 differed markedly. East Australian spring rainfall of 1982 was typical of El Niño, with significantly less rainfall than normal throughout east Australia. Unusually, during the 1997 event, east Australia received near average spring rainfall. In 2015, only a modest negative rainfall anomaly was recorded.

We found that differences between rainfall during the 1982 and 1997 events were mostly forced by sea surface temperature (SST) and were not solely due to a stochastic atmosphere as has been reported previously. Local SSTs in the regions directly to the north and northeast of Australia showed a strong relationship with rainfall that was largely independent of ENSO. An atmosphere-only general circulation model confirmed that the SST regions to the north and northeast of Australia contributed to the 1982 rainfall deficit, by reducing the availability of moisture to the east Australian region.

The model response to the observed 1982, 1997, and 2015 SSTs showed both the rainfall and circulation anomalies were well simulated for the 1982 and 1997 events. Only the rainfall was well simulated for 2015, with the observed circulation associated with the 2015 event either stochastically modified or was not well simulated by the model. The model results show that the rainfall deficit observed in 1982 was associated with SST-forced southeasterly wind

anomalies, whereas the near average rainfall in 1997 was associated with SST-forced near average winds. These results were aided by using multiple linear regression on observations to show that changes in wind anomalies were the most important circulation feature for SON rainfall in most of east Australia. Only in the Victorian region was sea level pressure (SLP) the most important for SON rainfall.

The wind anomalies in SON 1997 were near normal in part due to a record-breaking positive SLP anomaly to the north of Australia. We showed that this record anomaly was likely due to the 1997 El Niño developing earlier and stronger than other events. A strong SST anomaly in the eastern Pacific that peaked in SON 1997 was associated with an early eastward shift in the tropical Pacific maximum convection. The eastward movement of convection was associated with a greater increase in SLP over the Maritime Continent than is typical for SON during an El Niño. This process was not well simulated in both the atmosphere-only and Pacific pacemaker configuration of Community Earth System Model due to the model not able to simulate the shift in convection that was observed in SON.

Overall, this thesis shows that both SSTs local to Australia, and in the eastern Pacific can influence east Australian SON rainfall during strong El Niño events, with the potential modification from a stochastic atmosphere.

Publications during enrolment

van Rensch, P., Gallant, A.J.E., Cai, W., Nicholls, N., 2015. Evidence of local sea surface temperatures overriding the southeast Australian rainfall response to the 1997-1998 El Niño. *Geophys. Res. Lett.* 42, 9449–9456. https://doi.org/10.1002/2015GL066319

van Rensch, P., Arblaster, J., Gallant, A.J.E., Cai, W., Nicholls, N., Durack, P.J., 2019. Mechanisms causing east Australian spring rainfall differences between three strong El Niño events. *Clim. Dyn.* 53, 3641–3659. https://doi.org/10.1007/s00382-019-04732-1

Declaration

I hereby declare that this thesis contains no material which has been accepted for the award of any other degree or diploma at any university or equivalent institution and that, to the best of my knowledge and belief, this thesis contains no material previously published or written by another person, except where due reference is made in the text of the thesis.

This thesis includes two original papers published in peer reviewed journals. The core theme of the thesis is teleconnections of strong El Niño events to east Australian spring rainfall. The ideas, development and writing up of all the papers in the thesis were the principal responsibility of myself, the student, working within the School of Earth, Atmosphere and Environment under the supervision of Dr. Ailie Gallant, Assoc. Prof. Julie Arblaster, Dr. Wenju Cai, and Emeritus Prof. Neville Nicholls.

The inclusion of co-authors reflects the fact that the work came from active collaboration between researchers and acknowledges input into team-based research.

In the case of Chapters 2 and 3 my contribution to the work involved the following:

Thesis Chapter	**Publication Title**	**Status**	**Nature and % of student contribution**	**Co-authors name Nature and % of Co-author's contribution**	**Co-authors, Monash student**
2	Evidence of local sea surface temperatures overriding the southeast Australian rainfall response to the 1997-1998 El Niño	*Published*	*80%. Concept, methodology, analysis and writing*	*1)* Ailie Gallant, methodology and writing 10% *2)* Wenju Cai, methodology and writing 5% *3)* Neville Nicholls, methodology and writing 5%	*No (all)*
3	Mechanisms causing east Australian spring rainfall differences between three strong El Niño events	*Published*	*80%. Concept, methodology, analysis and writing*	1) Julie Arblaster, methodology and writing 5% *2)* Ailie Gallant, methodology and writing 5% *3)* Wenju Cai, methodology and writing 4% 4) Neville Nicholls, methodology and writing 4% 5) Paul Durack, data and writing, 2%	*No (all)*

I have renumbered sections and figures of published papers in order to generate a consistent presentation within the thesis.

Student name: Peter van Rensch

Student signature: **Date:** 24/04/2020

I hereby certify that the above declaration correctly reflects the nature and extent of the student's and co-authors' contributions to this work. In instances where I am not the responsible author, I have consulted with the responsible author to agree on the respective contributions of the authors.

Main Supervisor name: Ailie Gallant

Main Supervisor signature: **Date:** 24/04/2020

Acknowledgements

I would like to acknowledge and express my sincere gratitude to my supervisors Dr. Ailie Gallant, Assoc. Prof. Julie Arblaster, Dr. Wenju Cai, and Emeritus Prof. Neville Nicholls. They have supported me both professionally and personally throughout the numerous years of my PhD. I have tried to draw from their many and varied qualities that I hope to take with me. To mention a few, I would like to thank Ailie for her excitement for science, Julie for her broad depth of scientific knowledge, Cai for teaching me so much about the scientific world, and finally Neville, for being an excellent role model. I would also like to thank them for their support in helping me to maintain a good work/family balance, particularly Ailie and Julie who were also juggling their career with a young family.

There were numerous other people who contributed to this work, including Dr. Clara Deser and Adam Phillips for their scientific discussions, hospitality when visiting their institute, and for providing data that resulted in Chapter 4. Dr. Paul Durack who provided data and input to Chapter 3. Dr. Duncan Ackerley who taught me how to run the Australian Community Climate and Earth System Simulator. Also, I thank Assoc. Prof. Jason Evans and three anonymous reviewers for their valuable review of the papers included in this thesis.

This research was supported by an Australian Government Research Training Program (RTP) Scholarship, CSIRO, the Australian Research Council (ARC) Centre of Excellence for Climate System Science, and the Australian Climate Change Science Program. This research was undertaken with the assistance of resources and services from CSIRO High Performance Computing, and the National Computational Infrastructure (NCI), which is supported by the Australian Government. I also acknowledge the World Climate Research Programme's

Working Group on Coupled Modelling, which is responsible for the Coupled Model Intercomparison Project, and I thank the climate modeling groups for producing and making available their model output (listed in Table 2.1 of this thesis).

Personally, I would like to thank Tilo Ziehn, Ariaan Purich, Catia Domingues, Tim Cowan, Pandora Hope and many others at CSIRO, Monash University and the Bureau of Meteorology for their support throughout the years.

I am eternally grateful to my parents John and Riekie for giving me everything I needed to get where I am today. My sisters and their families for all the support they have given me. Finally, I thank my family; William and Emma for their fun and distractions when I needed it, and my wife, Lisa. I am forever grateful to Lisa who at times took over my role at home when I needed to pour my efforts into these pages. Of everything I accomplished in this thesis, her efforts in raising our two children has been greater; in that regard this thesis is as much an achievement of hers as it is of mine.

Table of Contents

1 Introduction

1.1 Background

Australia relies on rainfall for most of its water security. The refilling of dams and flowing river systems require rainfall on a regular basis. However, rainfall in Australia can be sporadic, with long-lasting droughts that are at times broken by wide-spread floods. Due to its sporadic nature, any predictability in rainfall is valuable for adequate planning of the agriculture, water resource and emergency management sectors.

There are numerous potential avenues for rainfall prediction, be that in the atmosphere, through the Southern Annular Mode (SAM, Hendon et al., 2007), and the Madden-Julien Oscillation (MJO, Wheeler et al., 2009); or in sea surface temperatures (SSTs, Nicholls, 1989; Taschetto et al., 2016). SSTs have the greatest potential of long-term seasonal prediction due to their long-lasting anomalies and known physical processes of air-sea interactions. Ocean phenomena such as the Indian Ocean Dipole and the El Niño-Southern Oscillation (ENSO) have the potential to assist in rainfall forecasting for at least one season in advance. In addition, SSTs to the north of Australia have been shown to have an influence on southern Australian rainfall (Nicholls, 1984a, 2010; Watterson, 2010). The statistical links between SSTs and Australian rainfall are well founded. Future improvements in seasonal forecasting of Australian rainfall relies on a greater understanding of how various SST phenomenon, such as ENSO, teleconnect their impact to Australian rainfall.

Although there is now a greater appreciation of the interactivity of all tropical ocean basins (Cai et al., 2019), by focusing on strong El Niño events, this thesis will perform an in-depth

investigation of each step that links tropical Pacific SST and east Australian spring (September-November, SON) rainfall. These steps include:

- How properties of remote tropical Pacific SSTs affect the link.
- The influence that SSTs local to Australia can have on the link.
- The SST forced atmospheric circulation.
- The influence of a stochastic atmosphere on the link.
- Finally, how the resulting circulation influences seasonal rainfall.

1.2 The El Niño-Southern Oscillation

ENSO is a coupled atmosphere-ocean phenomenon localised in the tropical Pacific Ocean. It is the largest contributor to global interannual climate variability and has an irregular cycle of roughly 3-7 years (Rasmusson and Wallace, 1983; Timmermann et al., 2018). There are two extreme phases of ENSO that have been described extensively in the literature. These extreme phases are distinct from normal, often called “neutral”, conditions (Fig. 1.1a). One of the extreme phases has been named as “La Niña” (Fig. 1.1b). A La Niña occurs when SSTs along the equatorial Pacific, just east of the dateline, cool significantly by roughly 0.5° C below average (Hoerling et al., 1997; Dommenget et al., 2013). The atmospheric circulation associated with a La Niña is effectively an intensification of neutral years. The opposite phase, known as an “El Niño” (Fig. 1.1c), is distinguished by warm SST anomalies greater than roughly 0.5° C in the central to eastern Pacific region (Hoerling et al., 1997; Dommenget et al., 2013). During El Niño, the Walker Circulation weakens, slackening the easterly winds; convection follows the SST anomalies and occurs further east than during normal conditions (Rasmusson and Wallace, 1983).

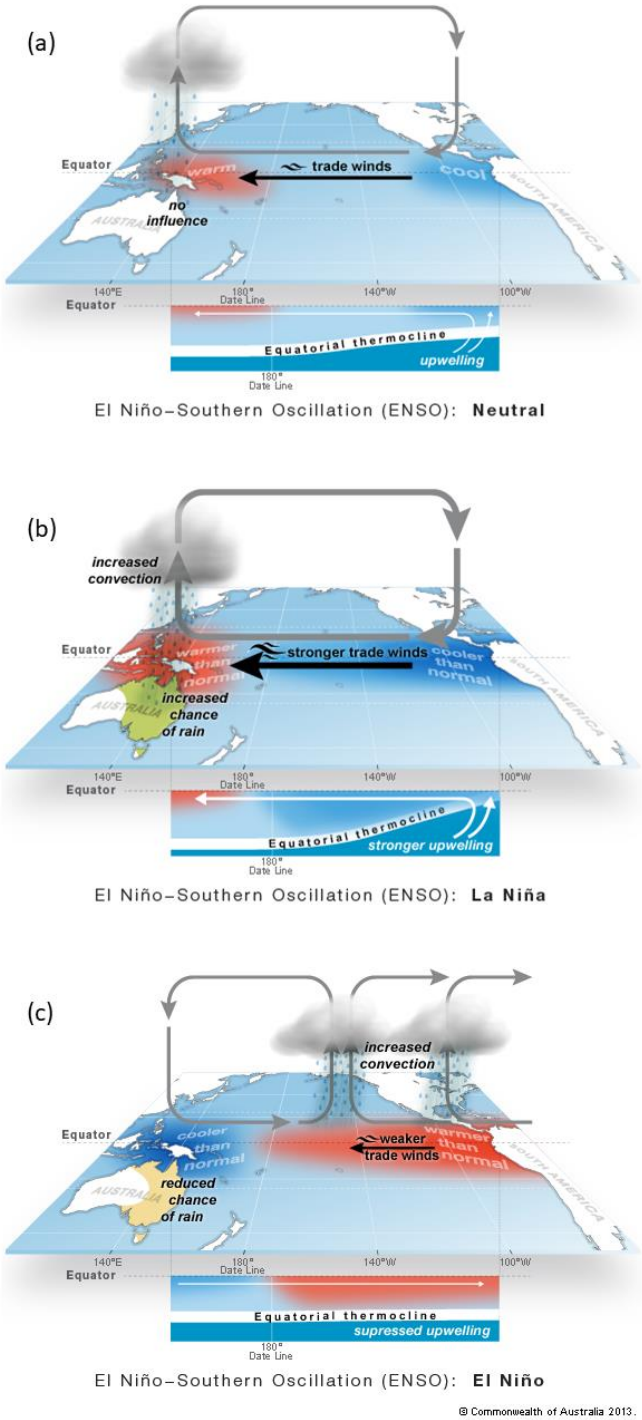

Fig. 1.1: Diagram of SSTs, winds and subsurface temperature in the tropical Pacific during (a) neutral, (b) La Niña, and (c) El Niño conditions. Adapted from the Australian Bureau of Meteorology (http://www.bom.gov.au/climate/about/australian-climate-influences.shtml?bookmark=enso).

El Niño events have shown two spatial structures (Kao and Yu, 2009; Kug et al., 2009; Timmermann et al., 2018). The first has its maximum SST anomalies in the central tropical

Pacific near the International Dateline and has a similar spatial structure, but opposite in sign, to La Niña (Dommenget et al., 2013). The second structure records the maximum SST anomalies in the eastern tropical Pacific (Dommenget et al., 2013; Timmermann et al., 2018; Santoso et al., 2019). Eastern Pacific El Niño typically have a stronger magnitude SST anomaly than the central Pacific El Niño (Kao and Yu, 2009; Kug et al., 2009).

As the phenomenon is a coupled system, El Niño events need both atmospheric and oceanic conditions to be favourable for events to initiate. Firstly, there needs to be a widespread warm temperature anomaly in the subsurface ocean (surface to roughly 150 m depth) of the equatorial Pacific (Wyrtki, 1985; Jin, 1997; Fig. 1.1c). This anomaly can arise from wind stress anomalies in the previous years, in conjunction with oceanic boundary wave reflection (Boulanger et al., 2004). Then from about March, the western Pacific will need to experience regular anomalous westerly wind events to initiate oceanic equatorial downwelling Kelvin waves, which travel to the east and prohibit upwelling of cool subsurface waters in the eastern tropical Pacific (Vecchi and Harrison, 2000; Boulanger et al., 2004; Lengaigne et al., 2004). Reduced upwelling allows warm SST anomalies to develop in the central to eastern tropical Pacific, further promoting westerly wind events and resulting in a positive feedback of El Niño growth. The peak of the El Niño event typically coincides with austral summer months, typically December or January (Rasmusson and Carpenter, 1982; Okumura and Deser, 2010). The El Niño event typically decays in February with the Pacific returning to roughly neutral conditions by March (Harrison and Vecchi, 1999). El Niño events show evidence of coupling to the seasonal cycle (Rasmusson and Carpenter, 1982; Timmermann et al., 2018). The reasons for this seasonal coupling are still unknown, but possibly due to seasonal variations making conditions favourable or unfavourable for El Niño growth (Chen and Jin, 2019). Most El Niño events are isolated in time by neutral years and can be considered

independent (Kessler, 2002), although it is possible that a La Niña event can directly follow an east Pacific El Niño event (Wyrtki, 1985; Jin, 1997; Kug et al., 2009; Dommenget et al., 2013).

1.3 ENSO and climate predictability

The ENSO phenomenon provides one of the greatest opportunities for interannual climate predictability. Not only are ENSO events the strongest mode of interannual variability in many locations around the world, their long-lasting nature and the distinct features of their development can give many months warning of their peak. The positive feedbacks between SSTs and winds, and SST persistence, gives some confidence that if an ENSO event is developing during the austral winter, the anomalies will continue until the end of austral summer. This has the potential to provide up to six months of warning before an El Niño peak. However stochastic process, such as a lack of further westerly wind bursts can dampen the magnitude of the El Niño (Vecchi and Harrison, 2000; Boulanger et al., 2004). The ability to forecast an El Niño event prior to its onset is not possible with today's level of understanding of the physical mechanisms that produce and maintain an El Niño. However, there is currently a global push to develop decadal forecasting which may improve our multi-year knowledge of ENSO events (Boer et al., 2016; DiNezio et al., 2017; O'Kane et al., 2020).

The ability to forecast an ENSO event is most useful not for the ENSO event itself, but rather the accompanying teleconnections that exist between the extreme phases of ENSO and regional climates. Namely, the extreme phases of ENSO are strongly related to interannual variations in temperature and precipitation in some locations. ENSO events have the largest influence on regional climate in the tropical Pacific Ocean, but their effects are also seen on the edges of the Pacific basin and beyond (Ropelewski and Halpert, 1987; Frauen et al., 2014).

It is these areas where ENSO events are felt via their socioeconomic effects and also the regions from which ENSO obtained its name. During El Niño events, fish stocks off the north-western coast of South America can be severely impacted. Typically, this region experiences upwelling, drawing nutrient rich water to the surface and providing a base for marine ecosystems. However, when an El Niño event occurs, upwelling in this region is suppressed reducing the nutrient abundance (Barber and Chavez, 1983). The reduced nutrients and warmer water drives fish stocks away from this region cutting off a vital food resource for many northwest South American communities. Warmer water local to northwest South America also increases the atmospheric moisture content, increasing the chance of extreme rainfall events in this region (Sanabria et al., 2018; Sulca et al., 2018). As El Niño events peak roughly at Christmas time, the Spanish speaking and predominately Christian South American population associate these events with the birth of “El Niño”, or in English “The Boy” Jesus Christ. Conversely, “La Niña” means “The Girl” in Spanish. This not only explains part of the origin of the acronym “ENSO,” but also highlights the importance of this phenomenon to the local South American community to associate this event with divinity.

On the western edge of the Pacific basin, the climate of the Maritime Continent, which encompasses the islands and archipelagos of tropical southeast Asia including Indonesia and Papua New Guinea, are also influenced by ENSO events. This region is close to the ascending branch of the Walker Circulation and is therefore strongly influenced by convection. In conjunction with the Indian Ocean Dipole, La Niña events can dramatically increase Maritime Continent dry season rainfall (Lestari et al., 2019), or shift rainfall zonally away during El Niño, leaving the region in drought (Hamada et al., 2012). The effects of ENSO extend even further west away from the Pacific, with the atmospheric circulation of the Indian Ocean also greatly affected by different phases of ENSO. The term “Southern Oscillation” originates from the

almost global scale seasonal oscillations in sea level pressure (SLP) that was detected to the south of India (Walker, 1924). Walker (1923, 1924) found this oscillation in SLP, and its association with the strength of the Indian monsoon – suggesting it could be used for seasonal prediction. Later it was found that this SLP oscillation was linked to the SSTs in the tropical Pacific Ocean linking the term "El Niño-Southern Oscillation" (Bjerknes, 1966, 1969). Continuing west, east African rainfall shows a complex relationship with ENSO, with El Niño typically associated with increased rainfall there (Indeje et al., 2000).

The influence of ENSO is not localised to the tropics – SLP in the north and southern Pacific basins are significantly related to the variability exhibited in the tropical Pacific. The Pacific-North American pattern and the Pacific-South American pattern are well known features in the monthly to seasonal SLP field (Hoskins and Karoly, 1981; Karoly, 1989). Studies have attributed these patterns to equivalent-barotropic Rossby waves emanating from divergence anomalies in the upper levels of the troposphere, which is associated with the changed convection features during ENSO events (Hoskins and Karoly, 1981; Sardeshmukh and Hoskins, 1988; Karoly, 1989). There is some dispute as to whether the Pacific-South American pattern is the result of Rossby waves, due to the inability for Rossby waves to propagate through the vorticity barrier associated with the midlatitude jet (O'Kane et al., 2017). However, despite the uncertainty of the mechanisms in which these features operate, the association between ENSO and the extratropics is well established (Ropelewski and Halpert, 1987; Kiladis and Diaz, 1989), and includes regions such as Australia (McBride and Nicholls, 1983; Chung and Power, 2017), New Zealand (Kidson and Renwick, 2002; Ummenhofer and England, 2007), Antarctica (Renwick, 2002; Turner, 2004), North America (L'Heureux et al., 2015; Johnson and Kosaka, 2016; Deser et al., 2017), the Arctic (Lee, 2012), and possibly Europe (Katsafados et al., 2005).

1.4 ENSO and Australia

The strong relationship between Australian rainfall and ENSO gives Australia a seasonal forecasting advantage compared to other regions which do not have as strong relationship, e.g. North America, Europe (Ropelewski and Halpert, 1987). The link between Australian rainfall and ENSO was so strong that the link was known before a firm understanding of the ENSO phenomenon was established. Quayle (1929) detailed the monthly relationship between 10 northern Victorian rainfall stations and Darwin air pressure, finding the relationship was strongest in winter and spring. As rainfall and SLP datasets improved in spatial coverage and temporal length, more robust signals were confirmed, and the spatial details were defined. Seasonal variations in the strength of the ENSO-Australian rainfall relationship were discovered, showing that SON possesses the strongest and most widespread relationship than in any other season (McBride and Nicholls, 1983).

Despite the strong relationship between ENSO and Australian rainfall, there are also complexities within this relationship. The relationship is non-stationary, with regions of significant relationship shifting spatially with time (McBride and Nicholls, 1983; Gallant et al., 2013; Ashcroft et al., 2016). A waxing and waning of the ENSO-Australian rainfall relationship was shown to be in coherence with the change of phase of the Interdecadal Pacific Oscillation (Power et al., 1999), suggesting decadal fluctuations in the Pacific could explain some of the non-stationarity of the relationship. An asymmetry in the Australian rainfall response of La Niña events compared to El Niño events was detected, with La Niña causing a greater increase in rainfall than a similar magnitude El Niño would cause a decrease in rainfall (Power et al., 2006). This asymmetry is greatest in the north of Australia, with southern Australia showing a more symmetric relationship between La Niña and El Niño (Chung and Power, 2017). The

ENSO-Australian rainfall relationship also exists within a strongly stochastic atmosphere, with any ENSO event only able to increase the chance of a rainfall anomaly, not guarantee it (Dix and Hunt, 1995).

Quayle (1929) not only showed the link between Australian rainfall and what is now known as ENSO, he also postulated that the physical process of the link is through large-scale pressure modulations modifying storm paths. There have been numerous studies investigating the link between ENSO and Australian rainfall, but a limited number have explored the physical process of the link. The relationship between SLP and rainfall in the extratropics is ubiquitous, allowing the possibly overstated assumption that the Southern Oscillation pressure anomalies drives rainfall there. Other hypotheses suggest a zonal shift of convection towards and away from northern Australia during La Niña and El Niño events respectively could influence rainfall in that region (Cai et al., 2010).

In the south of Australia, Rossby wave trains emanating from an ENSO coherent Indian Ocean is a suggested mechanism by which ENSO events influence this region (Cai et al., 2011b; McIntosh and Hendon, 2018). ENSO could also influence Australian rainfall through its relationship with the SAM and associated zonal wind anomalies (L'Heureux and Thompson, 2006; Hendon et al., 2007). Zonal wind anomalies show a strong relationship with rainfall along the eastern coast of Australia, both using direct wind measurements (Pepler et al., 2016a), and a meridional MSLP gradient (Rakich et al., 2008). Atmospheric thickness anomalies emanating from the Coral Sea region have also been proposed as an additional mechanism for ENSO to influence cut-off lows in southeast Australia (Risbey et al., 2009a). This is particularly pertinent as cut-off lows events account for 57 % of spring rainfall in

southeast Australia (Pook et al., 2006). The variety of mechanisms posed shows that a definitive explanation of how ENSO influences Australian rainfall remains elusive.

Despite the lack of clarity around the mechanisms by which ENSO influences Australian rainfall, the relationship between ENSO and Australian rainfall is engrained in Australian seasonal forecasting lore. Australia's agricultural sector are aware of the terms El Niño and La Niña and equate these with dry and wet years, respectively. This is despite the fact that, ENSO events can only explain up to 25 – 50 % of the rainfall variability across the country, but in many regions it is the best performing climate driver (Risbey et al., 2009b). Furthermore, links between ENSO and natural hazards, such as bushfire weather (Williams and Karoly, 1999; Harris and Lucas, 2019) and tropical cyclone occurrence (Nicholls, 1984b) reinforces the importance of our understanding of the impacts of ENSO.

1.5 Strong El Niño events

The El Niño events of 1982-1983, 1997-1998, and 2015-2016 all stand out as the strongest El Niño events of the satellite era (Huang et al., 2016). Given the previously described relationship between Australian rainfall and El Niño events, it would be reasonable to expect dry conditions to prevail across the continent during the austral spring during these years. Yet, these events were all associated with markedly different rainfall anomalies. The SON of 1982 saw below average rainfall for much of eastern Australia, in line with expectations of a strong El Niño on the Australian climate. In 1997, as the strong El Niño was building, expectations were for a repeat of the 1982 event in SON, however, this did not happen. Near-average rainfall was observed in eastern Australia during the SON of 1997 differing from the typical historical relationship. In 2015, rainfall was below average during SON, but the

anomalies were weaker than expected and were much weaker than 1982. Consistent large-scale impacts were observed in other regions of the globe for all three El Niño events, including reduced rainfall and wildfires in Indonesia (Pan et al., 2018) and flooding in Peru (Sanabria et al., 2018), so the impacts in Australia were unusual – especially during 1997.

The influence of a stochastic atmosphere interfering with the ENSO teleconnection could be the main factor differentiating these events (e.g. Walland, 1998; Brown et al., 2009). However, previous studies have shown that significantly warm SST anomalies to the north of Australia proved important for increasing north Australian rainfall during the 2010-2011 La Niña (Evans and Boyer-Souchet, 2012; Ummenhofer et al., 2015). In line with this finding, warmer than average SSTs off the east coast of Australia have been shown to be favourable for east coast low development (Pepler et al., 2016b). East coast lows explain roughly 23 % of annual rainfall along the eastern coast of Australia (Pepler et al., 2014). Whether local SSTs could be influencing east Australian precipitation during strong El Niño events has not been assessed. In addition, the three El Niño events have been shown to be indistinguishable from each other in terms of strength (Huang et al., 2016), but differences in the structure of the SST anomalies in the Pacific could influence the resulting Australian teleconnections. For example, the 2015 event showed characteristics of a central Pacific El Niño (Santoso et al., 2017), which has been shown to have a greater influence on east Australian SON rainfall (Wang and Hendon, 2007), however the rainfall from 2015 did not align with the 2002 central Pacific El Niño, or even the 1982 event.

1.6 Motivation of this study

This thesis will assess the mechanisms leading to the differences in east Australian springtime rainfall associated with the strong 1982, 1997, and 2015 El Niño events. The impetus of this study is that strong El Niño events have been projected to increase in frequency with increased greenhouse gases (Cai et al., 2014). At our present knowledge, if a strong El Niño were to occur, dry conditions in east Australia would be anticipated with any deviations attributed to stochasticity within the system. It is possible, however, seasonal rainfall forecasts could be improved through understanding all processes associated with the impacts of strong El Niño events. Improved seasonal rainfall forecasts would be valuable for planning in the agriculture, water resource and emergency management sectors.

The thesis is divided into three related studies. First, we assess the atmospheric response to 1982 and 1997 SSTs to determine the possible range of stochastic weather on the teleconnection to southeast Australian rainfall, using atmosphere only experiments from the Coupled Model Intercomparison Project phase 5 (CMIP5). Next, we assess the ENSO-independent relationship between SSTs to the north and northeast of Australia. We will then build upon this result using targeted atmosphere-only experiments of the Australian Community Climate and Earth System Simulator version 1.3 (ACCESS 1.3), which will also allow the assessment of the 2015 event. This will be presented following an observational assessment of the most important circulation features for SON rainfall, with a view to help explain how ENSO influences Australian rainfall on a seasonal timescale. Finally, we will assess the origin of a key circulation feature that contributed to the near average SON rainfall observed in east Australia during 1997.

2 Evidence of local sea surface temperatures overriding the southeast Australian rainfall response to the 1997-98 El Niño

This section is a reproduction of the paper “Evidence of local sea surface temperatures overriding the southeast Australian rainfall response to the 1997-1998 El Niño” published in Geophysical Research Letters by van Rensch et al. (2015), with section and figure numbers changed to fit the thesis structure. The supplementary material of van Rensch et al. (2015) is now included in the main text.

This chapter explores the influence that stochastic forcing in the atmosphere had on the teleconnection for southeast Australian rainfall during spring of 1982 and 1997 using CMIP5. It also statistically shows that local SSTs were important during the two El Niño events.

2.1 Abstract

El Niño events typically bring rainfall deficits to southeast Australia (SEA), for example during the El Niño of 1982-1983. However, SEA experienced near average rainfall during the similar El Niño of 1997-1998. Using an ensemble of atmospheric general circulation models (AGCMs) forced with observed SSTs, we demonstrate that the different September-November rainfall during the 1982 and 1997 events is primarily explained by differences in SST forcing from outside the central and eastern equatorial Pacific. The AGCMs reproduce an observed relationship between SEA rainfall and SSTs to the northeast of Australia. Significantly cooler northeast Australian SSTs during 1982-1983 shifted the rainfall distribution, making a rainfall deficit more likely (relative to the situation in 1997-1998). However stochastic atmospheric processes can modulate the El Niño and regional SST influence and the use of an ensemble of AGCM simulations allows the separation of the effects of stochastic atmospheric processes and SST forcing.

2.2 Introduction

The influence of ENSO on regional rainfall varies with location and also the type of ENSO event. The SST and pressure anomalies associated with an ENSO event can either directly affect rainfall of local regions [e.g. Pacific island nations (Murphy et al., 2014), Indonesia (Hendon, 2003) and northern Australia (Cai et al., 2011b)], or remotely through the propagation of Rossby waves [e.g. The Americas (Horel and Wallace, 1981; Karoly, 1989), southern Australia through the Indian Ocean (Cai et al., 2011b)]. SSTs during the El Niño phase also have two different modes, inducing different impacts on regional climates, such as in the Pacific (Murphy et al., 2014), and Australia (Brown et al., 2009; Frauen et al., 2014; Lim and Hendon, 2015). The modes are distinguished by the location of maximum warm SST anomaly, one in the central Pacific (Ashok et al., 2007; Kao and Yu, 2009); and another in the eastern Pacific. Lim and Hendon (2015) showed the impact of the 2002 central Pacific El Niño was greater than the 1997 eastern Pacific El Niño on Australian SON rainfall, due to the different location of the warm SST anomalies.

The 1982-83 El Niño was also an eastern Pacific type, similar to the 1997-98 El Niño (Fig. 2.1a and Fig. 2.1b); therefore, it would be expected to have the same regional impact. However, during SON of 1982 the eastern half of Australia experienced large rainfall deficits (Fig. 2.1c), consistent with the historical ENSO-Australian rainfall relationship from 1979-2008 (Fig. 2.1e). Unusually, the 1997-98 event, though more intense than the 1982-83 (McPhaden, 1999), resulted in near average SON rainfall in most of Australia (Fig. 2.1d). Brown et al. (2009) attributed the rainfall differences in southeast Australia (SEA) to variations in cut off low events, where more rainfall was received per cut off low in 1997 than during 1982. Back trajectory analysis showed that the air parcels feeding the 1997 cut-off lows were moisture

rich, due to time spent in the marine boundary layer over the oceans to the northeast of Australia (Brown et al., 2009). The parcel trajectories were the result of anticyclonic flow to the east of Australia (Brown et al., 2009), suggesting that the near-average rainfall in SEA during 1997 was contributed by an anomalous atmospheric circulation, but what fed this anomalous circulation is not clear.

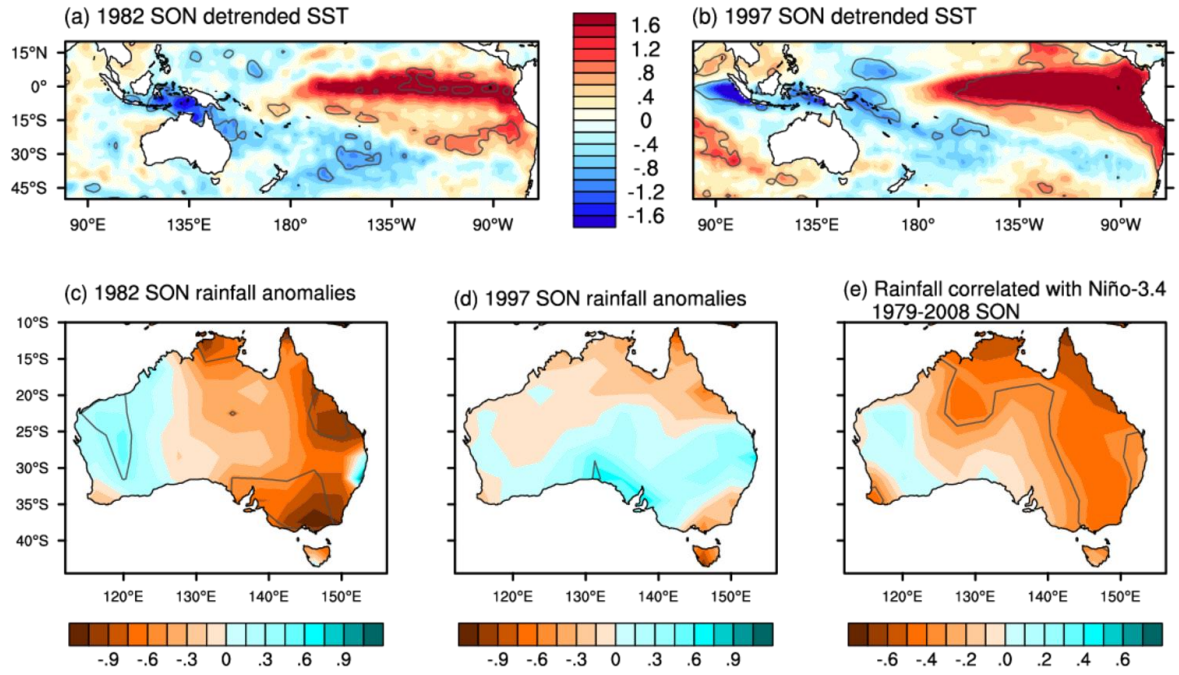

Fig. 2.1: (a, b) Detrended SON SST anomalies for 1982 and 1997, respectively, with grey contours showing values matching 2 standard deviations from the mean of detrended 1979-2008 SON SST. (c, d) SON rainfall anomalies for 1982 and 1997, respectively, with the grey contours showing values matching the 5th and 95th percentile of 1979-2008 SON rainfall. (e) Correlation coefficients of detrended SON rainfall versus detrended SON Niño-3.4, with grey contours showing statistically significant values at the 5% level.

Atmospheric general circulation model (AGCM) studies using different atmospheric initial conditions, but with identical SSTs, show diverse extratropical rainfall responses to the same ENSO forcing (Dix and Hunt, 1995; Sardeshmukh et al., 2000). This indicates that the

stochastic nature of the atmosphere can modify any remote SST forcing, reinforcing or diminishing the signal in any given year. In addition to atmospheric interference to the ENSO teleconnection, local SSTs can also have an impact on regional rainfall. For example in Australia, much warmer than normal local SSTs off the coast of northern Australia increased the rainfall in northeast Australia by 25% during the 2011 La Niña (Evans and Boyer-Souchet, 2012). These studies emphasize that the remote ENSO teleconnection can be affected by processes that may be independent from ENSO itself. The influence of processes such as a stochastic atmosphere and local SSTs may vary depending on the location of ENSO impact, making a global and consistent process difficult to isolate.

In this chapter, we focus on how processes in the Australian region may have influenced the dissimilar SON rainfall associated with the 1997 and 1982 El Niño events. Using a 100 member suite of AGCM simulations forced with observed SSTs, this study explores the extent to which the observed rainfall was affected by stochastic atmospheric processes and by local Australian SSTs in these events.

2.3 Data and methods

Our analysis employs the Atmospheric Model Intercomparison Project (AMIP) experiments from CMIP5 (Taylor et al., 2012). This set of experiments force the atmosphere component of each model with the same observed SST, sea ice and greenhouse gas concentrations from the period 1979-2008. We use 100 simulations from 31 models detailed in Table 2.1. Most models have multiple simulations where either the initial conditions or physics has been altered (Table 2.1). Such a large ensemble means that variability associated with stochastic atmospheric processes, which is not dependent on SSTs, will be reduced by averaging over

the ensemble. To remove any systematic bias between models we use rainfall anomalies from each simulation.

Table 2.1: List of models used in this study. The number of realisations is provided for each model, totalling 100 simulations. Additional notes are provided.

Model name	***Number of realisations***	***Notes***
ACCESS1-0	*1*	
ACCESS1-3	*2*	*Two different physics configurations.*
bcc-csm1-1	*3*	
bcc-csm1-1-m	*3*	
BNU-ESM	*1*	
CanAM4	*4*	
CCSM4	*6*	
CESM1-CAM5	*2*	*From years 1979-2005 only.*
CMCC-CM	*3*	
CNRM-CM5	*1*	
CSIRO-Mk3-6-0	*10*	
EC-EARTH	*1*	
FGOALS-g2	*1*	
FGOALS-s2	*3*	
GFDL-CM3	*5*	
GFDL-HIRAM-C180	*3*	
GFDL-HIRAM-C360	*2*	
GISS-E2-R	*12*	*Two different physics configurations (6 runs each). One physics configuration runs from years 1979-2005 only.*
HadGEM2-A	*6*	*Three different initialisation methods, distributed over 3 runs, 2 runs and 1 run.*
inmcm4	*1*	
IPSL-CM5A-LR	*6*	
IPSL-CM5A-MR	*3*	
IPSL-CM5B-LR	*1*	
MIROC5	*2*	
MIROC-ESM	*1*	
MPI-ESM-LR	*3*	
MPI-ESM-MR	*3*	
MRI-AGCM3-2H	*3*	*Three different physics configurations.*
MRI-AGCM3-2S	*1*	
MRI-CGCM3	*4*	*One run uses a different physics configuration.*
NorESM1-M	*3*	

We focus on SEA as this region has a strong relationship with ENSO (Fig. 2.1e), but is still remote from its direct influence. A time series of spatially averaged rainfall in mainland Australia south of 23°S and east of 143°E is used (outlined in Fig. 2.3a and Fig. 2.3b). We focus on SON, the season when the ENSO-Australian rainfall relationship is strongest (McBride and Nicholls, 1983). The SEA region receives an average SON rainfall of 161 mm ranging from 68 mm – 244 mm during the period 1979-2008.

In SEA, the model simulations capture the observed SON rainfall variance for 1979-2008 (Fig. 2.2a), where a two sample Kolmogorov–Smirnov test cannot distinguish a statistically significant difference (73% level) between the simulated and observed distributions. Therefore, we assume any variance between the simulations is due to stochastic atmospheric processes rather than model bias. The SEA rainfall distribution for the 100 simulations has a more Gaussian appearance than the observed with the simulated distribution unable to reproduce the observed non-Gaussian features such as the peak around -0.8mm/day (Fig. 2.2a). This is likely due to the small sample size of the observations, compared to the roughly 100 times larger sample size for the simulated distribution in Fig. 2.2a. The distributions for SEA rainfall from individual simulations also reveal non-Gaussian features, including peaks at various rainfall values (Fig. 2.2b). None of the individual 100 simulated distributions were significantly different to the observed distribution (using two sample Kolmogorov–Smirnov tests), suggesting that the differences seen in Fig. 2.2a are due to the small sample size of the observed distribution.

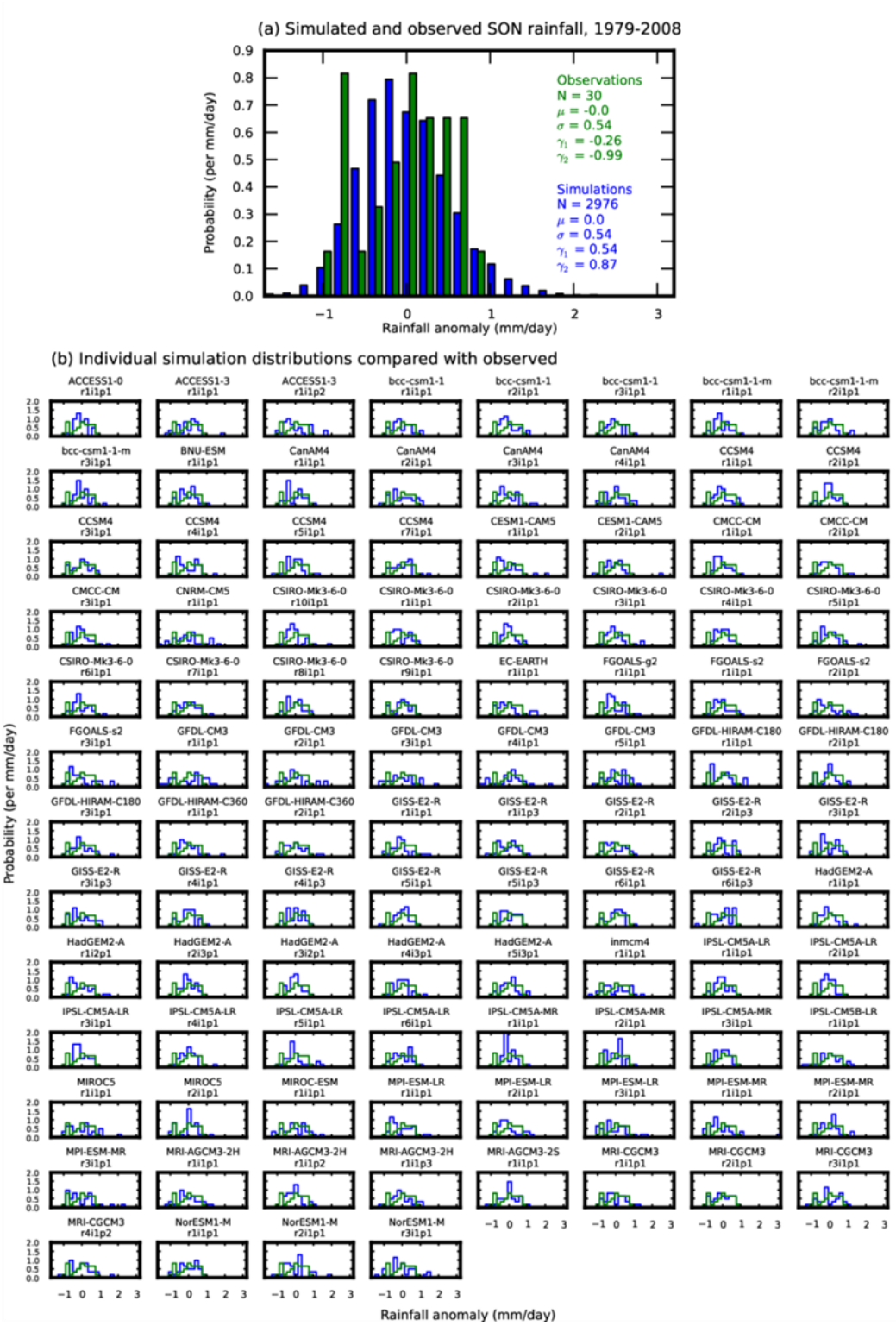

Fig. 2.2: (a) PDF of SON mainland SEA rainfall anomalies during 1979-2008 for (green) observations and (blue) all simulations. Sample size (N), mean (μ), standard deviation (σ), skewness (γ_1) and kurtosis (γ2) are provided. (b) As for (a), but for each individual simulation.

As most models run at different resolutions, we regrid all model data using bilinear interpolation to a 3.75˚ longitude by 3˚ latitude grid, which was the coarsest grid used by any model in the ensemble. Although localised extreme rainfall events are diminished, large-scale rainfall features are still resolved. Each simulation was forced with custom spatially and temporally gridded SST and sea ice concentrations that were derived from a monthly 1˚ by 1˚ gridded observational dataset (Hurrell et al., 2008). For our analysis we use this observational SST dataset in its native grid, from which we also derive all SST time series described in this chapter. For comparison to observations we use rainfall data from Version 2 of the Global Precipitation Climatology Project (Adler et al., 2003), which was also regridded to our common model resolution.

Some datasets, particularly the SSTs, have trends throughout the time period, therefore we detrend all data before performing any analysis in order to focus on interannual differences only. In addition to correlation we also use partial correlations to examine the relationships after removing the effects of a third predictor (Ashok et al., 2007). The statistical significance of the correlation coefficients was derived using a two-tailed Student's *t*-test.

2.4 Simulation of 1982 and 1997 rainfall using observed SSTs

The AGCM simulations suggest that the different observed Australian SON rainfall patterns in 1982 and 1997 were to be expected, given the observed SSTs. The ensemble mean rainfall for simulations forced with 1982 SSTs shows below average rainfall in the eastern half of Australia, similar to the observations (cf. Fig. 2.1c and Fig. 2.3a). However, the magnitude of ensemble mean rainfall anomaly is weaker than the observed anomaly, suggesting that stochastic atmospheric processes might have amplified the rainfall deficit. In 1997, the

ensemble mean rainfall generally captures the observed pattern and magnitude, with wetter than average rainfall across much of the Australian continent and dryer areas in the far northern and southern tips (cf. Fig. 2.1d and Fig. 2.3b). The similarity of the observed to the mean ensemble simulated rainfall patterns in the two years (despite the large differences between 1982 and 1997, and the fact that in the equatorial Pacific the SST patterns were

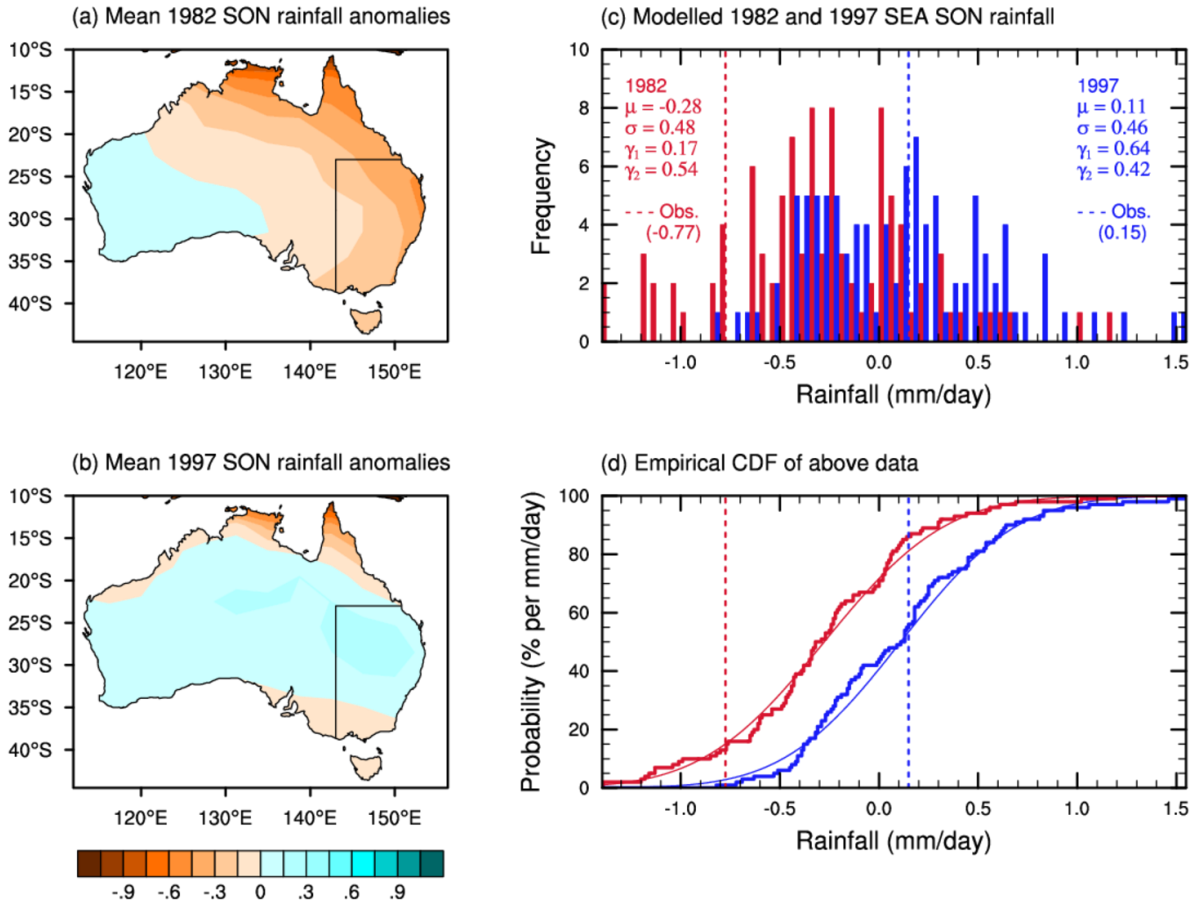

Fig. 2.3: (a, b) Ensemble mean SON rainfall anomalies of 100 atmospheric simulations for 1982 and 1997, respectively. (c) Histogram of 100 simulated rainfall anomalies in SEA [outlined by the boxes in (a) and (b)] for 1982 (red) and 1997 (blue), with mean (μ), standard deviation (σ), skewness (γ_1), kurtosis (γ_2) and observations (dashed lines, values in parentheses) displayed. (d) Bold lines show the empirical distribution function of the data in (c), thin lines show the cumulative distribution function of a fitted normal distribution from which our probability estimates in the text are derived. Vertical dashed lines show the observed rainfall, as in (c).

similar in the two years), suggests that the Australian rainfall patterns were largely influenced by SST forcing outside the tropical Pacific, with some influence from stochastic atmospheric processes.

The AGCM ensemble results suggest that the different SEA rainfall anomaly patterns in 1982 and 1997 were the result of a forcing that is not common to both years. A two sample Kolmogorov–Smirnov test shows less than 0.01% probability that the 1982 and 1997 SEA ensemble rainfall anomalies are from the same distribution. The distributions of simulated SEA rainfall for both 1982 and 1997 were deconstructed into individual model rainfall anomalies (Fig. 2.4), and their spread across the multi-model distribution confirms the ensemble mean was not the result of individual model biases.

Although the ensemble rainfall anomalies in years 1982 and 1997 have different mean values, they actually have similar inter-simulation variance (Fig. 2.3c). This suggests that stochastic behaviour inherent in the atmosphere is responsible for the spread of rainfall anomalies, rather than SST forcing. The rainfall spread results in the overlap of the 1982 and 1997 distributions, showing that it is possible to produce a similar rainfall anomaly for both 1982 and 1997 when choosing only one realisation. This highlights the highly stochastic nature of rainfall in this region even with identical SST forcing, and shows a capacity for stochastic processes to mask a strong teleconnection.

The ensemble mean SEA SON rainfall anomaly during 1982 (-0.28 mm/day) is less than half that of the observed (-0.77 mm/day, Fig. 2.3c), suggesting that random atmospheric processes acted to enhance the observed rainfall deficit. In fact, providing the models are realistic, we estimate that the probability of obtaining a rainfall anomaly less than or equal to the observed is 15% given the same SST forcing of 1982 (Fig. 2.3d).

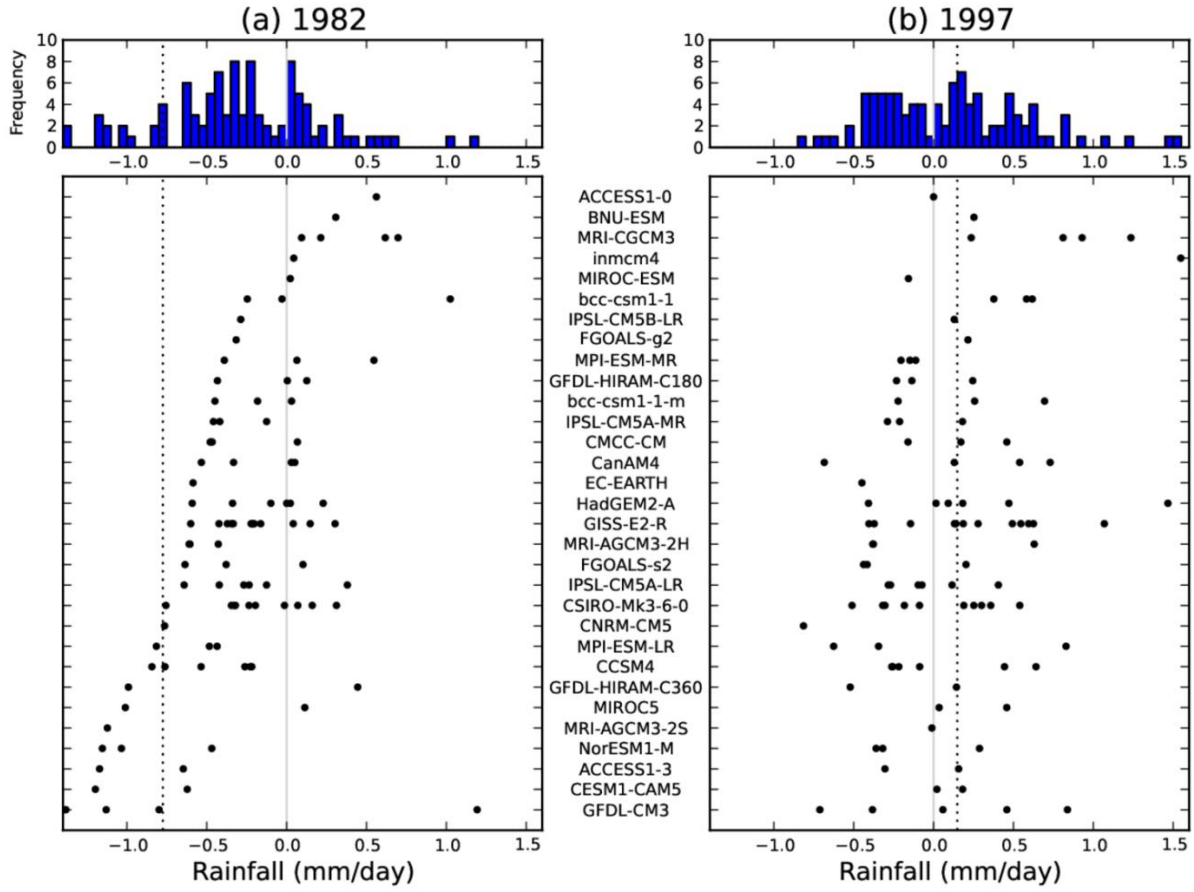

Fig. 2.4: Model breakdown of the SEA SON rainfall anomaly distributions shown in Fig. 2.3c for (a) 1982 and (b) 1997. The models descend by the minimum SON rainfall anomaly for 1982. The observations and zero anomalies are marked by black dotted and grey solid lines, respectively.

For the 1997 case, stochastic atmospheric processes did not drastically alter the observed rainfall anomaly. The ensemble mean SEA SON rainfall anomaly is 0.11 mm/day, compared with the observed 0.15 mm/day, with only a 53% probability of obtaining an equal or lesser rainfall to the observed (Fig. 2.3d). This makes the lack of rainfall anomalies even more at odds with the historical relationship between ENSO and SEA rainfall, which would expect a large rainfall deficit (Fig. 2.1e). Furthermore, when forced with 1997 SSTs there is only a 2.8%

chance of getting a rainfall deficit less than or equal to that observed in 1982, despite the fact that the El Niño event of 1997 was stronger than 1982 by several metrics (McPhaden, 1999).

Thus, the observed rainfall difference between 1982 and 1997 were likely forced by a difference in the observed SST, though the 1982 rainfall deficit appears to be exacerbated by stochastic atmospheric processes. Given that the 1982 and 1997 events had similar SST anomalies in the central and eastern equatorial Pacific, a difference in SST in other regions must have exerted an influence.

2.5 SST regions forcing SEA rainfall variations

Nicholls (1984a, 1989, 2010) demonstrated that SSTs around northern Australia were correlated with southern Australian rainfall. Confirming Nicholls's earlier results, SEA rainfall during the 1979-2008 period was positively correlated to local SST to the north and northeast of Australia ($r > 0.4$), and strongly negatively correlated ($r < -0.6$) in the central tropical Pacific (Fig. 2.5a). However, the correlations in Fig. 2.5a are computed from observational rainfall time series that are heavily influenced by a stochastic atmosphere.

To remove stochastic atmospheric influences and isolate the true forcing from the ocean, we use the AGCM ensemble mean of SEA SON rainfall to correlate with SSTs (Fig. 2.5b). This reveals stronger and more widespread statistically significant relationships between SSTs and SEA rainfall of generally the same sign as the observed (cf. Fig. 2.5a and Fig. 2.5b). Thus, these regions are more important for forcing Australian rainfall variability than is indicated by the observational analysis, which includes stochastic atmospheric processes that damp the teleconnection. Other modelling studies have been reluctant to use correlations involving ensemble mean rainfall because it artificially strengthens the teleconnection by not including

stochastic atmospheric variability (e.g. Grötzner et al., 2000). However, using the ensemble mean also provides a clearer picture of the SST regions that might be important for forcing regional climate over land, but whose signal is dampened by stochastic atmospheric processes in the observations. (cf. Fig. 2.5a and Fig. 2.5b).

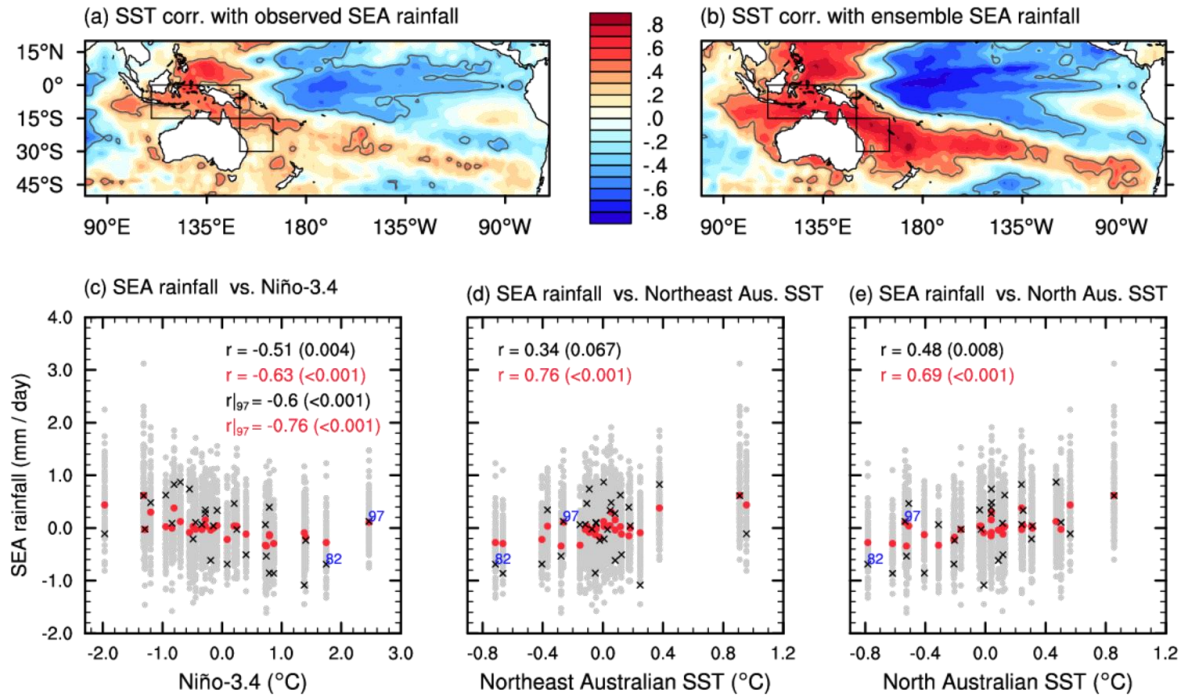

Fig. 2.5: (a, b) Correlation of grid-point SST with (a) observational and (b) AGCM ensemble mean time series of SEA rainfall anomalies during SON 1979-2008. Grey contours show statistically significant values at the 5% level, the two boxes show regions used for the SST time series in (d, e). (c-e) Scatter plots of SEA rainfall versus time series of (c) Niño-3.4, (d) northeast of Australia SST (15˚-30˚S, 150˚-165˚E) and (e) north of Australia SST [Equator-15˚S, 110˚-150˚E, as used in *Nicholls* (2010)] during SON 1979-2008. Black crosses show observations, grey circles show each individual simulation, and red circles show the simulation ensemble mean. The correlation coefficients, r, for the observations and ensemble mean rainfall are displayed in black and red, respectively, the associated p-values are in parentheses. The observational values of years 1982 and 1997 are labelled in blue. (c) also contains the r and p-values with the 1997 point excluded. All datasets were initially detrended.

To determine which regions were of importance to SEA rainfall anomalies during SON of 1982 and 1997, we compare the observed SSTs of these two years to the historical SST-SEA rainfall relationship. This identifies that the SSTs to the north [Equator-15˚S, 110˚-150˚E, as used in Nicholls (2010)] and northeast (15˚-30˚S, 150˚-165˚E) of Australia are significantly correlated with SEA rainfall (boxes in Fig. 2.5a and Fig. 2.5b), but also that they were significantly cool during the 1982 event (Fig. 2.1a). Section 2.4 showed that Australian rainfall in 1982 responded more strongly to SST forcing than in 1997 (Fig. 2.3d). Therefore, it is possible that the cool SSTs to the north and northeast of Australia during 1982 amplified the rainfall reduction in SEA. During 1997, the strong SST anomalies to the north/northeast of Australia were absent, contributing to near average rainfall.

We find that the SEA SON rainfall in 1997 is better represented by SSTs to the north and northeast of Australia than using Niño-3.4. In SON, 1997 was the strongest El Niño in the 1979-2008 period and is an outlier in the SEA rainfall versus Niño-3.4 linear relationship (labelled, Fig. 2.5c). Conversely, the scatter plots of SEA rainfall versus northeast Australian SST and north Australian SST show that 1997 fits within the historical linear relationships (labelled, Fig. 2.5 d and e). However, the strengths of the observed relationships between SEA rainfall and the local Australian SST time series (0.34 and 0.48) are not as strong as those with Niño-3.4 (-0.51; cf. Fig. 2.5 c, d, e).

The weak correlations that were observed when local Australian SSTs were used, as compared to Niño-3.4, are largely because stochastic atmospheric processes influence Australian SSTs. Removing stochastic processes by using the ensemble mean of the AGCMs highlights a stronger correlation between SEA rainfall and local Australian SSTs (0.69, 0.76) compared to the Niño-3.4 index (-0.63; i.e., red dots in Fig. 2.5 c, d, e). Excluding the year 1997 from the

Niño-3.4 correlation produces a comparable correlation with the local Australian SSTs (-0.76), further highlighting that the forced response in 1997 did not stem from the Niño-3.4 region in the eastern tropical Pacific.

The increased strength of the correlations when using ensemble mean rainfall is not because the individual ensemble members have a stronger correlation between SST and SEA rainfall than is observed. Using the same method as other modelling studies (e.g. Grötzner et al., 2000), the mean of correlation coefficients is actually weaker than the observed for all time series (Fig. 2.6). The increase in strength is a result of removing the damping from stochastic perturbations in the atmosphere.

With the effect of stochastic atmospheric processes removed, local Australian SSTs show a stronger relationship with SEA rainfall than ENSO, particularly during 1997. Moreover, northeast Australian SSTs show stronger correlations with SEA rainfall than the SSTs to the north of Australia. However, when isolating different east Australian regions for our rainfall time series, some subtle differences in the importance of the SST-rainfall relationships emerge and these are explored in the next section.

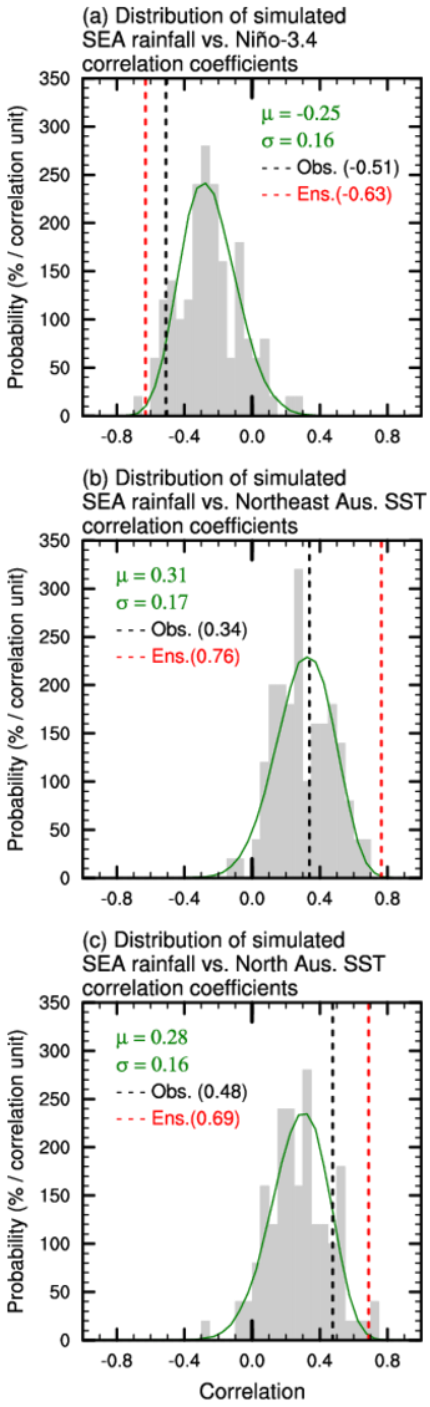

Fig. 2.6: Grey bars show the probability density functions of correlation coefficients for each individual AGCM simulation during SON 1979-2008. The correlation coefficients are for detrended SEA rainfall versus detrended (a) Niño-3.4, (b) northeast of Australia SST and (c) north of Australia SST time series. The green line shows a suite of rainfall time series derived by a 10^5 random resample of all simulations for each year. The mean (μ) and standard deviation (σ) of the distribution are provided. Observations and ensemble mean rainfall correlation coefficients are marked by black and red dashed lines, respectively.

2.6 Local SST contributions to the ENSO-Australian rainfall teleconnection

Assuming that the SSTs to the north and northeast of Australia influence Australian rainfall, it remains unclear if these regions act together or separately and how they are related to ENSO. To this end, we conducted analysis without the influence of stochastic atmospheric processes by using the AGCM ensemble mean rainfall. We find that the SSTs to the northeast of Australia have the strongest impact on SEA rainfall, as the partial correlation of north Australian SST with the effect of northeast Australian SST removed does not have a significant correlation over most of SEA (Fig. 2.7a). Additionally, the residual of northeast Australian SST with north Australian SST removed still shows a significant correlation with most of SEA rainfall (Fig. 2.7b), corroborating Brown et al. (2009).

The dominant relationship between northeast Australian SSTs and AGCM ensemble mean rainfall is not seen when examining those SSTs in relation to observed rainfall. Both north and northeast Australian SST residuals do not show significant correlations with observed rainfall in SEA (Fig. 2.7 e, f), suggesting that for the observations the influences of stochastic atmospheric processes are large.

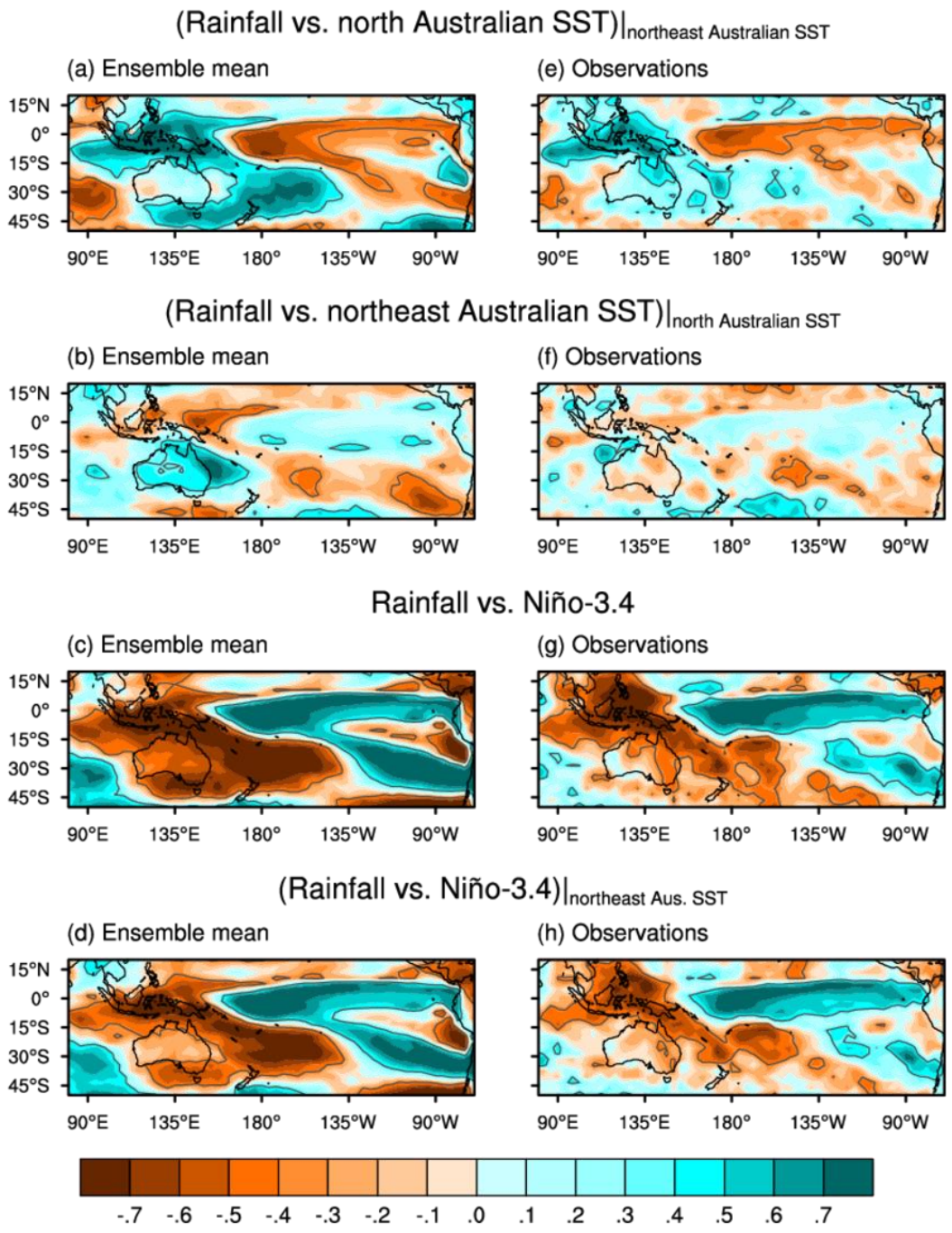

Fig. 2.7: Partial correlation coefficients of ensemble mean rainfall versus (a) north Australian SSTs with northeast Australian SSTs removed and (b) northeast Australian SSTs with north Australian SSTs removed. (c) Correlation coefficients of ensemble mean rainfall versus Niño-3.4. (d) Partial correlation coefficients of ensemble mean rainfall versus Niño-3.4 with northeast Australian SSTs removed. (e-h) as for (a-d), but using observational rainfall instead of the ensemble mean rainfall. Grey contours show statistically significant values at the 5% level. All datasets were initially detrended.

Our results show that the response of SEA rainfall to ENSO is modulated by SSTs to the northeast of Australia. Without the influence of stochastic atmospheric processes much of Australian rainfall is related to ENSO (Fig. 2.7c). However, removing the effect of SSTs to the northeast of Australia, ENSO is no longer correlated with rainfall in a large portion of Australia, including in over half of the SEA region (Fig. 2.7d). Strong correlations remain only in the far south of eastern Australia and in the far northern tip of Australia. Interestingly, this pattern of residual ENSO impact looks similar to the observed and modelled SON rainfall in 1997 (cf. Fig. 2.1d, Fig. 2.3b and Fig. 2.7d), further suggesting that atypical northeast Australian SSTs played a role during that year.

The relationship between northeast Australian SSTs and ENSO ($r = -0.56$) appears to be derived through north Australian SSTs, as removing the influence of north Australian SSTs using partial correlation leaves no relationship ($r = -0.01$). This indicates that although northeast Australian SSTs have a stronger influence on rainfall, the influence of ENSO is introduced into this region through north Australian SSTs. The large number of links between ENSO and rainfall may provide opportunities for the signal to be lost due to other processes, such as what occurred during 1997.

The observations agree with the AGCM results, with the Niño-3.4 residual displaying a weak relationship with SEA rainfall (cf. Fig. 2.7 g and h). These results are robust to variations in the definition of northeast Australian SSTs (not shown).

2.7 Summary and discussion

The extreme 1982 El Niño was associated with a severe rainfall deficit in SEA (as expected from the long-term relationship between El Niño and SEA rainfall), but the more extreme

1997 El Niño resulted in near average rainfall in this region. We find that SST forcing outside the central and eastern equatorial Pacific must have played a role in determining the rainfall, and that the differing rainfall anomalies in the two years was not solely due to stochastic atmospheric processes. Through AGCM simulations, we have shown that cool SST anomalies to the north and northeast of Australia during 1982 increased the likelihood of a rainfall deficit in this region. However, during 1997 these local SSTs were only slightly below normal, and thus had little impact on the rainfall anomaly distribution, leading to slightly above-normal SEA rainfall despite the concurrent extreme El Niño.

The SSTs to the north and northeast of Australia were found to have different degrees of impact on rainfall in most of SEA. We found that the SSTs to the northeast of Australia have the greatest effect on rainfall, but that this is only revealed when stochastic atmospheric processes are removed. The mechanisms by which the SSTs influence rainfall were not explored in this study, however Brown et al. (2009) shows that moisture transport from the SST to the northeast of Australia played a major role in feeding the cut off lows during 1997. We postulate that the warmer northeast Australian SSTs during 1997 than during 1982 enhanced moisture flux to the atmosphere, providing a greater moisture source, and/or the SSTs induced an anomalous circulation directing moisture rich air into the region (Brown et al., 2009). An investigation of these mechanisms will form the basis of future work.

This study indicates that local SSTs can act as a conduit for ENSO to teleconnect with a remote region, but as the 1997 case shows, these local SSTs can have an independently varying component. This provides additional complexity when forecasting rainfall using ENSO metrics, but may provide an opportunity to increase the forecast skill when incorporating the effect of these local SSTs.

3 Mechanisms causing east Australian spring rainfall differences between three strong El Niño events

This section is a reproduction of the paper “Mechanisms causing east Australian spring rainfall differences between three strong El Niño events” published in Climate Dynamics by van Rensch et al. (2019), with section and figure numbers changed to fit the thesis structure.

This section describes the dynamical reasons for the differences in east Australian spring rainfall between the three events. Also, this section examines the physical process linking local SSTs and rainfall during the 1982 El Niño in particular.

3.1 Abstract

Strong El Niño events have had significant impacts on society through their association with extreme events, such as droughts and floods. However, questions remain as to the robustness of strong El Niño events in forcing regional climate variability. The strong 1982, 1997 and 2015 El Niño events were of similar type and strength, but in eastern Australia they were associated with differing spring rainfall anomaly magnitudes and patterns. To understand these differences, we first determined the most important processes for teleconnecting the El Niño signal to east Australian spring rainfall using historical relationships with winds and sea level pressure. Then, using a 60-member atmospheric model ensemble, we estimated the influence of sea surface temperatures (SSTs) on Australian atmospheric circulation and rainfall during these three El Niño events relative to internal variability. We found that the different east Australian spring rainfall anomalies for each of the three El Niño events are best explained by differences in the strength of the meridional wind component of the regional circulation. All three El Niño events exhibited a positive sea level pressure anomaly to the south of Australia, which was associated with rainfall deficits along the southeast Australian coast. The experiments indicate the regional atmospheric circulation and rainfall differences were forced by SSTs during spring of 1982 and 1997, with their influence on the circulation in 2015 remaining unclear. We also show that SSTs adjacent to Australia further contributed to the modelled rainfall differences mainly by regulating moisture availability.

3.2 Introduction

El Niño events affect climate around the globe (Ropelewski and Halpert, 1987), with strong El Niño events showing significant and at times unique regional impacts, such as cold surges in China (Geng et al., 2017), droughts in Indonesia (Pan et al., 2018) and floods in Peru (Sanabria et al., 2018). Understanding the regional impacts of these strong El Niño events, and the mechanisms by which these impacts occur, is needed to improve regional forecasting of the climatic response to future strong El Niño events. Better isolating regional responses to strong El Niño events, and their impacts on society, is imperative given that strong El Niño events are projected to increase in frequency with increasing greenhouse gas concentrations (Cai et al., 2012, 2014; Wang et al., 2017).

In eastern Australia, ENSO is most significantly related with rainfall during austral spring (McBride and Nicholls, 1983; Chung and Power, 2017), where El Niño events are typically associated with less than average rainfall. This relationship held for the El Niño event in 1982, which was one of the three strongest El Niño events of the satellite era (Santoso et al., 2017). A significant rainfall deficit was observed in spring of 1982, in agreement with the anomalously warm central equatorial Pacific SSTs. In 1997, however, regional east Australian rainfall deviated from the typical ENSO-east Australian spring rainfall relationship and rainfall was near average. This occurred despite the fact that the 1997 El Niño event rivalled or even exceeded the 1982 event in magnitude (Santoso et al., 2017). Eighteen years later, the strong El Niño of 2015, which had its equatorial Pacific SST anomaly closer to Australia, recorded only slightly less than average east Australian spring rainfall. The diversity of the responses in east Australian rainfall to similarly strong El Niño events highlights that there is still much about the ENSO-regional rainfall response that is yet to be understood.

Differences in the effects of El Niño on east Australian spring rainfall have been attributed to two factors. The first is differences in SST patterns, both in the proximity of maximum equatorial Pacific SST anomalies to Australia (e.g. Wang and Hendon, 2007), and of SSTs off the coast of Australia, such as to the north and northeast of Australia (Chapter 2; van Rensch et al., 2015). The second is the effect of stochastic atmospheric processes acting independently of El Niño (i.e., atmospheric internal variability), in masking the signal of the El Niño event (e.g. Brown et al., 2009). ENSO indices (e.g. the Southern Oscillation Index) show correlations of up to 0.6 with Australian rainfall (McBride and Nicholls, 1983; Chung and Power, 2017), leaving a large portion of rainfall variance unexplained by ENSO. Chapter 2 (van Rensch et al., 2015) showed that stochastic atmospheric processes exacerbated the southeast Australian spring rainfall deficit observed in 1982, using a large ensemble of atmosphere-only models from CMIP5 that was forced with observed SSTs (Taylor et al., 2012). However, Chapter 2 (van Rensch et al., 2015) also showed that differences in SST patterns significantly contributed to the southeast Australian spring rainfall differences between the 1982 and 1997 strong El Niño events. This suggested that there are differences in the mechanisms linking El Niño and southeast Australian rainfall that required further examination.

The mechanisms whereby El Niño influences east Australian rainfall are unclear. Past studies describe El Niño influencing east Australian rainfall through local pressure changes associated with the western pole of the Southern Oscillation (Cai et al., 2011b; Frauen et al., 2014), or by shifting convection and moisture away from Australia as it follows the region of warm SSTs (Cai et al., 2010; King et al., 2015; Chung and Power, 2017). Additionally, ENSO-coherent wave trains emanating from the Indian Ocean Dipole have been suggested as a mechanism for ENSO to affect southern Australia during spring (Cai et al., 2011b; McIntosh and Hendon, 2018). Other hypotheses focus on the influence of El Niño on regional synoptic events such

as cut-off lows in the Mallee region (see Fig. 3.1a for location) in southeastern Australia (Brown et al., 2009; Risbey et al., 2009a), where cut-off lows are influenced by atmospheric thickness anomalies originating from SSTs to the north and northeast of Australia (Risbey et al., 2009a).

A difficulty in determining the mechanism by which El Niño influences regional rainfall is that different processes are likely important for different regions. The mechanisms by which El Niño affects regional weather (e.g. cut-off low events in southeastern Australia) may not be the same as its influence on regions further north. Differing impacts on the frequency and intensity of daily rainfall in eastern Australia during ENSO events suggests that regional differences in processes exist (Nicholls and Kariko, 1993; Pui et al., 2012). ENSO events tend to affect the frequency of spring wet days throughout eastern Australia, except for east of the Great Dividing Range (see Fig. 3.1a for location; Pui et al., 2012). Furthermore, ENSO shows a relationship to the intensity of wet days in the Mallee region (Pui et al., 2012), which could be due to the influence of cut-off lows described by Risbey et al. (2009a) and Brown et al. (2009). While this suggests a physical explanation exists for the ENSO-rainfall relationship in the Mallee region, whether there are similar explanations for other regions of Australia is not known.

In addition to atmospheric processes, SST anomalies unrelated to El Niño may also have an influence on the rainfall teleconnection. For example, a modelling study has shown that during the 2010-2011 La Niña event, unusually warm SSTs for a La Niña event to the north and northeast of Australia led to an increase in rainfall in northeastern Australia by roughly 25% (Evans and Boyer-Souchet, 2012). The SSTs to the northeast of Australia have been statistically shown to be influential to the ENSO-southeast Australian rainfall relationship

(Chapter 2; van Rensch et al., 2015), corroborating the mechanism described by Risbey et al. (2009a). Chapter 2 (van Rensch et al., 2015) found evidence that the significantly cool SSTs to the north and northeast Australia during spring of 1982 reduced rainfall in southeast Australia, whereas the near average local SSTs during 1997 led to near average rainfall. However, the mechanism by which this region of SST influences rainfall is unknown.

The El Niño events of 1982, 1997 and 2015 were the strongest in the satellite era (Santoso et al., 2017). Given the known ENSO-rainfall relationship in east Australia, a strong El Niño would lead to an increased chance of a large spring rainfall deficiency. The fact that this did not occur in all three of these years suggests there might be aspects of this relationship that are yet to be identified. Chapter 2 (van Rensch et al., 2015) found that SSTs played a significant role in determining the observed rainfall anomalies in both 1982 and 1997, and this chapter expands on that result by examining the seasonal scale mechanisms that led to the observed rainfall anomalies in 1982, 1997 and additionally, 2015. We start by using historical data to identify how typical El Niño events and variations in the atmospheric circulation influence east Australian springtime rainfall. Differences in circulation over Australia between the three events are then assessed in terms of their influence on rainfall. The contribution of SST forcing on the differences in circulation are then assessed in the context of internal variability of the atmosphere using a large ensemble of atmosphere-only model simulations of the three strong El Niño events. Finally, Chapter 2 (van Rensch et al., 2015) showed that SSTs local to Australia had an influence on Australian rainfall during 1982 and 1997, but that chapter did not explore the mechanism by which this occurs. In this chapter we quantify the influence of local SSTs on Australian rainfall and examine the mechanisms using targeted atmosphere-only model experiments.

3.3 Methods

Here we provide a summary of the methods used in our analysis, including the observational and reanalysis datasets, as well as details of the atmospheric general circulation model used and the experiments we performed. We used the Australian Water Availability Project (AWAP) dataset for observed Australian rainfall (Jones et al., 2009), and the ERA Interim (ERAI) reanalysis provided the observed SLP, specific humidity, and wind fields (Dee et al., 2011). We restricted our analysis to the austral spring season from September – November (SON), and we used a 30-year climatological base period from 1979-2008. We defined east Australia as mainland Australia east of 143°E (excluding Tasmania, Fig. 3.1a); this region was further divided as defined in Section 3.4.

Internal atmospheric stochasticity can confuse the detection of teleconnections forced from SSTs. The present hypothesis describes SSTs modifying the large-scale climate system, under which shorter time-scale weather – and its inherent stochasticity – occurs. One way to detect the impact of SSTs in a stochastic atmosphere is by using a model with many ensembles. Studies have used models with a range of ensemble sizes to understand the influence of ENSO on the Pacific-North American pattern (Sardeshmukh et al., 2000; Deser et al., 2017), and also Australian climate (Dix and Hunt, 1995; Grötzner et al., 2000; Frederiksen et al., 2001; King et al., 2015; Karoly et al., 2016). The studies with large ensemble sizes (greater than 25 realisations) have been shown to have a greater chance of accurately capturing the atmospheric mean state of SST forcing, but many more ensembles are needed to capture the variance (Sardeshmukh et al., 2000), or extremes (Karoly et al., 2016). Chapter 2 (van Rensch et al., 2015) used a large ensemble of different atmospheric CMIP5 models forced with observed SSTs (AMIP, Taylor et al., 2012), but such an analysis includes inter-model biases in

the way each model simulates the Earth's climate, not just differences due to stochastic processes simulated by any one model.

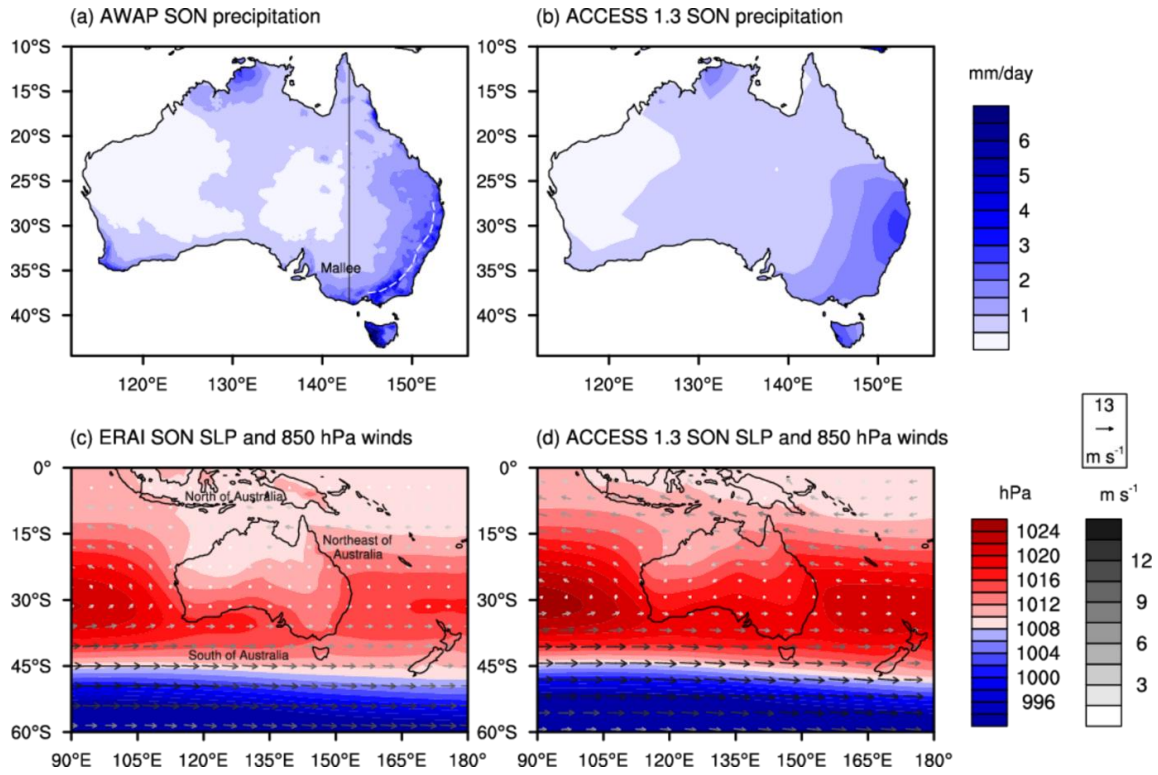

Fig. 3.1: Mean (a) AWAP precipitation and (c) ERA Interim sea level pressure with 850 hPa winds during SON, 1979-2008. (b and d) as for (a and c), but using data from the ACCESS 1.3 control run forced with climatological SSTs and sea ice concentrations from 1979-2008 (1979-2008Clim, see Table 2.1). Eastern Australia is indicated in (a) as mainland Australia (excluding Tasmania) east of the vertical line at 143°E. The Mallee region is also labelled in (a), with the white dashed line roughly indicating the major peaks of the Great Dividing Range. Regions to the north, northeast and south of Australia are labelled in (c).

In an attempt to separate the true SST forcing from stochastic atmospheric processes with unchanging model biases, we conducted a large ensemble using a single model, the Australian Community Climate and Earth System Simulator (ACCESS) 1.3 atmospheric model, forced with observed SST and sea ice concentrations (Durack and Taylor, 2018). The ACCESS 1.3 atmosphere model is based on the Hadley Centre Unified Model version 7.3 (Bi et al., 2013),

and was run at the N96 horizontal resolution (1.25° latitude by 1.875° longitude) with 38 vertical levels, identical to its CMIP5 submission. Our experiments were performed by repeating the required annual SST and sea ice field from April to March for 60 years, thereby producing a 60-member annual ensemble. We kept the atmospheric greenhouse gas concentrations and aerosol emissions fixed to 1990 values so the experiments had a constant forcing. Only the SST and sea ice boundary conditions were changed for each experiment, however the effects of atmospheric gas and aerosol concentrations may still be embedded in the SST and sea ice fields that forced our model.

The experiments performed are summarised in Table 3.1. They include a control run (1979-2008Clim), using twelve-monthly climatological SST and sea ice concentrations from 1979-2008. Three separate simulations using observed SST and sea ice concentrations from 1982, 1997 and 2015 (named 1982Control, 1997Control, and 2015Control, respectively). In addition, experiments were carried out in which we interchanged localised SST patterns between the three events e.g. the 1982 SSTs to the northeast of Australia were placed in the global 1997 SST field. The regions where the SSTs were swapped are to the northeast of Australia (15°S–30°S, 150°E–165°E, outlined in Fig. 3.9a), and to the north of Australia (Equator–15°S, 110°E–143°E, but including the entire Gulf of Carpentaria, outlined in Fig. 3.10a). A 5° latitude and longitude border surrounding the regions was spatially smoothed to remove discontinuities.

Table 3.1: All experiment codes with a summary of global SSTs and sea ice concentrations used, and the experiments where SST from different years were patched into different regions. All experiments repeated the 12-monthly SST and sea ice concentrations for 60 years, producing a 60-member ensemble.

Code	Global	Northeast Australia	North Australia
1979-2008Clim	*1979-2008 12-month climatology*	-	-
1982Control	*1982*	-	-
1997Control	*1997*	-	-
2015Control	*2015*	-	-
1982NEAus1997	*1982*	*1997*	-
1997NEAus1982	*1997*	*1982*	-
2015NEAus1982	*2015*	*1982*	-
1997NAus1982	*1997*	-	*1982*

Repeating an SST pattern from a particular year for 60 years may introduce a soil moisture bias from SST forced changes in rainfall. In eastern Australia, our model showed no consistent trends in SON upper level soil moisture in all of the experiments, however the model suffered from a soil moisture trend in the lowest levels (1.085 - 2.872 m), particularly in the 1982Control experiment. No significant trends were simulated in east Australian rainfall, therefore the soil moisture trend is unlikely to have impacted our results. In addition, our model suffers from a global soil moisture decline in all levels, but particularly in the lower levels. The 1979-2008Clim experiment exhibited a sharp decrease in global soil moisture at the beginning of the simulation. To minimise this decline, we ran the 1979-2008Clim experiment for 100 years, using only the last 60 years. Additionally, we started our other experiments from the 1979-2008Clim experiment after it had completed 40 years of simulation.

The model broadly reproduced the mean 1979-2008 climate as represented in AWAP and ERAI (Fig. 3.1). As observed, more rainfall was simulated in eastern Australia than western

Australia (c.f. Fig. 3.1 a and b). However, the model simulated less rainfall than observed in southeast Australia, possibly due to the relatively coarse model resolution missing up to 1700 m of orographic effects along the Great Dividing Range. The mean winds in this region were stronger in the model than compared to ERAI, and this was also the case in the north of Australia (c.f Fig. 3.1 c and d). The wind strength bias corresponded with a simulated subtropical ridge that is about 4 hPa stronger during SON than in ERAI. Overall, the model simulated the observed characteristics of the Australian circulation, but with a greater intensity.

3.4 Local processes governing Australian spring rainfall variability

Rainfall variability in eastern Australia is significantly associated with ENSO (Fig. 3.2a). However, the region is too remote from the central and eastern tropical Pacific to feel any direct effects of the ENSO SST anomalies on the local atmospheric circulation. Therefore, any signal from El Niño is thought to be caused by pressure and circulation anomalies over the Australian continent that have been induced by the El Niño-related SST anomalies. SLP varies over the Australian continent coherently with ENSO events as Australia is usually situated under the western pole of the Southern Oscillation (Fig. 3.2b). Furthermore, El Niño is related to significant southerly wind anomalies over eastern Australia (Fig. 3.2b). Though these relationships show that the circulation is an important conduit by which ENSO events could influence Australian rainfall, it remains unclear as to whether it is the large-scale changes in local SLP or wind that are most important for ENSO to influence local rainfall, and also if the mechanisms are consistent across the entire Australian region.

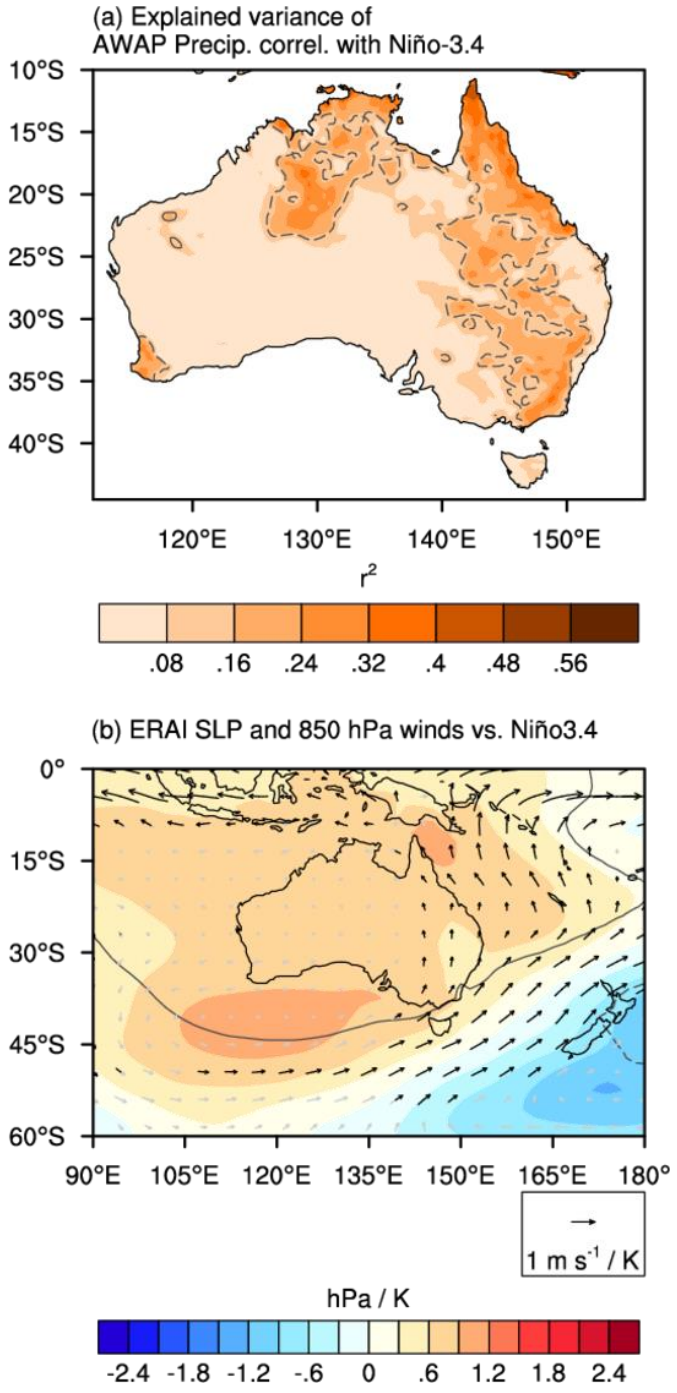

Fig. 3.2: (a) Explained variance (r^2) of AWAP precipitation correlated with the Niño-3.4 time series for SON, 1979-2008. The solid and dashed grey contours show the positive and negative significant correlation coefficients (r), respectively. (b) Regression of ERA Interim SLP and 850 hPa winds versus the Niño-3.4 time series for SON, 1979-2008. The solid and dashed grey contours show the positive and negative significant regressions, respectively. The black vectors show significant values in at least one wind component. Significance in all plots are defined as the 0.05 p-value using Student's two-sided t-test.

Previous studies focusing on southeast Australian rainfall variability have found links to variations in local and regional pressure and wind. This knowledge may help us understand how large-scale circulation changes in El Niño events influence rainfall. For example, the subtropical pressure ridge shows a significant relationship with southern Australia rainfall, particularly in the cooler months (e.g. Larsen and Nicholls, 2009; Cai et al., 2011a; Timbal and Drosdowsky, 2013). Additionally, increased rainfall in regions of southeast Australia have been found to be related to anomalous northerly winds (Whetton, 1988) and northerly flow (Theobald et al., 2015). The northerly winds were shown to originate from geostrophic balance of a pressure gradient induced by high and low pressure anomalies/systems in the vicinity (Whetton, 1988; Theobald et al., 2015). These studies show that local pressure and local wind (or remote pressure anomalies, through geostrophic balance) are important for rainfall in regions of Australia. Quantifying these relationships in all regions of Australia provides the means to understand the simple dynamics associated with variations in seasonal rainfall. Consequently, matching these relationships with the regional circulation patterns during the three strong El Niño events provides a way to elucidate how the circulation influenced the observed rainfall for each El Niño event.

Using multiple linear regression, we isolated which of observed SLP, zonal wind or meridional wind anomalies have historically had the strongest relationship with observed spring rainfall in different regions of Australia (Fig. 3.3). We calculated the multiple linear regression coefficients of anomalous AWAP rainfall regressed onto normalised anomalies of SLP (Fig. 3.3a); 850 hPa zonal wind (Fig. 3.3b); and 850 hPa meridional wind (Fig. 3.3c), at each individual grid point of the ERAI reanalysis. We then identified the strongest regression coefficient in Fig. 3.3a, Fig. 3.3b, and Fig. 3.3c at each grid-point and shaded grid-points with weaker coefficients. Thus, regions without shading in the figure are the regions in which the

respective circulation process (i.e. SLP, zonal wind, or meridional wind) is the most dominant influence on rainfall.

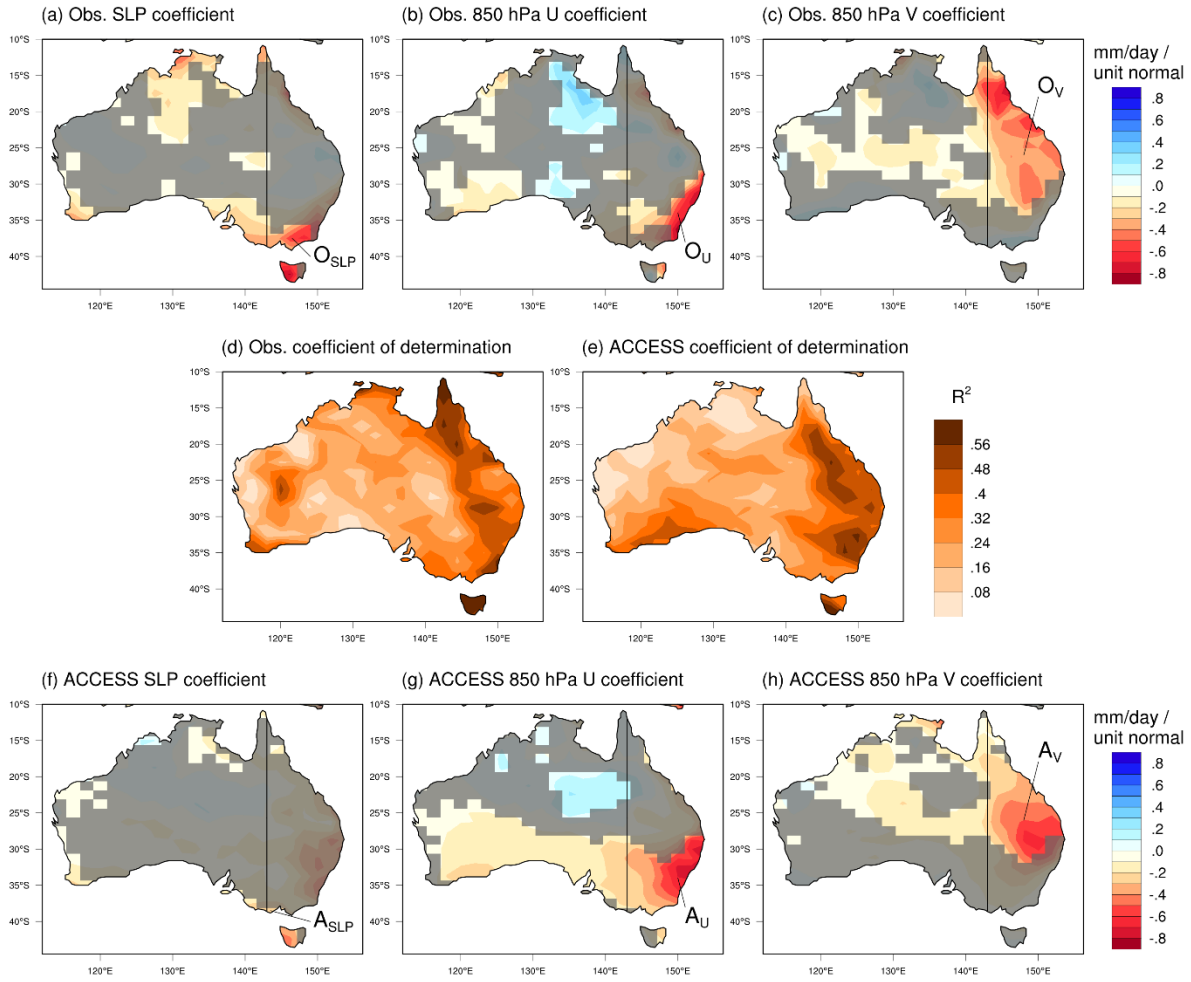

Fig. 3.3: Grid-point multiple linear regressions of AWAP precipitation anomalies versus normalised (a) sea level pressure, (b) 850 hPa zonal wind, and (c) 850 hPa meridional wind anomalies from ERA Interim for SON, 1979-2008. In (a-c), the areas without shading in each panel shows a stronger magnitude regression coefficient than the remaining two panels. (d, e) Explained variance of rainfall using the three observed and ACCESS regression coefficients, respectively. (f-h) as (a-c), but using all fields from the ACCESS 1979-2008Clim experiment. Regions of interest east of 143°E [e.g. O_{SLP} in (a)] are labelled for use in the text and define the regions used in Fig. 3.4. Label conventions are described in Section 3.4.

Our analysis indicates that SLP and component wind anomalies can explain approximately 30-50% of the spring rainfall variance in much of east Australia (Fig. 3.3d). The explained variance shown in Fig. 3.3d is the upper limit of influence that any large-scale climate mode (e.g. ENSO) could have on rainfall by modifying SLP and/or wind anomalies. Indeed, the explained variance is equal or greater than that found using the leading large-scale climate mode (e.g. ENSO, Indian Ocean Dipole, atmospheric blocking) in each location of Australia (Risbey et al., 2009b). Thus ENSO alone shows roughly the same spatial structure as Fig. 3.3d, but explains only about 14-32% of the rainfall variance (Fig. 3.2a) in contrast to the 30-50% explained by SLP and component wind anomalies.

To test the performance of the ACCESS model, we calculated the multiple linear regression analysis just described using the 1979-2008 climatological control simulation, which showed a similar explained variance to the observed (c.f. Fig. 3.3e and Fig. 3.3d). The model was able to simulate the large region of strong meridional wind coherence with rainfall, similar to the observations. However, the model showed a greater emphasis on zonal wind and less on SLP in the south of Australia. This difference could be due to reduced orographic effects, or the strong mean wind model bias in this region (Fig. 3.1d). These results show that the ACCESS model is able to produce similar circulation-rainfall relationships to the observed, but there are some deficiencies that may have implications on the modelled results.

The regions that are not shaded grey in Fig. 3.3a-c and Fig. 3.3f-h are those where different characteristics of the local circulation are important for rainfall. However, these local characteristics might be associated with a large-scale circulation feature that is also associated with rainfall. This large-scale circulation could be useful for comparison to the circulation associated with El Niño events. To elucidate this, we regressed SLP, and 850 hPa

wind, onto three different regional time series of spatial mean east Australian rainfall defined using those regions most closely associated with either SLP (subscript "SLP"), zonal wind (subscript "U"), or meridional wind (subscript "V") as shown in Fig. 3.3, and east of 143°E. This was performed for both observations (Fig. 3.4a-c) using the regions in Fig. 3.3a-c (labels with an "O" prefix), and for ACCESS (Fig. 3.4d-f) using the regions in Fig. 3.3f-h (labels with an "A" prefix). Generally, for all regions in east Australia (i.e. all rainfall time series), less rainfall than average is associated with significantly positive SLP anomalies in northwest Australia and significantly negative SLP anomalies to the southeast of Australia in the vicinity of New Zealand (roughly 53°S, 165°E, Fig. 3.4). Changes in location of these negative and positive SLP anomalies govern changes in SLP and wind anomalies in different regions of east Australia, which are then associated with rainfall (Fig. 3.4). This is true for both observations and ACCESS, and will be further discussed in the following subsections.

Our analysis agrees with previous studies (e.g. Cai et al., 2011b; McIntosh and Hendon, 2018), which suggested that the El Niño related positive SLP anomaly to the south of Australia (Fig. 3.2b) can influence southeast Australian rainfall. A positive SLP anomaly centred on the coast, west of the Mallee region is evident in the regression with O_{SLP} rainfall (Fig. 3.4a), however, rainfall outside of the O_{SLP} region (i.e. rainfall in the O_U and O_V regions) appears unrelated to SLP (Fig. 3.4 b and c). The limited relationship between east Australian rainfall and SLP to the south of Australia could be a reason why ENSO explains a limited portion of the observed variance in east Australian rainfall compared to the circulation diagnostics (c.f. Fig. 3.2a and Fig. 3.3d). Furthermore, the significant relationship between a negative SLP anomaly in the vicinity of New Zealand to a decrease in east Australian rainfall (Fig. 3.4) could further lessen the influence of ENSO to east Australian rainfall, as this region of SLP is largely not significantly related to ENSO (Fig. 3.2b).

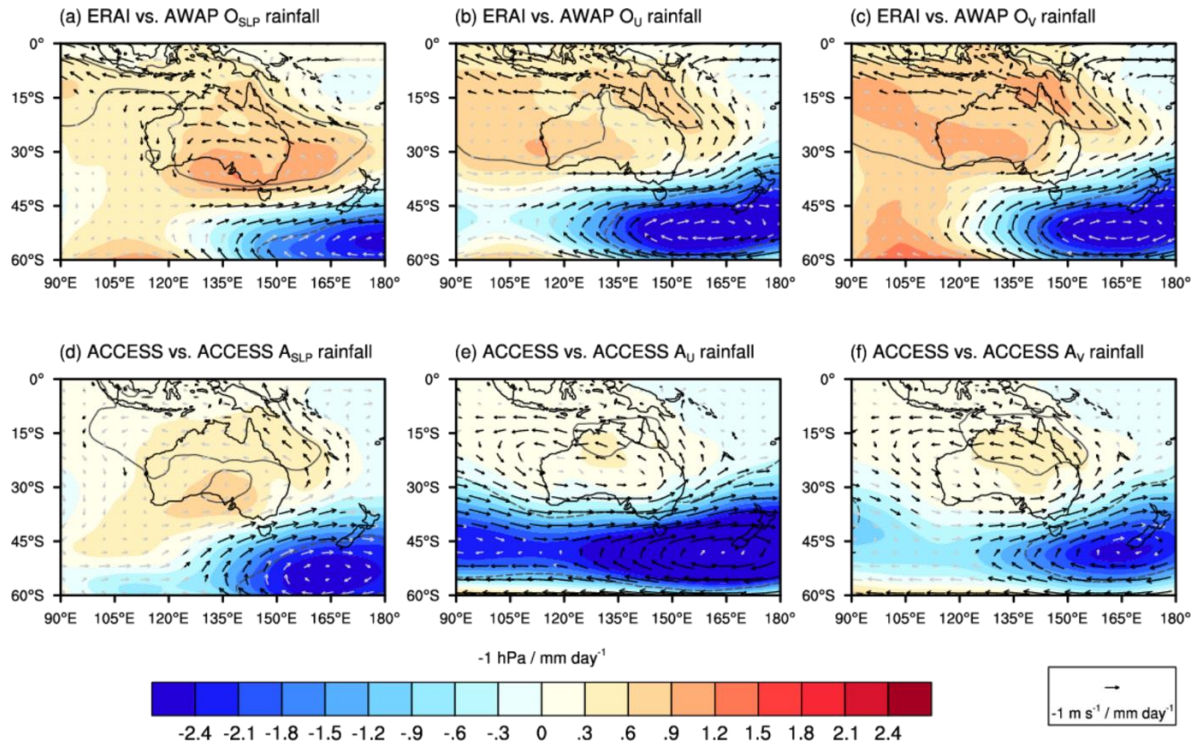

Fig. 3.4: Regressions of ERA Interim SLP and 850 hPa winds versus spatial mean rainfall time series east of 143°E and the region (a) O_{SLP}, (b) O_U, and (c) O_V, defined in Fig. 3.3a, Fig. 3.3b, and Fig. 3.3c, respectively. (d-f) as (a-c), but using SLP, 850 hPa winds and rainfall from the ACCESS 1979-2008Clim experiment, with the regions A_{SLP}, A_U, and A_V, defined in Fig. 3.3f, Fig. 3.3g, and Fig. 3.3h, respectively. All regressions have been multiplied by -1 to show conditions associated with less than average rainfall. Plotting conventions as described in Fig. 3.2b.

3.4.1 East Australian rainfall and SLP

In southeast Australia (O_{SLP} region), local positive SLP anomalies are more strongly related to a springtime rainfall deficit than local wind direction (Fig. 3.3a). The large-scale circulation associated with rainfall in this region shows a widespread SLP anomaly over most of Australia (Fig. 3.4a). The location of this SLP anomaly is in a similar location to the mean subtropical ridge (Fig. 3.1c), the intensity of which has been shown to have a significant relationship with

rainfall in southeast Australia (Cai et al., 2011a; Timbal and Drosdowsky, 2013). The ACCESS model was not able to simulate the SLP-rainfall relationship to the same spatial extent as in the observations (i.e. the region of A_{SLP} is smaller than the region of O_{SLP}, c.f. Fig. 3.3 f and a). Despite this, the widespread simulated circulation associated with rainfall in A_{SLP} shows a similar pattern to ERAI (c.f. Fig. 3.4 d and a).

3.4.2 East Australian rainfall and zonal wind

Along the eastern coast of the southern half of Australia (O_U region), zonal wind is more related to rainfall than SLP or meridional wind, where westerly winds are associated with less rainfall (Fig. 3.3b). The O_U region shows large rainfall totals in SON compared to other regions of Australia, which can largely be attributed to orographic effects caused by the mountains of the Great Dividing Range that extends just inland along the east coast (Fig. 3.1a). Easterly onshore winds result in uplift of moisture rich maritime air when it comes in contact with the eastern side of the range, whereas drier westerly winds from the continental interior are uplifted on the western side of the range, leading to even drier air being advected to the eastern side of the range. Rainfall on the eastern side of the range has historically shown a weak relationship with ENSO, although it strengthens in the southern regions (Fig. 3.2a). Northern Victoria and southern New South Wales, just east of the Mallee region, also show a strong relationship between rainfall and zonal wind; the reason for this is not easily explained. However, this region exhibits weaker regression coefficients compared with other areas of east Australia, and shares a similar magnitude between SLP and both components of 850 hPa wind, suggesting processes less related to the circulation could be more important for rainfall in this region.

The large-scale circulation associated with rainfall in the O_U region shows the negative SLP anomaly in the vicinity of New Zealand extending further west than for rainfall in the O_{SLP} and O_V regions (cf. Fig. 3.4 b, a and c). This extension of the negative SLP anomaly results in a more zonally oriented wind anomaly over the southeast coast of Australia (Fig. 3.4b). In the region to the south of Australia, where there is a significant positive regression between SLP and ENSO (Fig. 3.2b), O_U rainfall and SLP are not significantly related (Fig. 3.4b). The incoherence between O_U rainfall and SLP in this region to the south of Australia could be a reason that ENSO is not able to exert a greater relationship with rainfall along the east coast of Australia.

The ACCESS model performs well in reproducing the large-scale winds associated with rainfall seen in observations (c.f. Fig. 3.4 b and e), despite ACCESS showing a larger spatial extent of rainfall – zonal wind coherence than observed (c.f. Fig. 3.3 g and b). However, discrepancies were seen in the simulated large-scale negative SLP anomaly in the vicinity of New Zealand, which zonally extends further west than observed and also simulates a weaker positive SLP anomaly over northern Australia (c.f. Fig. 3.4 e and b).

3.4.3 East Australian rainfall and meridional wind

In the remainder of east Australia (O_V region), meridional winds have the strongest relationship to rainfall when compared to SLP and zonal wind, with southerly wind anomalies associated with a rainfall deficit in this region (Fig. 3.3c). This is likely due to the availability of moisture-rich air masses from the tropics described in other studies (Whetton, 1988; Theobald et al., 2015). This region is distinct in terms of its ENSO relationship, with ENSO phases only associated with changes to the frequency of daily rainfall events, whereas daily rainfall frequency and intensity are associated with ENSO further south (Pui et al., 2012).

ENSO is also significantly related to meridional wind anomalies throughout east Australia (Fig. 3.2b), suggesting that it is the ENSO induced change in meridional winds that could drive the ENSO-rainfall relationship in the O_V region.

As for the O_U case, the large-scale circulation associated with rainfall in the O_V region does not show a significant positive SLP anomaly to the south of Australia as seen in Fig. 3.2b (Fig. 3.4c). This indicates that the ENSO related SLP anomaly to the south of Australia is not important for rainfall in the central and northern regions of east Australia. The large-scale circulation that is significantly related to O_V rainfall again shows a negative SLP anomaly in the vicinity of New Zealand, but also a positive anomaly over northeast Australia (Fig. 3.4c). A similar anomalous SLP structure is seen related to ENSO (Fig. 3.2b), indicating that it is through these SLP anomalies that that ENSO could influence east Australian rainfall.

The ACCESS model performs well in simulating the spatial extent of rainfall – meridional wind coherence (i.e. the regions of O_V are similar to A_V, Fig. 3.3 h and c, respectively), and the rainfall related large-scale circulation (c.f. Fig. 3.4 f and c). However, as seen with the modelled regressions using A_U rainfall (Fig. 3.4e), the negative SLP anomaly extents too far west compared to observed (c.f. Fig. 3.4 f and c), but in this case the westward extension did not show a significant relationship with A_V rainfall (Fig. 3.4f).

3.5 Processes influencing Australian spring rainfall during the three strong El Niño events

In the previous section, we examined the relationship between the local circulation and rainfall in east Australia. Using those relationships, we now examine the role of the regional

atmospheric circulation in producing the different east Australian rainfall anomalies that were observed during the three strong El Niño years of 1982, 1997 and 2015. In this section we examine SLP, humidity, and wind anomalies during austral spring in ERAI and the 60-member ensemble mean of the ACCESS atmospheric general circulation model.

When forced with 1979-2008 climatological SSTs, the model simulated a median east Australian spring rainfall rate of 1.51 mm/day, which is comparable to the AWAP data of 1.43 mm/day (Fig. 3.5). As a comparison to other models, the ACCESS 1.3 atmosphere model ranked in the top 11 % of CMIP5 models forced with time-varying 1979-2008 SSTs for simulating an SON mean daily rainfall rate in southeast Australia closest to that observed (using model data from Section 2, not shown). One notable difference between our climatological simulation and the observed east Australian rainfall is the inability for the model to accurately simulate spring seasons with low rainfall, i.e., the modelled 5th percentile is comparable to the observed 25th percentile. This model bias is common, in that models tend to drizzle more often than is observed (Stephens et al., 2010). Another factor could be that this experiment lacked time varying SSTs, which has been shown to reduce regional rainfall variance due to a lack of forcing from large magnitude SST anomalies (Taschetto et al., 2016). This effect was evident in the 1982 SSTs forced experiment, where the model was able to simulate the 5th and 25th percentiles with a similar rainfall value as the AWAP data, unlike the 1979-2008 climatological control (Fig. 3.5).

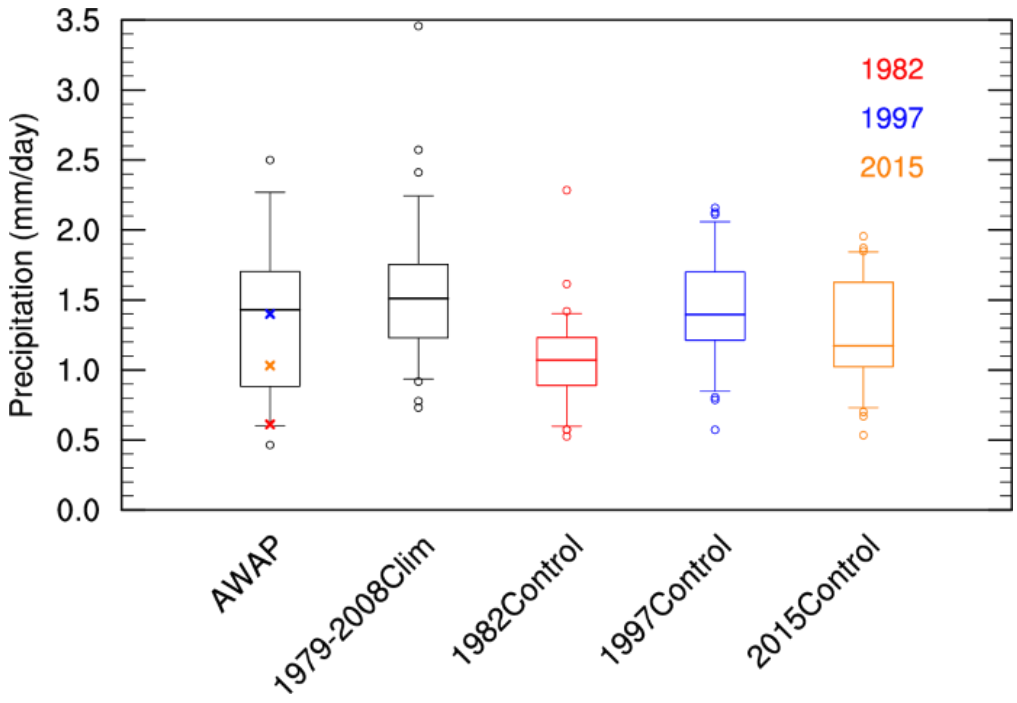

Fig. 3.5: Box and whisker plots of spatial mean SON precipitation in eastern Australia (as depicted in Fig. 3.1a) for the AWAP dataset from 1979-2008; the ACCESS 1979-2008 mean SST climatology experiment; and the 1982, 1997, 2015 SST experiments. The centre bars show the median, the boxes outline the interquartile range, and the whiskers show the 5th and 95th percentile ranges, with circles showing the remaining values. The years 1982, 1997 and 2015 in the AWAP dataset are also shown by red, blue and orange crosses, respectively.

The model median east Australian spring rainfall of each of the three experiments forced with SSTs during the three El Niño events captured the ranking of the three events seen in the AWAP data. The model median rainfall for the 1997 experiment was just below the climatological control median with 1.40 mm/day, followed by 2015 with 1.17 mm/day and finally 1982 simulated a median of 1.07 mm/day (Fig. 3.5). All three El Niño experiments showed a suppression of high seasonal-mean daily rainfall rates compared to the climatological run and AWAP data. This was most evident in the 1982 experiment with over 95% of the 1982 SON realisations falling below the median values for the climatological

control. This highlights the large role that SSTs had in reducing east Australian rainfall during spring of 1982.

In the following subsections we will analyse what influence SSTs from all three El Niño events had on east Australian rainfall, SLP, and 850 hPa humidity and winds. Note that all three simulated years showed significantly greater than climatological rainfall in different regions of Western Australia, which was generally not seen in the observations to the same extent (Fig. 3.6). As Western Australia has historically shown a relatively weak relationship with ENSO events during spring (Fig. 3.2a), we do not focus on this region.

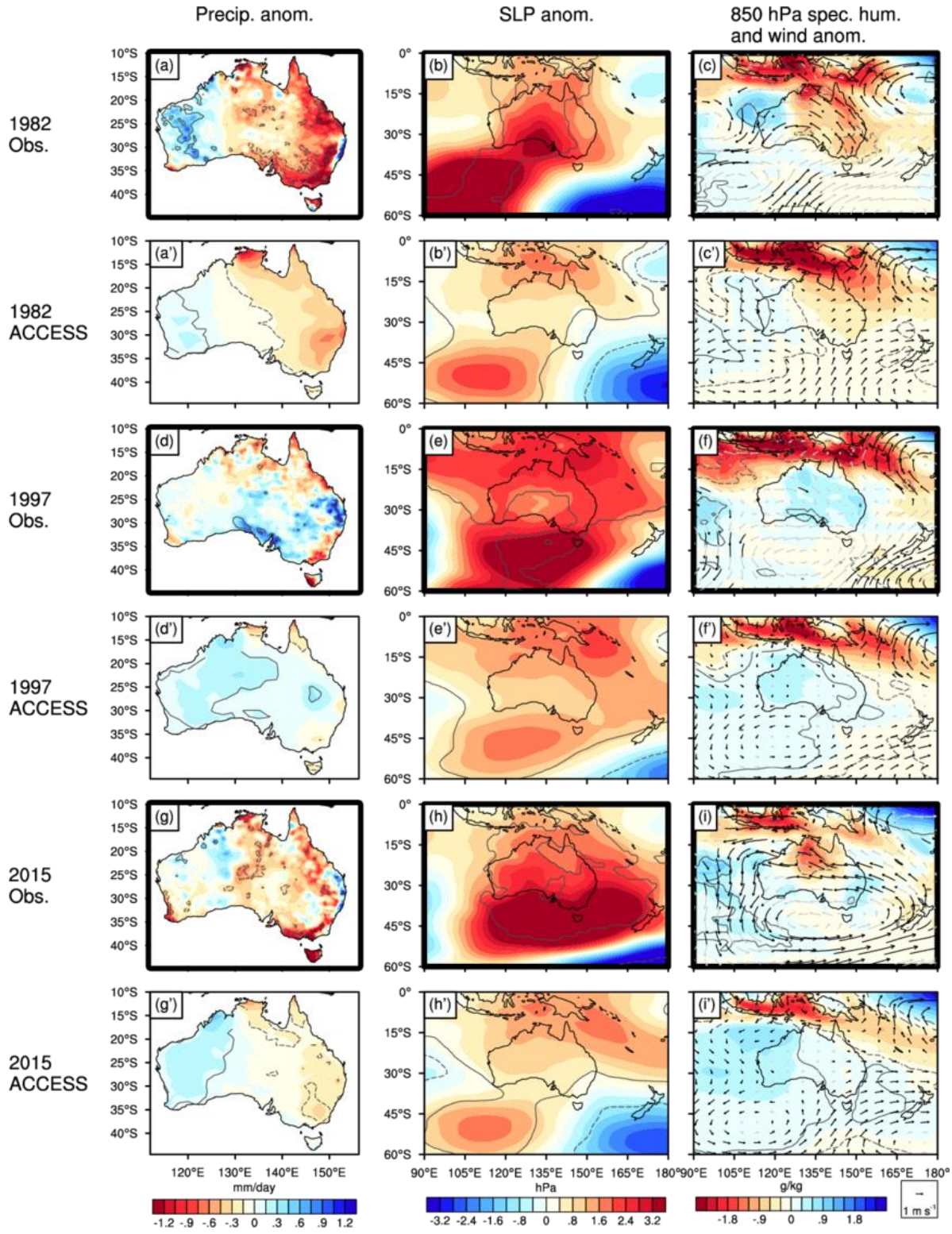

Fig. 3.6: Spring anomalies for observed and modelled (left column) precipitation, (middle column) sea level pressure, and (right column) 850 hPa humidity and wind. Rows with bold panel borders indicate the observed anomalies for (top) 1982, (middle) 1997 and (bottom) 2015. The rows with thin panel borders, and with an added apostrophe to each panel letter,

show the respective ACCESS anomalies. The observed fields use AWAP for precipitation and ERA Interim for sea level pressure, humidity and wind. The solid and dashed grey contours indicate significant positive and negative shading values, respectively. Black vectors indicate significant wind anomalies. Significant values are defined as the 5th and 95th percentiles for observations, and the 0.05 p-value using Student's two-sided t-test for ACCESS.

3.5.1 The 1982 El Niño event

In 1982, spring rainfall was far below average in much of east Australia (Fig. 3.6a). This generally agreed with what could be expected given the historical relationship between ENSO and Australian rainfall (McBride and Nicholls, 1983). The observed circulation over Australia during this event showed a strong, positive SLP anomaly extending southeast of Western Australia (roughly 50°S, 105°E) into the central southern coast of Australia (roughly 35°S, 130°E), and negative SLP anomalies to the southeast (centred at 55°S, 165°E) and northeast of Australia (roughly 13°S, 175°E, Fig. 3.6b). These SLP anomalies induced a southeasterly wind anomaly throughout much of east Australia (Fig. 3.6 b and c), coincident with a moisture deficit (Fig. 3.6c). The observed rainfall deficit was consistent with the relationships of southerly wind anomalies with O_V rainfall, and positive SLP anomalies with O_{SLP} rainfall, previously described in Fig. 3.3c and Fig. 3.3a, respectively. Likewise, an anomalously easterly component of the zonal wind was associated with slightly increased rainfall in a region east of the Great Dividing Range (Fig. 3.6a), as per the relationship between rainfall and zonal wind in this region (O_U, Fig. 3.3b).

The ensemble mean of the atmosphere model experiment forced with 1982 SSTs captured the patterns of rainfall and SLP anomalies of the 1982 atmospheric circulation, but they were weaker than the AWAP anomalies (Fig. 3.6 a' and b'). Also, the model erroneously simulated a widespread positive SLP anomaly to the north of Australia (centred 10°S, 135°E), extending southeast just off the northeast coast, which in turn impacted the simulated 1982 winds (Fig. 3.6 b' and c'). This resulted in significant southwesterly wind anomalies situated over east Australia, with southeasterly wind anomalies located further east than in ERAI (Fig. 3.6 c and c'). The lack of an anomalous easterly component of the wind in the model ensemble mean coincided with a lack of positive rainfall anomalies along the central east coast (Fig. 3.6 a' and c'), as per the observed and modelled relationship (O_U and A_U in Fig. 3.3 b and g, respectively). Throughout east Australia the simulated wind anomalies corresponded with a weak, although still significant, decrease in simulated moisture over east Australia (Fig. 3.6c'). This may explain why the simulated mean rainfall anomalies were not as low as observed. However, it is likely that stochastic influences played some role as the model forced with 1982 SSTs was able to simulate a spring mean rainfall lower than observed in 1982 (Fig. 3.5).

3.5.2 The 1997 El Niño event

The springtime east Australian rainfall during the 1997 El Niño was unusual based on the strength of the event. Less than average spring rainfall could have been likely in east Australia during 1997 given the historical relationship between ENSO and rainfall. What was observed, however, was close to average east Australian spring rainfall (Fig. 3.5), with some locations near the central eastern coast receiving substantially above average rainfall in 1997 (Fig. 3.6d). Eastern Australia experienced an almost spatially uniform increase in spring SLP by about 2 hPa. This type of response is considered typical of an El Niño and is normally

attributed to the western pole of the Southern Oscillation. The increase in mean SLP across the continent was seemingly the combination of significant positive SLP anomalies to the north and south of Australia, and an eastward displacement of the negative SLP anomaly to the south of New Zealand compared to the 1982 event (Fig. 3.6e). Anomalously positive SLP in the northern and southern tips of eastern Australia is associated with less than average rainfall there (see Fig. 3.3a), as was observed in 1997 (Fig. 3.6d).

In response to the almost spatially uniform SLP anomaly during spring of 1997, almost no substantial wind anomalies were observed over eastern Australia (Fig. 3.6f). Winds are historically more closely associated with rainfall variability in central and north eastern Australia compared to SLP (O_U and O_V, Fig. 3.3 b and c, respectively). With no major wind anomalies during 1997, the expectation would be for no significant rainfall change, as was observed (Fig. 3.6d). In agreement with the weak wind and rainfall anomalies, there were also no statistically significant changes to moisture over the continent (Fig. 3.6f), which produced conditions favourable for near average rainfall over central-eastern Australia.

A previous study suggested the springtime rainfall and circulation anomalies in 1997 were primarily caused by internal stochastic variability (Walland, 1998). However, the model ensemble mean was able to reproduce many characteristics of the observed pattern, suggesting that a significant component of the near-normal rainfall was likely induced by SST forcing (Fig. 3.6 d'-f'). The simulated positive SLP response extending to the north of Australia – which was spuriously simulated in 1982 simulations – is more closely aligned with the reanalysis in 1997 (c.f. Fig. 3.6 e and e'). Furthermore, the SLP anomalies simulated with 1997 SSTs are stronger than those simulated with 1982 SSTs (and 2015 SSTs, which will be described in Section 3.5.3, c.f. Fig. 3.6 e', b' and h'). This suggests that although the model may have

difficulty simulating the observed SLP response extending to the north of Australia in other strong El Niño years, the impact of SSTs in 1997 was strong enough to overcome the apparent model bias in this region.

3.5.3 The 2015 El Niño event

The 2015 El Niño event saw spring rainfall anomalies similar to that expected from the historical ENSO-east Australian rainfall relationship, with less than average rainfall observed in much of eastern Australia (Fig. 3.6g). However, the rainfall deficits were not as large or as significant as in 1982. The 2015 event was associated with a strong positive SLP anomaly centred over Tasmania, extending from south of the western coast of Australia to New Zealand, encompassing southeast Australia (Fig. 3.6h). The negative SLP anomaly to the south of New Zealand was displaced further to the southeast than in the 1997 event (Fig. 3.6h), which would have disrupted the typical rainfall-related circulation seen in Fig. 3.4 b and c. The positive SLP anomaly to the south of Australia induced significant easterly wind anomalies over eastern Australia (Fig. 3.6i), corresponding with a slight increase in moisture and rainfall along the east coast (Fig. 3.6 g and i). A significant rainfall deficit in southeastern Australia was consistent with positive SLP anomalies there (Fig. 3.6 g and h), as per the SLP-rainfall relationship in the O_{SLP} region (Fig. 3.3a). The lower-than-average rainfall over the remainder of eastern Australia was not clearly associated with the wind and SLP relationships shown in Fig. 3.3. Lower-than-average rainfall in the O_V region is associated with southerly wind anomalies (Fig. 3.3c). However, the spring of 2015 was dominated by easterly anomalies, with only a weak meridional wind anomaly component. The weak meridional wind anomaly could have been associated with the weak rainfall anomalies, but it is also possible that other processes were associated with rainfall in this region during spring of 2015.

Similar to what was observed, the model ensemble mean showed less rainfall than average throughout much of eastern Australia. However, the model was not able to simulate some fine-scale features of rainfall that were observed in the AWAP data. These included the positive rainfall anomalies observed along the east coast (roughly the O_U region) and significant negative anomalies observed along the southeast coast (roughly the O_{SLP} region, Fig. 3.6 g and g'). The inability of the model to simulate these rainfall features was associated with model ensemble mean SLP, wind and humidity anomalies that differed from the reanalysis. The expansive positive SLP anomaly that encompassed southern Australia in 2015 is not evident in the model ensemble mean (c.f. Fig. 3.6 h and h'); instead the simulated mean position of the positive SLP anomaly was similar to 1982, with a strong negative SLP anomaly to the south of New Zealand (c.f. Fig. 3.6 b' and h'). As a result, westerly and southwesterly wind anomalies were simulated over eastern Australia, but, unlike 1982, there was no significant change in moisture availability (c.f. Fig. 3.6 c' and i'). Thus, either the model simulated the observed east Australian rainfall anomalies with a different circulation to the observed, or a process unrelated to the circulation, but related to 2015 SSTs, was more important for rainfall during this event.

Focusing on the circulation, the difference between the ACCESS and ERAI SLP anomalies during 2015 raises two possibilities. Either ACCESS is not capable of simulating the observed response (due to model deficiencies or experimental design), or the SST-forced positive SLP anomalies in 2015 were modified by a stochastic atmospheric process unrelated to SSTs (i.e. atmospheric internal variability). ACCESS performed well in simulating the 1982 and 1997 SLP anomaly patterns (Fig. 3.6 b' and e'), showing that the model is capable of simulating observed anomalies when forced with observed SSTs. Furthermore, the simulated SLP anomaly patterns between the 1982 and 2015 events were similar (Fig. 3.6 b' and h'), showing

that the model forced with 2015 SSTs simulated a similar pattern to another strong El Niño event. This suggests the model can perform well with similar SST forcing, however, our experiment design excludes observed 2015 greenhouse gas and aerosol concentrations which may have contributed to the observed SLP anomaly in SON 2015.

If the observed SLP anomaly in 2015 was modified by a stochastic process unrelated to SSTs, it may be possible for ACCESS to simulate an SLP anomaly similar to the observed in an individual ensemble member. Here we show the zonal mean SLP in the region of the observed 2015 SLP anomaly (110°E –170°E) for ERAI and all realisations of the ACCESS experiments (Fig. 3.7). Out of the 60 realisations forced with 2015 SSTs, ACCESS failed to simulate a zonal SLP anomaly closely resembling that observed in 2015, but did simulate some similar features, now described. The model simulated zonal SLP anomalies 1.5 – 2 hPa weaker than observed in the same location, and simulated zonal SLP anomalies of similar strength to that observed 3° – 10° further south. The model was able to simulate a zonal SLP anomaly almost identical to that of 2015, but only when forced with 1997 SSTs. Overall, this suggests that the SLP anomaly observed in 2015 was an unusual event, and with enough realisations it may be possible for the model to simulate a similar SLP anomaly when forced with 2015 SSTs. However, as it stands now, the ACCESS model appeared to suffer from a bias when simulating the observed positive SLP anomaly.

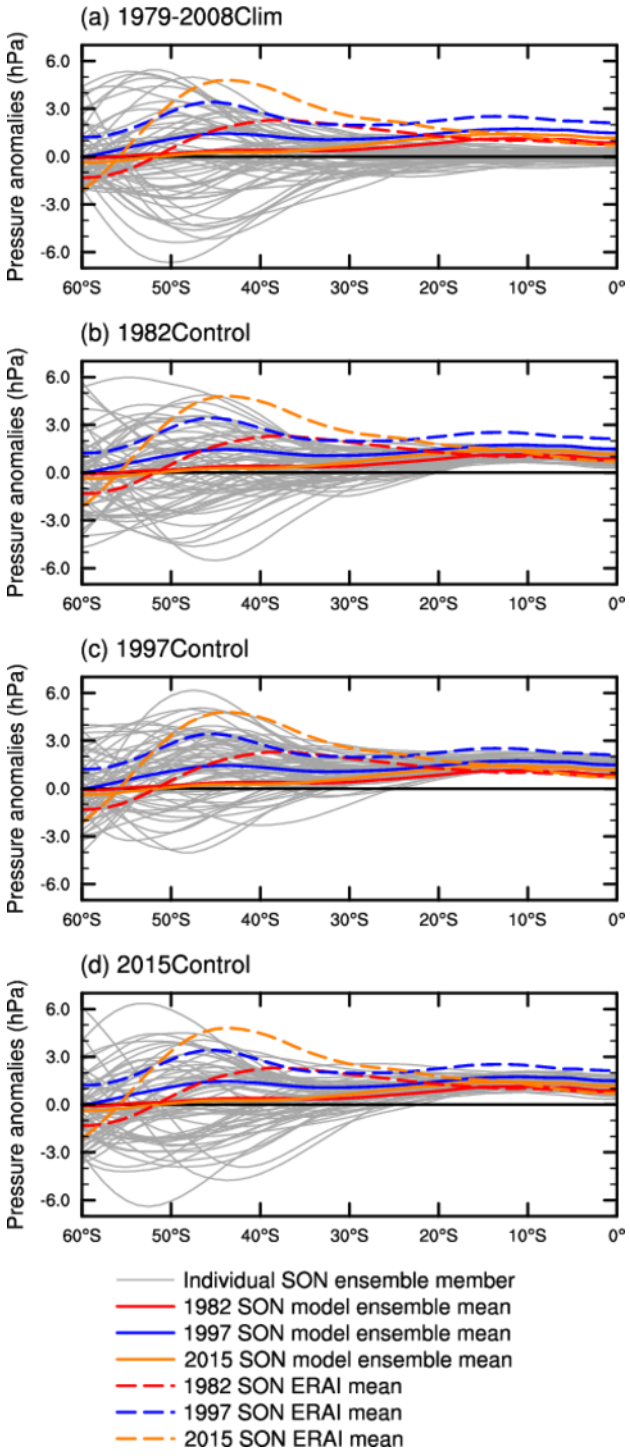

Fig. 3.7: Zonal mean sea level pressure anomalies from 110°-170°E during spring. The coloured dashed and solid lines show ERA Interim anomalies and ACCESS model ensemble mean anomalies, respectively. Red, blue and yellow show 1982, 1997, and 2015, respectively. The grey lines show the individual realisations of (a) the 1979-2008 control, (b) the 1982, (c) the 1997, and (d) the 2015 experiments.

3.6 The role of local SSTs on Australian spring rainfall during strong El Niño events

3.6.1 SST off the northeast coast of Australia

Chapter 2 (van Rensch et al., 2015) hypothesised that the SSTs to the northeast of Australia around the Coral Sea had a modulating role on the ENSO – southeast Australian rainfall teleconnection. Using partial correlations on observed and modelled data Chapter 2 suggested that the cool SSTs to the northeast of Australia in 1982 contributed to reduced rainfall in southeast Australia, whereas the near average SSTs in the same region in 1997 contributed to near average rainfall. In this section we test the hypothesis of Chapter 2 by using results from targeted model simulations where SSTs to the northeast of Australia were swapped between the three strong El Niño events. These experiments will allow us to determine the contribution that this region of SSTs had on east Australian rainfall during these strong El Niño events. We swapped the SSTs rather than using an idealised strong El Niño SST composite (e.g. Frauen et al., 2014), because we did not want to smooth the SST in regions remote from the tropical Pacific, as these regions may also have an influence on Australian rainfall. This way we know any changes seen in the experiments are due to the change in northeast Australian SSTs and not due to an absence of another SST anomaly.

The introduction of 1982 SSTs to the northeast of Australia in the 1997 and 2015 simulations resulted in a 17-19% reduction of median east Australian spring rainfall compared to their respective control runs (Fig. 3.8). These results support the hypothesis described in Chapter 2 (van Rensch et al., 2015) that local SST patterns strongly contributed to the severely reduced rainfall in eastern Australia in 1982. When the 1982 SSTs to the northeast of Australia were

patched into global 1997 SSTs, the median east Australian spring rainfall reduced from 1.40 mm/day in the 1997 control experiment to 1.14 mm/day. For the experiment where 1982 SSTs were patched into global 2015 SSTs, the median rainfall rate was 0.97 mm/day, lower than the median rainfall of even the 1982 control experiment (Fig. 3.8).

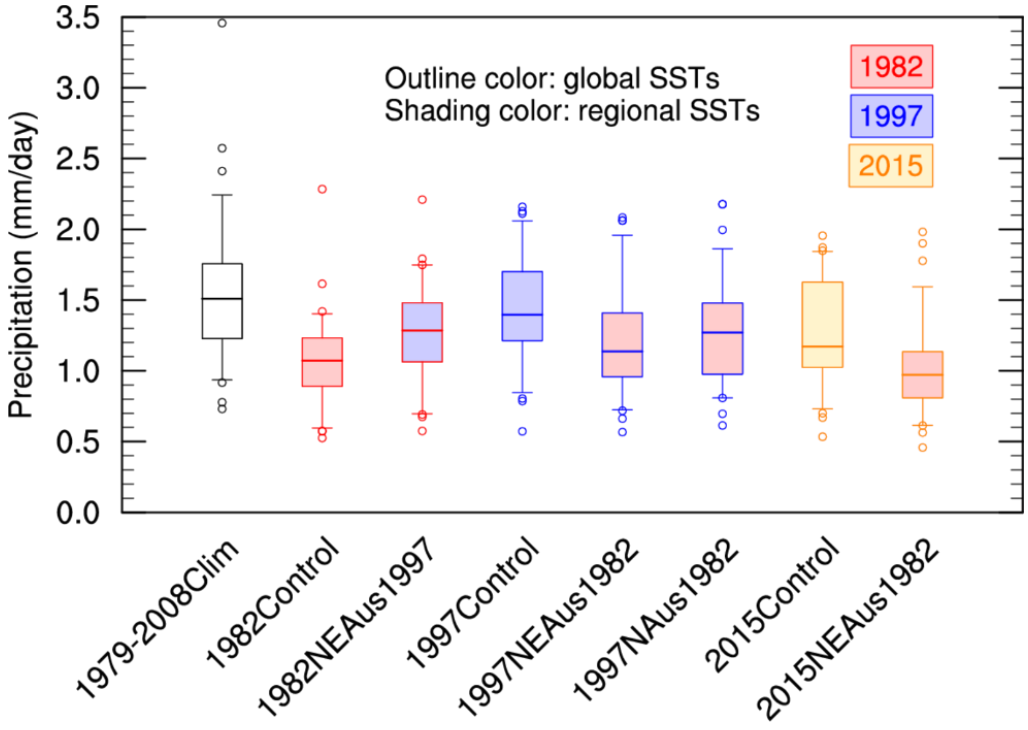

Fig. 3.8: As Fig. 3.5, but for the 1979-2008 mean SST climatology experiment; the 1982, 1997, 2015 SST experiments; and the swap experiments: global 1982 SST with 1997 SST to the northeast of Australia (1982NEAus1997), global 1997 SST with 1982 SST to the northeast of Australia (1997NEAus1982), global 2015 SST with 1982 SST to the northeast of Australia (2015NEAus1982), and global 1997 SST with 1982 SST to the north of Australia (1997NAusLE1982). The colour of the box and whisker outline indicates the year of global SSTs used in the experiment, with shading inside the box indicating the year of the SSTs in the swapped region.

Conversely, patching the 1997 SSTs to the northeast of Australia, with 1982 SSTs elsewhere, resulted in a 21% increase in median east Australian spring rainfall compared to the 1982

control experiment. However, the value of 1.29 mm/day is still drier than the 1997 control experiment. Thus, the model shows that the SSTs to the northeast of Australia can contribute between 17 % and 21 % of the rainfall change during these strong El Niño events.

The SSTs to the northeast of Australia largely influenced simulated Australian rainfall locally in the northeast of the country (Fig. 3.9 a-c), with little influence in the southeast as described in Chapter 2 (van Rensch et al., 2015). When the cooler 1982 SSTs to the northeast of Australia are patched into global 1997 SSTs, significantly less near-surface moisture was simulated around the swapped region and extended into northeast Australia (Fig. 3.9d). The opposite is true for the reverse experiment, where near average 1997 SSTs to the northeast of Australia simulated more moisture when patched into global 1982 SSTs (Fig. 3.9e). These changes in moisture were not associated with a statistically significant change in the circulation (Fig. 3.9d and Fig. 3.9e), suggesting that the SSTs to the northeast of Australia influence rainfall through a moisture availability process. The moisture availability process works by SSTs controlling evaporation of moisture to the atmosphere above it, this moisture is then transported over land through sub-seasonal anomalous flow, influencing local rainfall producing systems (e.g. Brown et al., 2009).

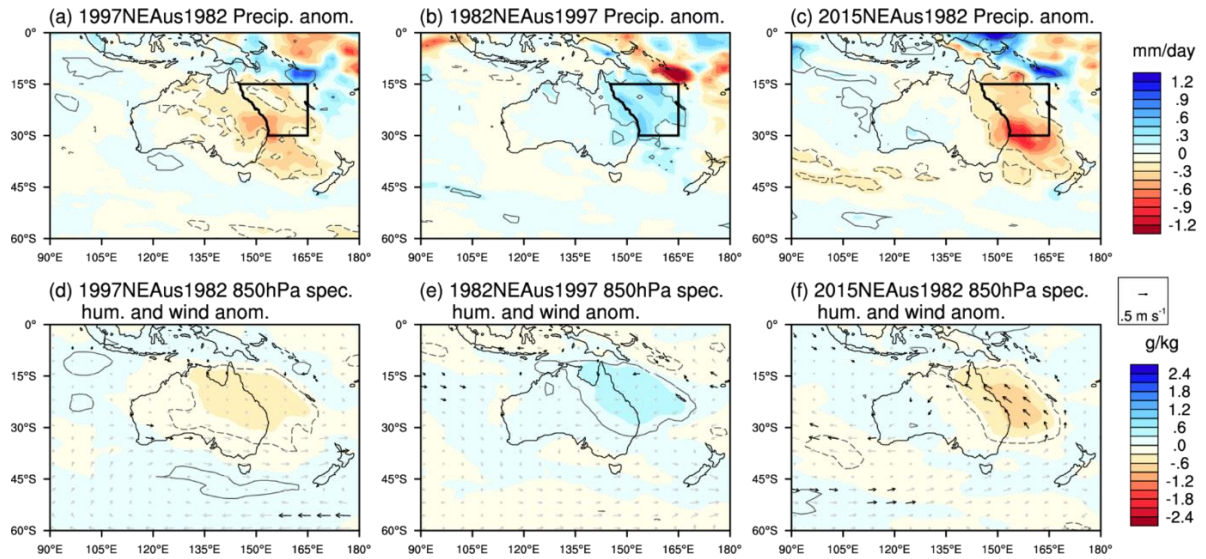

Fig. 3.9: The influence of SSTs to the northeast of Australia in the ACCESS atmosphere model. (a) Precipitation anomalies from the experiment forced with 1997 SSTs globally with 1982 SSTs to the northeast of Australia, relative to the 1997 control experiment. (b) Precipitation anomalies from the experiment forced with 1982 SSTs globally with 1997 SSTs to the northeast of Australia, relative to the 1982 control experiment. (c) Precipitation anomalies from the experiment forced with 2015 SSTs globally, with 1982 SSTs to the northeast of Australia, relative to the 2015 control experiment. (d-e) as (a-c), respectively, but showing 850 hPa specific humidity and wind anomalies. Similar plotting characteristics were used for the respective plots in Fig. 3.6, only the reference wind vector is halved. The region where the SSTs were swapped is outlined by bold in a-c.

When the cooler 1982 SSTs off the northeast of Australia is patched into the global 2015 SSTs, significant southeasterly wind anomalies were simulated over the region compared to the 2015 control (Fig. 3.9f). This was in addition to changes in moisture availability (Fig. 3.9f). The additional dynamical response simulated in this experiment does not enhance the east Australian rainfall reduction above those from the companion experiment that used global 1997 SSTs (Fig. 3.8; -17% in the 2015NEAus1982 experiment versus -19% in the 1997NEAus1982 experiment). The lack of additional rainfall response associated with a change in circulation suggests that northeast Australian SSTs mainly influence east Australian

rainfall through changes to moisture availability, rather than via changes in atmospheric circulation.

3.6.2 SST to the north of Australia

Chapter 2 (van Rensch et al., 2015) also investigated the link between SSTs directly to the north of Australia around the Maritime Continent and rainfall in southeast Australia, but that chapter showed that this region did not have as strong an influence as the SSTs to the northeast of Australia. However, previous studies have shown that this region has a significant relationship with southeast Australian rainfall during the cooler months of the year (Nicholls, 2010; Watterson, 2010; Timbal and Hendon, 2011). Here we investigate the effect of the significantly cool 1982 SSTs to the north of Australia if they had happened during the 1997 event. The introduction of cool SSTs off northern Australia showed a modest 9% reduction in median east Australian spring rainfall compared to the 1997 control experiment (Fig. 3.8). Compared to the 19% reduction in the companion experiment using SSTs to the northeast of Australia, this corroborates that it is the SSTs in the northeast region that is most important for regulating rainfall, as noted in Chapter 2 (van Rensch et al., 2015).

The north of Australia experiment showed significantly less rainfall than the 1997 control experiment extending from central northern Australia into central eastern Australia (Fig. 3.10a). There is evidence that rainfall was influenced by a similar moisture availability process to that of northeast Australian SSTs. This is because a region of significantly less humidity than the 1997 control was simulated over a similar region to the rainfall anomalies, but with few significant changes to the atmospheric circulation (c.f. Fig. 3.10 b and a). However, a significant circulation response was simulated over southeast Australia extending to New

Zealand in the north of Australia experiment (Fig. 3.10b), with the associated circulation reminiscent of a cyclonic Rossby wave response to thermal forcing as described by Hoskins and Karoly (1981). Comparing this experiment to the 1979-2008 climatological experiment reveals that the apparent Rossby wave train seen in the winds of Fig. 3.10b was expressed by a westward shift in the negative SLP anomaly compared to the 1997 control (c.f. Fig. 3.10d and Fig. 3.6e'). This resulted in a significant intensification of the winds in southeast Australia and a small region of significantly less rainfall compared to the 1979-2008 control (Fig. 3.10 d and c).

Based on our experiments, it appears that changes due to the moisture availability process rather than changes in circulation have a greater influence on eastern Australian rainfall (Fig. 3.8). However, this is regionally dependent, with a greater influence from the moisture availability process in the north of Australia (Fig. 3.9a and Fig. 3.10a), with areas further south being influenced by circulation changes (Fig. 3.10 b and d). These findings tend to agree with other studies showing a significant link between SST to the north of Australia and rainfall in southeast Australia (Nicholls, 2010; Watterson, 2010; Timbal and Hendon, 2011). The appearance of a dynamical response to changes in north of Australia SSTs and not to changes in northeast Australian SSTs is consistent with the finding that tropical anomalies are more efficient in inducing Rossby wave trains than subtropical anomalies (Hoskins and Karoly, 1981).

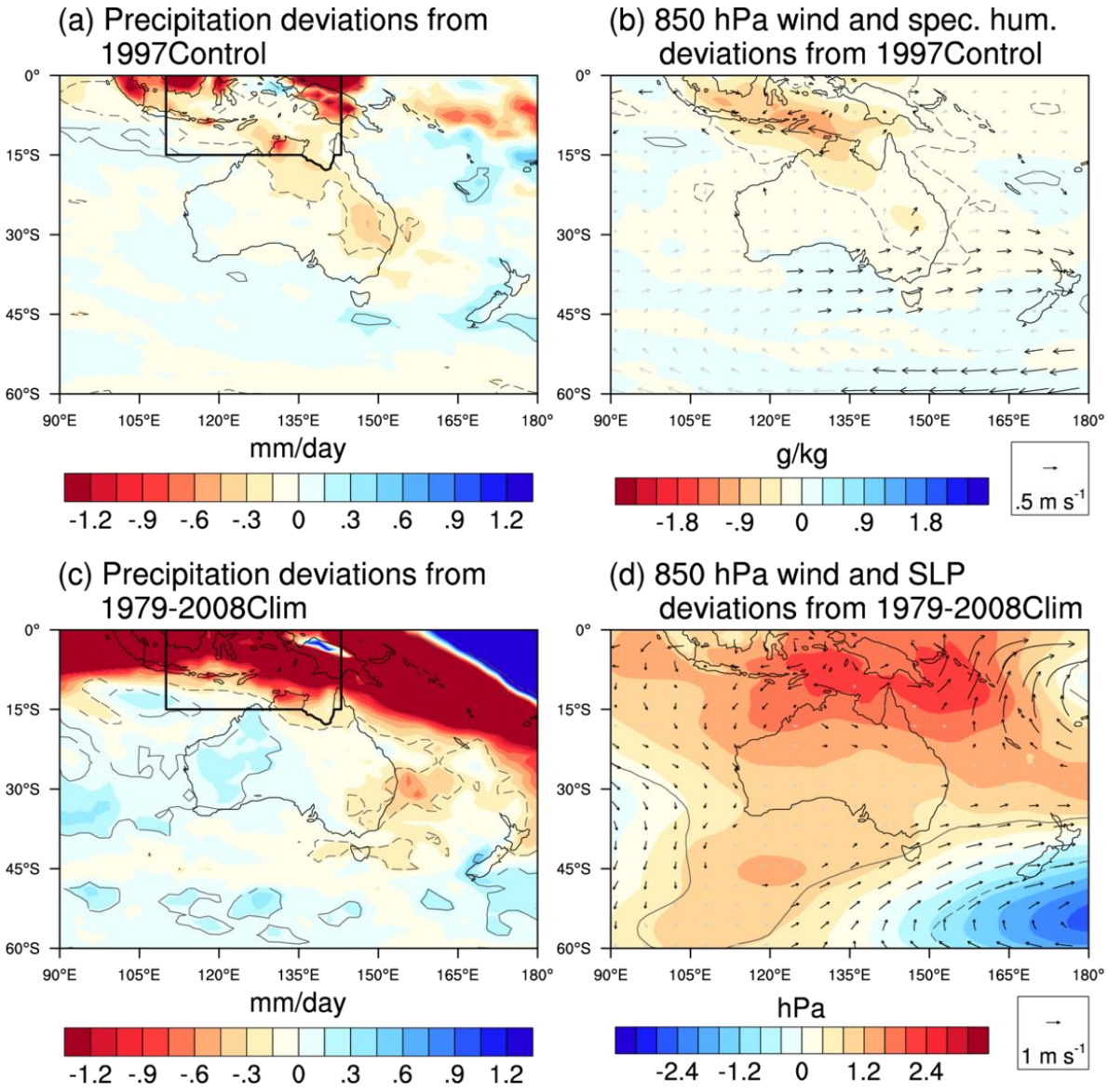

Fig. 3.10: Anomalies of the experiment forced with 1997 SSTs globally with 1982 SSTs to the north of Australia relative to (a, b) the 1997 control experiment, and (c, d) the 1979-2008 climatological control experiment. Left column shows precipitation anomalies, right column shows 850 hPa humidity and wind anomalies. Similar plotting characteristics were used for the respective plots in Fig. 3.6, only the reference vector in b is halved. The region where the SSTs were swapped is outlined by bold in a and c.

3.7 Summary and discussion

In this study we examined the influence of El Niño events on east Australian spring rainfall, with a focus on the three strongest El Niño events since 1979. The mechanism of how ENSO events influence Australian rainfall has been discussed in the literature for some time (Cai et al., 2010, 2011b; Frauen et al., 2014; King et al., 2015). We have clarified the possible mechanisms by focusing on seasonal scale circulation patterns, e.g. SLP and wind anomalies, and their relationship with local rainfall. Based on linear regression, the three strongest El Niño events might be expected to lead to a clear reduction in spring rainfall (McBride and Nicholls, 1983; Risbey et al., 2009b), however, the eastern Australian SON rainfall varied from very dry to normal. Significantly below average eastern Australian spring rainfall was recorded in 1982, near-average rainfall in 1997, and slightly below average rainfall in 2015. We used reanalysis and the ACCESS 1.3 atmospheric general circulation model to expose the different mechanisms for how El Niño can influence rainfall. We found significant SST-forced signals in the spring circulation over eastern Australia during the 1982 and 1997 El Niño events, with the SST influence on the circulation during 2015 remaining unclear.

The typical El Niño related circulation features, and the deviations experienced during the three strong El Niño events, are summarised in a schematic (Fig. 3.11). All three strong El Niño events were associated with a distinct positive SLP anomaly to the south of Australia (“H” in Fig. 3.11), with the exact location and spatial extent changing from the typical ENSO signal for all three events. Previous studies have attributed this positive SLP anomaly to an ENSO signal transmitted through the Indian Ocean (Cai et al., 2011b; McIntosh and Hendon, 2018). A negative SLP anomaly was consistently observed to the southeast of Australia near New Zealand, during the three events (“L” in Fig. 3.11), which has not been highlighted in previous

studies. This negative SLP anomaly near New Zealand shows a significant relationship with less than average rainfall throughout eastern Australia, whereas SLP in the "H" region (Fig. 3.11) shows a weak rainfall relationship. This suggests that the positive SLP anomaly associated with strong El Niño events is of less importance to eastern Australian rainfall than previously thought, with a greater influence apparently arising from the downstream negative SLP anomaly. It is important to note, however, that for the central and north eastern Australian region, rainfall is more strongly related to local wind anomalies, which may be associated to a variety of SLP anomaly positions and magnitudes in any one year. Further analysis on synoptic timescales (e.g. Risbey et al., 2009a; Theobald et al., 2015), particularly for the northeast Australian region, could improve our understanding of the sensitivity of wind and SLP to rainfall.

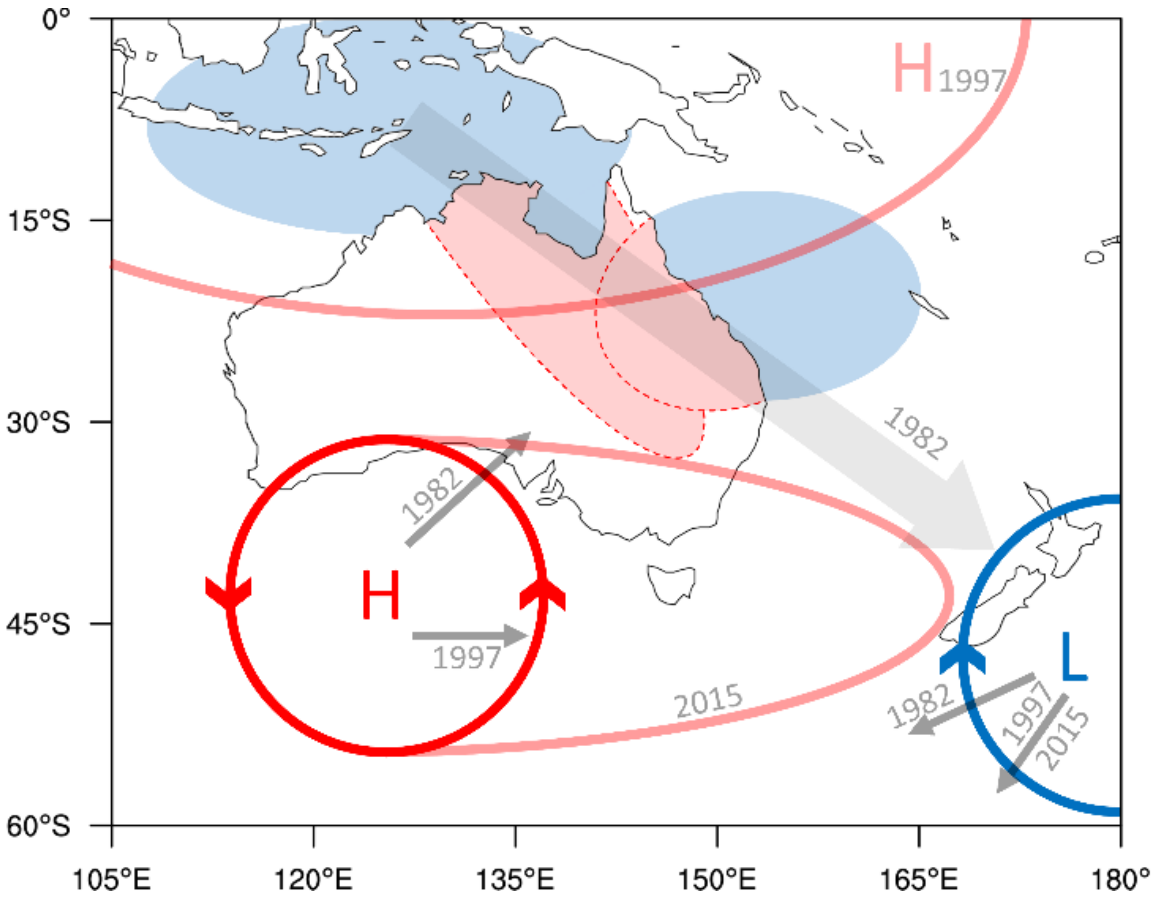

Fig. 3.11: Schematic summarising the key pressure and wind anomalies associated with typical El Niño events and the deviations during strong El Niño events. Solid red and blue lines show positive (H) and negative (L) SLP anomalies, respectively, with an indication of the associated wind. Regions of SST (blue shading) and their moisture anomalies (red shading outlined by red dashed lines) can influence east Australian rainfall during strong El Niño events. The faint red lines indicate large deviations from the typical pressure anomalies during a strong El Niño event (indicated by year). The thin grey arrows indicate how the anomalies shifted from the ideal El Niño circulation during the indicated year. The thick grey arrow indicates the influence of a remote teleconnection occurring during spring of 1982.

The 1982 strong El Niño event showed an example of a shift in positive SLP anomaly that contributed to less eastern Australian rainfall than average. During this event, the "H" anomaly in Fig. 3.11 shifted northeast compared to typical El Niño events resulting in

significant positive SLP over southeast Australia and significant southeasterly wind anomalies over eastern Australia, both resulting in significantly less rainfall there. Furthermore, cool SST anomalies to the northeast of Australia during spring of 1982 exacerbated the spring rainfall deficit by 17-21% by reducing moisture availability. These influential SST regions to the northeast, and to a lesser extent to the north of Australia, are highlighted in Fig. 3.11 by blue shading. The land areas influenced by these SST moisture sources are shown by red dashed lines and shading. This local SST effect was observed during all three El Niño events, but is most noticeable when there are strongly anomalous SSTs, as in 1982. Furthermore, the SSTs to the north of Australia showed a remote teleconnection with SLP to the southeast of Australia, contributing to the more eastward shift of the "L" anomaly in Fig. 3.11. However, the effect of this region would only have led to a 9% reduction in east Australian rainfall. The influence that the 1982 El Niño had on eastern Australia is historically regarded as a typical El Niño response. This study shows that it was the local SSTs that induced a significant change to regional rainfall in 1982, suggesting there was an atypical regional response during this strong El Niño event. The importance of the SST regions adjacent to Australia in Fig. 3.11 highlights a possible source of predictability of spring rainfall in some regions of Australia. Indeed, there is potential for these areas to be utilised to improve the accuracy of seasonal forecasts during strong El Niño events. Increased monitoring and prediction using the SSTs in these regions would show whether this is the case.

The 2015 event was associated with a widespread extension of the positive SLP anomaly (faint extension of the "H" anomaly, Fig. 3.11), related to a significant reduction in spring rainfall along the southeast coast of Australia. The simulation of the 2015 event is inconclusive as to the extent of forcing from SST anomalies. This suggests that either the model is not able to simulate what was observed in 2015 from either model deficiencies, experimental design (e.g.

constant greenhouse gas concentrations), or that what was observed in 2015 is a rare occurrence where the SST response was modified by a stochastic atmosphere. The latter seems the most likely based of Karoly et al. (2016), which used a similar model (HadAM3P, with a nested HadRM3P regional model) to conclude that atmospheric variability provided the largest contribution to the record low Tasmanian rainfall in October 2015, than both the concurrent El Niño and anthropogenic climate change (Karoly et al., 2016). Additionally, a large-scale driver of atmospheric variability, the negative SAM, was found to have contributed to the Australian spring rainfall deficit during the 2002 El Niño event (Lim and Hendon, 2015). However, in SON of 2015 the SAM was positive, with an index value of 1.75 based on the method used in Marshall (2003), whereas in both 1982 and 1997 the SAM was negative, with values of -1.10 and -1.81, respectively. It is possible that the positive SAM could have contributed to the observed circulation patterns of the 2015 El Niño event, but this requires further analysis.

The near-average east Australian spring rainfall during the 1997 El Niño event was associated with near-average winds over the region, corroborating the work of Brown et al. (2009) where they found near-average moisture availability during this event. The near-average winds appear to be the result of a combination of SST-forced positive SLP anomalies to the north and south of Australia (faint north of Australia "H_{1997}" and eastward shift of southern "H", Fig. 3.11). The positive SLP anomaly to the north of Australia observed in spring of 1997 was not observed in the 1982 and 2015 events. Likewise, although the model appeared to show a positive SLP bias to the north of Australia in all three El Niño events, the SLP anomaly was the strongest when forced with 1997 SSTs. The model results indicated a distinct SST-forced dynamical reason for east Australian spring rainfall in 1997 to have been near average. This dynamical reason for the eastern Australian spring rainfall in 1997 can be put into context of

the asymmetry in the ENSO – Australian rainfall relationship. It has previously been shown that La Niña events have a greater relationship with Australian rainfall than El Niño events (Power et al., 2006; Cai et al., 2010; King et al., 2015; Chung and Power, 2017). The question remains as to whether the dynamics of the 1997 event is unique, or whether historical and future events may exhibit similar characteristics. If so, this may help contextualise the origins of the nonlinear ENSO – Australian rainfall relationship, and help improve seasonal rainfall forecasts for future events.

Overall, this study emphasises that particular attention must be paid to the structure of both local Australian and tropical Pacific SST anomalies for forecasting the regional Australian rainfall response to future strong El Niño events. Improvements to forecast skill and climate projections may be possible by focusing on the representation of SSTs in these key regions and their teleconnections. This was highlighted by the well simulated eastern Australian spring rainfall when forced with both 1982 and 1997 SSTs, despite the differing rainfall anomalies observed during these two El Niño events. In terms of climate projections, this suggests that if the frequency of strong El Niño events increases in the future, as currently projected, this may not equate to less rainfall in east Australia, e.g. if El Niño events like 1997 become more frequent. However, as our large ensemble experiments suggest, any forcing from SSTs only has the ability to shift the distribution of likely atmospheric states. The resulting observed rainfall and circulation anomaly associated with a future strong El Niño event may also be influenced by stochastic atmospheric processes, as may have occurred during the 2015 El Niño event.

4 The record high Maritime Continent sea level pressure during the strong El Niño of 1997

This section is original work that has not yet been published in a journal.

This section continues the findings in the previous chapter (van Rensch et al., 2019) regarding the 1997 event. The significantly high SLP anomaly to the north of Australia during SON of 1997 was one of its most distinguishing features for the unusual east Australian rainfall. This section examines the origins of this SLP anomaly in terms of remote forcing from the tropical Pacific.

4.1 Abstract

The El Niño of 1997-1998 was, by many metrics, the strongest El Niño event of the satellite era. The event was punctuated by some unusual features, including a record high September – November (SON) sea level pressure (SLP) over the Maritime Continent in 1997. This SLP anomaly is important for explaining the east Australian SON rainfall anomaly that was atypical for an El Niño, as shown in Chapter 3 (van Rensch et al., 2019). However, the reason for the extreme high SLP over the Maritime Continent during SON 1997 is unknown. We show that the extreme SLP over the Maritime Continent was the result of the early peak of extreme east Pacific SSTs. The east Pacific SST anomalies in SON 1997 reached levels typically seen in other strong El Niño events during December – February (DJF), when the event normally peaks. The early onset warm east Pacific SSTs promoted record breaking convection in the east Pacific and were associated with the location of strongest tropical Pacific convection reaching the furthest east in SON. The location of strongest convection is considered to be the rising branch of the Walker Circulation. With the location of strongest convection furthest away from the Maritime Continent, this promoted an unusual build-up of mass over the Maritime Continent region associated with the localised reversal of the Walker Circulation – a process that is typical for strong El Niño in DJF, but not in SON. Using a partially coupled ocean-atmosphere model, we confirm that the early onset of strong eastern Pacific SSTs in SON 1997 alone is enough to simulate a record positive SLP anomaly in the Maritime Continent region. However, the magnitude of the observed anomaly was underestimated by the model. The weaker Maritime Continent SLP response in the model is likely due to the inability of the atmospheric component of the model to simulate a realistic eastward shift in maximum convection during SON, and cooler mean tropical Pacific SSTs. These findings have implications for the realistic

simulation of teleconnections from similar early peak events, both in seasonal forecasting and in climate projections.

4.2 Introduction

The 1997-1998 El Niño event was the strongest event in the eastern Pacific since at least 1979 when comprehensive observations began (Y.-K. Lim et al., 2017). The event significantly affected global and regional climate. Globally, the mean surface temperature broke the hottest year on record at the time in 1998, which was attributed to both the ending El Niño and excessive greenhouse gases (Angell, 2000). Regionally, countries surrounding the Pacific experienced more extreme weather and climate events than during typical El Niño events. In the eastern Pacific, extreme floods occurred in Peru (Sanabria et al., 2018), and in the western Pacific extreme meteorological drought and fires occurred in Indonesia (Pan et al., 2018). However, some regions, which are typically strongly affected by El Niño, did not experience such a marked effect. For example, drought was forecast during the monsoon in India, and less SON rainfall was predicted for east Australia. However, near average rainfall was experienced in both regions (Kumar et al., 2006; Brown et al., 2009; van Rensch et al., 2015, 2019; Chapter 2; Chapter 3).

Forecasting the 1997-1998 El Niño was a challenge for both statistical and dynamical models of the time (Barnston et al., 1999; Landsea and Knaff, 2000). Some models could forecast the onset and decay of the event well, but no models were able to forecast the magnitude of the event (Landsea and Knaff, 2000). This event continues to be a challenge and a test case for more advanced dynamical models, e.g., for testing forecast improvements from the inclusion of atmospheric initial conditions in addition to the standard oceanic initial conditions (Shi et

al., 2011). For a model to accurately simulate the magnitude of the 1997-1998 event, it needs to be able to simulate the processes leading to and amplifying this event. The 1997-1998 event had a preconditioned warm ocean mixed layer across much of the equatorial Pacific (McPhaden, 1999) . This warm layer was the result of anomalously strong trade winds in 1996, causing an oceanic Rossby wave reflection on the western Pacific boundary (Boulanger et al., 2004). A strong westerly wind event in March 1997 then initiated the 1997 El Niño event by exciting equatorial downwelling Kelvin Waves which travelled eastwards, reducing oceanic upwelling and warming the surface in the east Pacific (McPhaden, 1999; Wang and Weisberg, 2000). Frequent westerly wind events throughout 1997 further added to the strength of the SST anomaly in the eastern Pacific (McPhaden, 1999; Wang and Weisberg, 2000; Boulanger et al., 2004). The strength of the March 1997 westerly wind event has been attributed as the reason for this event becoming so strong much earlier than other strong El Niño events, such as the 1982-1983 event (Boulanger et al., 2004).

The early onset of the 1997-1998 El Niño, and its unprecedented magnitude, allowed for accurate forecasts of many regional teleconnections due to persistence alone, but in some regions this failed. Persistence from 1997 June-August allowed for an accurate 1997-1998 December – February (DJF) seasonal forecast in North America (Barnston et al., 1999). However, in 1997 SON the persistence rainfall forecast performed somewhat poorly in eastern Australia, even though Australia typically experiences the strongest effects from El Niño in this season (McBride and Nicholls, 1983). Chapter 3 (van Rensch et al., 2019) found that the 1997 SON rainfall in eastern Australia deviated from a typical El Niño year due to a combination of a positive SLP anomaly over the Maritime Continent, and a positive SLP anomaly to the south of Australia. Chapter 3.5 identified that both of these SLP anomalies were forced by sea surface temperature (SST) anomalies, since they were able to be

reproduced by AGCMs driven by observed SSTs. The anomaly to the south of Australia is a typical feature of El Niño acting through the Indian Ocean Dipole (Cai et al., 2011b). Chapter 3.6 showed SSTs off the northeast and northern coasts of Australia did not have a significant influence on Maritime Continent SLP, suggesting either SSTs from other regions had a greater influence, or the observed anomaly was stochastically forced. The origin of the positive Maritime Continent SLP anomaly in SON 1997 will be the focus of this chapter.

In Chapter 3.5, we showed that the ACCESS 1.3 atmosphere model simulated a significantly positive SLP anomaly over the Maritime Continent for all three strong El Niño events. Whereas, this was only observed during the 1997 El Niño. Furthermore, the model failed to simulate the observed magnitude of the SLP anomaly over the Maritime Continent during SON 1997, suggesting that the model suffers from a deficiency in simulating the processes leading to the anomaly. Atmospheric models have struggled to simulate the negative rainfall anomaly over the Maritime Continent region during the 1997-1998 event (Kang et al., 2002), which could be related to the SLP issue. Allowing coupling between the atmosphere and sea surface showed an improvement in the negative Maritime Continent rainfall anomaly in June-August 1997, as well as generally improving the representation of rainfall in the Maritime Continent region (Zhu and Shukla, 2013). Whether regional air-sea coupling improves the ability of the model to simulate the observed Maritime Continent SLP during strong El Niño events is unknown.

In this chapter, we will examine the key factors that promoted the high Maritime Continent SLP during SON of 1997. This will clarify the processes that were associated with the near average east Australian rainfall during SON of the 1997 El Niño. Firstly, we will identify the record nature of the 1997 SON Maritime Continent SLP and show how this was not detected

in the Southern Oscillation Index (SOI). Then, we examine the evolution of the 1997 SON Maritime Continent SLP in observations and determine important factors conducive for its development. Finally, we examine how well the CESM1.1 model can simulate the 1997 Maritime Continent SLP in two configurations. One, when the atmosphere is forced with global SSTs, and another when forced with SSTs only in the central-eastern tropical Pacific with free air-sea coupling elsewhere. The ability of the model to simulate the important factors for Maritime Continent SLP will also be assessed. Overall, this work may help contextualise the unusual 1997 SON east Australian rainfall and potentially improve the forecasting of the impacts associated with future strong El Niño events.

4.3 Methods

This study performed statistical analysis of observational and general circulation model data. In order to establish the link between Pacific SSTs and SLP in the Maritime Continent during the 1997 event, metrics of the Walker Circulation were examined. We analysed the Troup SOI and station SLP data for Darwin (12.4° S, 130.8° E) and Tahiti (17.7° S, 149.4° W), as this is a common metric for El Niño-related SLP and the Walker Circulation. The Troup SOI spans 1876-2018 and was obtained from the Australian Bureau of Meteorology, who used a 1933-1992 climatology[1]. We used ERA Interim data for gridded SLP (Dee et al., 2011), and defined the Maritime Continent region as 15° N – 15° S, 120° E – 150° E. We confirmed that our results regarding the Maritime Continent SLP are robust by comparing to HadSLP2 and the NCEP/NCAR reanalysis (Kalnay et al., 1996; Allan and Ansell, 2006; not shown). Outgoing longwave radiation (OLR) was used as a proxy for convection. Changes in regions of strongest

[1] http://poama.bom.gov.au/climate/current/soihtm1.shtml

convection in the tropical Indo-Pacific gave an indication of the region of strongest ascent in the Walker Circulation. Here, we used an OLR dataset based on interpolated satellite data (Liebmann and Smith, 1996).

To assess relationships between variables we used linear regression and both Pearson's and Spearman's rank methods for correlation. Comparing the deviations between the two methods gave an indication of nonlinearity or outliers in the relationship. Nonlinear relationships are particularly noticeable in relationships with convection, due to deep convection not initiating until reaching an SST threshold (Gadgil et al., 1984), and can therefore appear as outliers. Pearson's correlation is sensitive to outliers within the time series, whereas Spearman's rank correlation eliminates outliers by using the ranks of the data to perform a Pearson's correlation.

We examined results from two experiments using the CESM1.1 model (Hurrell et al., 2013). Both experiments are comprised of 10-member ensembles and are forced by historical greenhouse gas concentrations and other external forcings (such as aerosols) until 2005 after which RCP8.5 forcings were used. The experiments used the Extended Reconstructed SST version 3b (ERSSTv3b) dataset for their SST boundary conditions, and we also use this dataset for our observations. The ERSSTv3b dataset combines ship and buoy measurements into a gridded SST product as detailed in Smith et al. (2008), but the version "b" excludes satellite data. The first experiment used the atmosphere-only model and assessed the influence of global SSTs on the atmosphere by forcing the atmospheric component of the model with ERSSTv3b SSTs from 1979-2015 for consistency with the observations. As this experiment finished at the end of 2015, we could not compare our results with DJF 2015-2016 for this experiment.

The second experiment, known as a "pacemaker" experiment, was used to assess the influence of SSTs in the eastern tropical Pacific alone. The experiment allowed a fully coupled CESM1.1 model to evolve freely, except for in the tropical eastern Pacific region (10 °S – 10 °N, 160 °W – 90 °W). In this region, the SSTs were relaxed to the ERSSTv3b time-varying anomalies added to the coupled model climatology. ERSSTv3b anomalies were used as opposed to raw values, because using raw values would likely introduce a spurious spatial inhomogeneity greater than any observed interannual variability. Linear tapering was performed outside the tropical eastern Pacific region to 20 °S – 20 °N and 180 ° – American coast. The pacemaker experiment used in this study allowed for freely evolving air-sea dynamics around the Maritime Continent, but maintained the historical evolution of El Niño, neutral and La Niña years. We examined model output from the same CESM1.1 pacemaker experiment as Deser et al. (2017), which was previously used to examine the influence of El Niño and La Niña events on Northern Hemisphere atmospheric pressure. The pacemaker experiment was analysed from 1979-2013. The start year was again used for consistency with observations, with the end year being the final year of the experiment. Comparison to the 2015-2016 El Niño was therefore not possible in this experiment.

4.4 The 1997-1998 El Niño in observations

4.4.1 The structure of the 1997-1998 event along the equator

The SOI is designed to identify ENSO events by examining a proxy for the zonal pressure gradient south of the equatorial Pacific, achieved by comparing the Darwin SLP with that of Tahiti. However, the 1997 El Niño event shows the SOI can be deficient in capturing extreme

SLP at either one of these sites. The SOI recorded its strongest negative SON and DJF values in 1982 and 1982-1983, respectively (Fig. 4.1a). This record SOI was associated with the concurrent strong El Niño event in 1982-1983, and retained the record even after the strong El Niño events of 1997-1998 and 2015-2016 (Fig. 4.1a). Darwin explains roughly 5% more of the SOI variance than Tahiti in SON (72% versus 67%, from 1876-2018). Despite Darwin explaining more of the variance, the SOI conceals a prominent feature in Darwin during SON of 1997 - a record high SLP in SON (Fig. 4.1a). The record high Darwin SLP in SON 1997 did not translate to the SOI because Tahiti recorded a slightly positive SLP anomaly rather than a negative anomaly typically seen during El Niño (e.g. SON 1982, Fig. 4.1a, b).

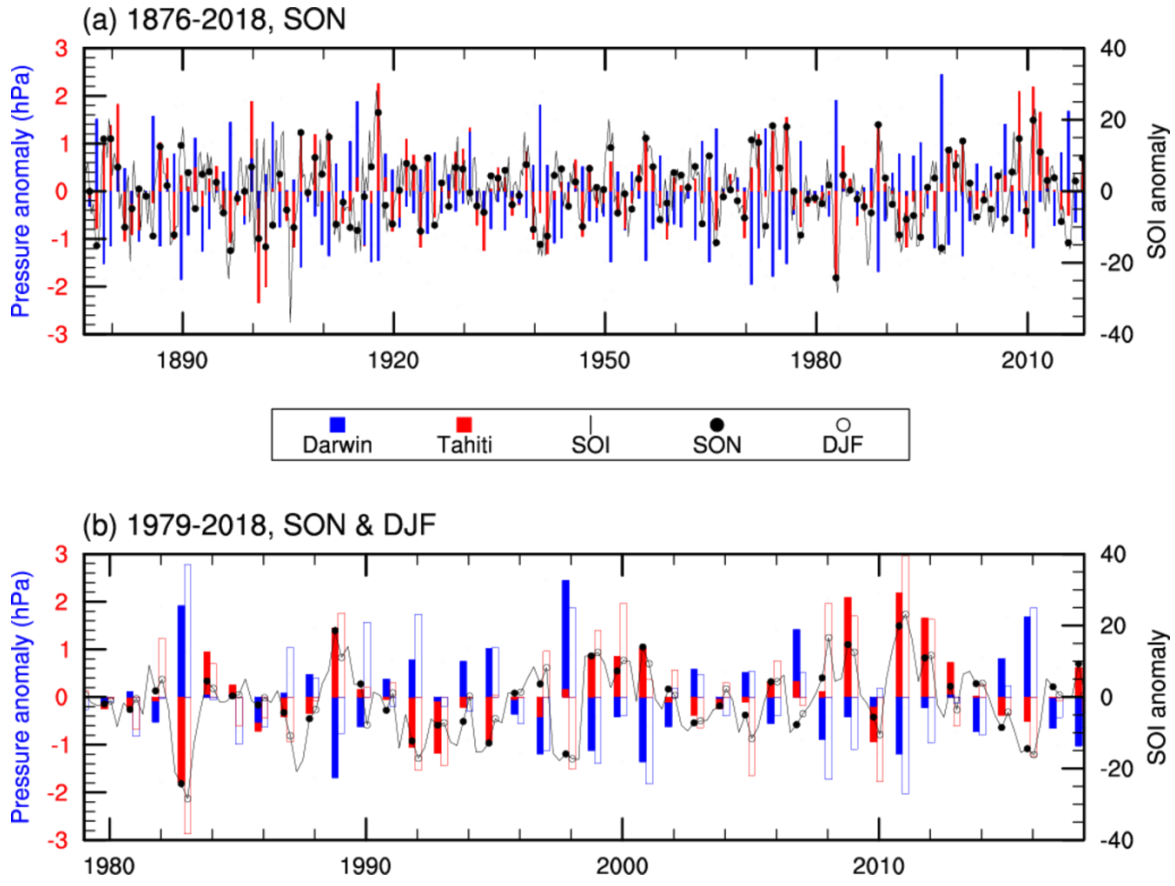

Fig. 4.1: (a) SON Darwin (blue bars) and Tahiti (red bars) SLP anomalies, overlayed with monthly SOI (black line) and SON SOI values (filled black circles) for the period 1876-2018. (b) As (a), but for the period 1979-2018 and showing DJF Darwin and Tahiti SLP anomalies and DJF SOI values using open bars and circles, respectively.

The SOI failed to capture an extreme property of the 1997 El Niño event in SON due to the large spatial extent of the western pole of the Southern Oscillation. The record high Darwin SLP in SON 1997 was associated with a zonally widespread high SLP anomaly stretching along the equator from the western Indian Ocean to roughly Tahiti longitudes at 150° W (Fig. 4.2a). At Tahiti longitudes, the 1997 event shows a large disparity with the two other strong El Niño – with 1997 SLP showing near average, but 1982 and 2015 SLPs showing a strong negative anomaly (Fig. 4.2a). Using the SOI as an indication of El Niño strength, may therefore be unreliable. To improve the SOI index for strong events, the SLP at 100 °W showed a similar negative SON SLP anomaly for all three strong El Niño events (Fig. 4.2a). Comparing the SLP at 100 °W to Darwin SLP would show a greater Southern Oscillation intensity in SON 1997 event than in SON of both 1982 and 2015. Another criticism of the location of the eastern SOI station (currently Tahiti) is that it is too far south of the equator at 17 °S, but this analysis indicates that an equatorial location would still be deficient for strong El Niño events. Unfortunately, there has historically been limited station data availability in the equatorial region around 100 °W. Although, reconstructed, or reanalysed data could be used instead of station data, as used in the Equatorial SOI which covers the 100 °W domain. Therefore, the widespread SLP effect must be kept in mind when attempting to detect historical strong El Niño events using the SOI. It is also important to note that the 1997 El Niño event was only exceptional in the SON season; in DJF the SLP gradients become more similar between the three strong El Niño events, particularly the 1982-1983 and 1997-1998 events (Fig. 4.1a and Fig. 4.2b).

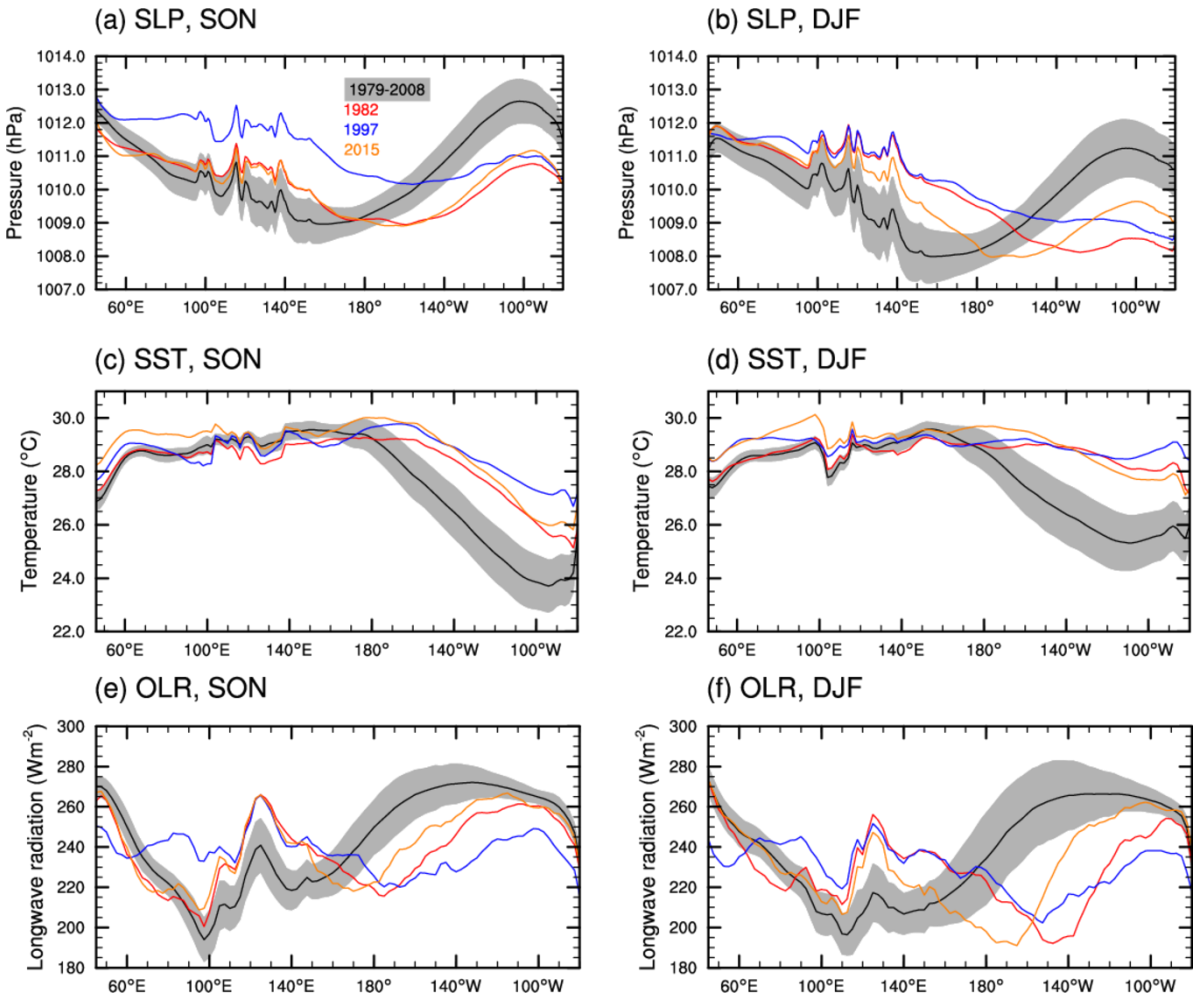

Fig. 4.2: Observed meridional mean SLP, SST, and OLR from 5S – 5N in the Indo-Pacific basin for (left) SON, and (right) DJF. Black lines and grey shading show the 1979-2008 mean and ±1 standard deviation anomaly from 1979-2008, respectively. Red, blue and yellow lines show the 1982-1983, 1997-1998, and 2015-2016 years, respectively.

During El Niño events, SLP and SST are closely linked in the tropical Pacific (Bjerknes, 1969). The record Darwin SLP occurred when areas of the eastern tropical Pacific also experienced record warm SSTs, suggesting these records might also be linked. In the SON of 1997, the equatorial SSTs in the far eastern Pacific (around 100 °W) were approximately three standard deviations warmer than normal, and over 1 °C warmer than the two other strong El Niño events examined (Fig. 4.2c). The SSTs during SON of 1997 around the Maritime Continent did not show a significant anomaly (Fig. 4.2c), despite the roughly three standard deviations

positive SLP anomaly in the same region (Fig. 4.2a). The SON SSTs in the Maritime Continent region were more negative during 1982 than in 1997, suggesting local SSTs were less important for the record high 1997 SON Maritime Continent SLP than the far eastern Pacific SSTs. The SSTs in the eastern Indian Ocean were significantly cold in SON 1997 (Fig. 4.2c), associated with a concurrent strong positive Indian Ocean Dipole (Saji et al., 1999), which could have formed from internal Indian Ocean dynamics (Webster et al., 1999).

Convection in the tropical eastern Pacific during SON had a greater magnitude in 1997 compared to 1982 and 2015, as indicated from OLR values (Fig. 4.2e). A common feature for El Niño events is the eastward progression of the maximum convection and minimum SLP away from the Maritime Continent (Deser and Wallace, 1990). During SON 1997 the location of maximum convection and minimum SLP in the Pacific basin was the furthest east of all strong El Niño events (Fig. 4.2 e and a). The eastward shift of the maximum convection and minimum SLP points to the shift of the ascending region of the Walker Circulation. The ascending location moving further east away from the Maritime Continent, where it is typically situated, could provide a greater opportunity for SLP to increase in the Maritime Continent region. In addition, a more widespread increase in eastern Pacific convection east of the location of maximum convection may favour a westward transport of mass over the Maritime Continent, further increasing the SLP there. The OLR profiles in DJF show 1997-1998 and 1982-1983 shift further east (Fig. 4.2f), with a similar Maritime Continent SLP anomaly (Fig. 4.2b), whereas 2015-2016 did not show as extensive eastward shift (Fig. 4.2f), or as high Maritime Continent SLP (Fig. 4.2b).

4.4.2 The evolution of the 1997-1998 event

Examining the evolution of SLP, SST and convection fields exposes the timing of these events and can provide information about which factors are most important for the development of the record SLP over the Maritime Continent in the SON of 1997. The relationship between SST, SLP and rainfall around the Maritime Continent region has been thoroughly examined (e.g. Nicholls, 1984c; Hendon, 2003). To summarize for our context, Fig. 4.3 shows those regions of SST and convection that have historically shown the strongest correlation with SLP over the Maritime Continent. The SLP over the Maritime Continent is most strongly related to SSTs in the eastern tropical Pacific in both SON and DJF, with correlations as high as 0.8 and showing a stronger relationship than SSTs local to the Maritime Continent (Fig. 4.3). This indicates that the eastern Pacific El Niño events, rather than central Pacific El Niño events are more strongly related to Maritime Continent SLP. Therefore, if eastern Pacific SSTs are anomalously warm, Maritime Continent SLP would likely be anomalously high. The change in sign seen in the DJF correlation around Indonesia in Fig. 4.3b is likely associated with the change in mean winds that occurs with the traversal of the Intertropical Convergence Zone (Hendon, 2003). Convection in the Maritime Continent and around 170 °W along the equator shows a strong correlation/anticorrelation dipole with Maritime Continent SLP (Fig. 4.3). The Maritime Continent correlation between convection and SLP is weaker in magnitude than the anticorrelation around 170 °W in SON, but reaches parity in DJF (Fig. 4.3b). Given these relationships, in the following analysis we use the Niño3 region to highlight the relationship of eastern Pacific SSTs with Maritime Continent SLP and, similarly, the Niño4 region for central Pacific convection.

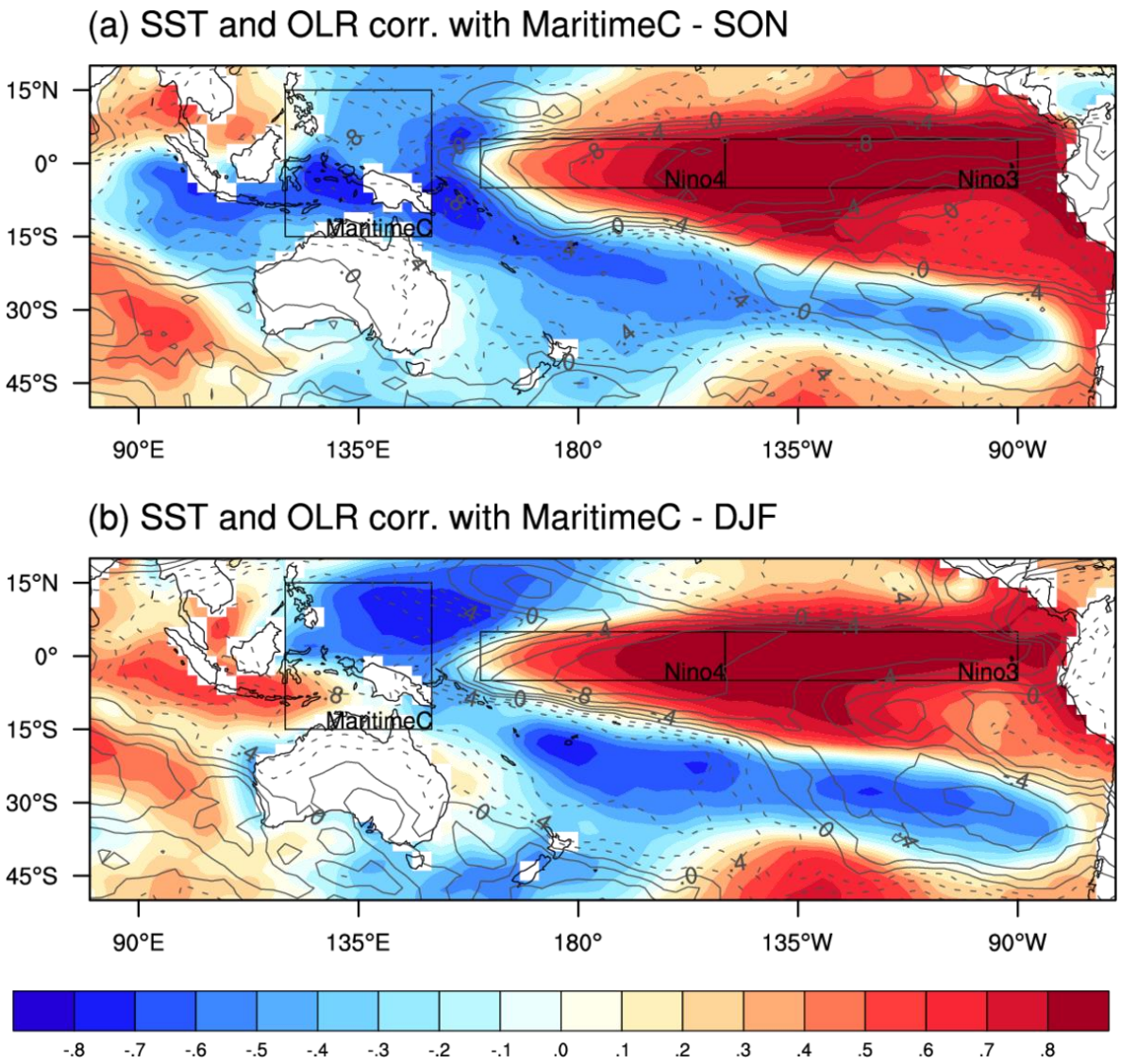

Fig. 4.3: Correlation of Maritime Continent (15° S – 15° N, 120° E – 150° E) SLP with (colour) SSTs and (contours) OLR during (a) SON, 1979-2008, and (b) DJF, 1980-2009. OLR correlation contours are from -0.8 to 0.8 by 0.2 intervals, with solid and dashed lines showing negative and positive correlations, respectively.

The record high SLP in the SON of 1997 over the Maritime Continent intensified and peaked earlier than both 1982 and 2015 events (Fig. 4.4a). The SLP anomaly appeared in conjunction with a similarly early intensification in SST and convection anomalies in the eastern equatorial Pacific (Fig. 4.4 a, b, c and c'). The early peak in SLP anomaly also coincided with an earlier eastward shift in the maximum convection over the equatorial Pacific when compared to

other strong El Niño events (Fig. 4.4d). The positive SLP anomaly over the Maritime Continent started developing in August of 1997 reaching a peak in November before reducing in magnitude in December (Fig. 4.4a). The peak of this SLP anomaly rivalled that of a subsequent peak in February 1998 and also in January-February 1983 and January 2016 (Fig. 4.4a). The Niño3 SST anomalies represent SST anomalies in the eastern equatorial Pacific Ocean (outlined in Fig. 4.3) and in 1997, these developed before the SLP anomaly over the Maritime Continent. In the Niño3 region, the SST anomalies rapidly increased in May-June 1997 compared to the other two strong El Niño events, followed by a more typical warming rate (Fig. 4.4b). The 1997 Niño3 SSTs reached roughly its maximum anomaly in November, maintaining a similar anomaly until January. Although the peak SLP anomaly over the Maritime Continent and the peak Niño3 SST match during November 1997, the reduction in Maritime Continent SLP anomaly in December does not corroborate with the maintenance of Niño3 SST anomaly into December (c.f. Fig. 4.4 b and d).

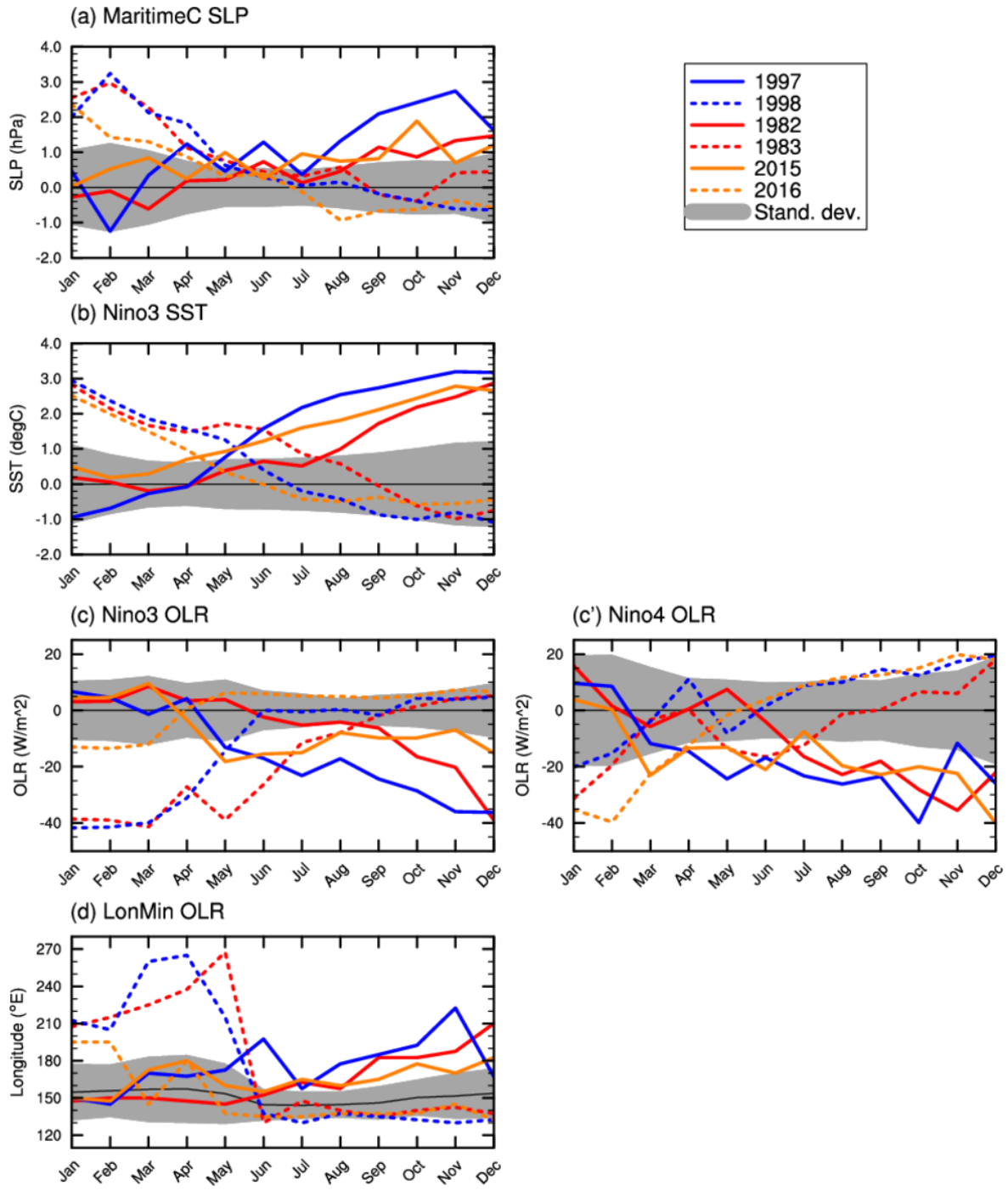

Fig. 4.4: Observed monthly evolution of (a) Maritime Continent SLP anomalies, (b) Niño3 SST anomalies, (c) Niño3 OLR anomalies, (c') Niño4 OLR anomalies, (d) longitude of minimum OLR from 5° S – 5° N, 130° E-270° E. Plotting conventions as in Fig. 4.2, with dashed lines showing the following years of each El Niño event.

Convection in the tropical central and eastern Pacific also shows a strong relationship with SLP over the Maritime Continent (Fig. 4.3). Convection in this region is likely part of the link between east Pacific SST anomalies and SLP over the Maritime Continent through the Walker Circulation (Bjerknes, 1969; Deser and Wallace, 1990). In the second half of 1997, convection in the Niño3 region showed a substantial increase compared to the other two El Niño events (Fig. 4.4c), in line with the increase in SST anomalies. A build-up of convection was also observed in the Niño4 region in 1997 (Niño4 region outlined in Fig. 4.3), but in this region the convective activity was not significantly different from the other two strong El Niño events (Fig. 4.4c'). While convection in the Niño4 region shows the strongest positive correlation with SLP over the Maritime Continent (Fig. 4.3), the Niño3 region also shows a strong correlation. The Niño3 region also shows the greatest difference in convection anomalies between the 1997 event and the other strong El Niño events, suggesting this region could be more important for the record Maritime Continent SLP.

However, the magnitude of the convection in the east Pacific cannot account for the weakening of the positive SLP anomaly over the Maritime Continent from November into December 1997 (Fig. 4.4a). Here we hypothesise that the longitude of maximum tropical convection might also play a role (e.g. Deser and Wallace, 1990). Niño3 SST and Niño3 convection increased concurrently from April-May 1997 (Fig. 4.4 b and c), however the Maritime Continent SLP anomaly developed from roughly July-August (Fig. 4.4a). From roughly July-August 1997 the location of maximum convection starts to move eastwards reaching the furthest east in November 1997 (Fig. 4.4d), coinciding with the 1997 peak in Maritime Continent SLP (Fig. 4.4a). The location of maximum convection for the 1997 El Niño was also furthest east earlier than any other strong El Niño event (Fig. 4.4d). From November to December 1997 the maximum convection temporarily shifted westward to around one

standard deviation of its typical position (Fig. 4.4d), corresponding with the temporary reduction of Maritime Continent SLP (Fig. 4.4a). This suggests that the location of maximum convection is important for Maritime Continent SLP during the 1997 El Niño event, as suggested at the end of the previous section. A key differentiator for the 1997 El Niño to produce the record Maritime Continent SLP in SON could be that the maximum convection shifted earlier than other strong El Niño events, which is related to the early development of warm east Pacific SSTs.

4.4.3 Causes of the record SLP over the Maritime Continent in SON of 1997

As described above, the 1997-1998 event showed many record-breaking characteristics during SON, such as the highest SLP anomalies over the Maritime Continent, the warmest eastern tropical Pacific SSTs, and the most intense east Pacific convection of any strong El Niño event in the observational record. To determine the key processes associated with the high SLP anomaly, we examined the historical relationships between Maritime Continent SLP and metrics discussed in the previous sections. We also argued that the reason that this El Niño event was considered particularly strong in SON, was because it matured earlier in the seasonal cycle than other El Niño events. To highlight this, we compared SLP anomalies over the Maritime Continent with raw Niño3 SST, Maritime Continent SST, Niño3 OLR and longitude of minimum OLR (location of maximum convection) in SON and DJF (Fig. 4.5). We used SLP anomalies to ease comparison between seasons with different climatological SLP, but doing so did not change the relationships.

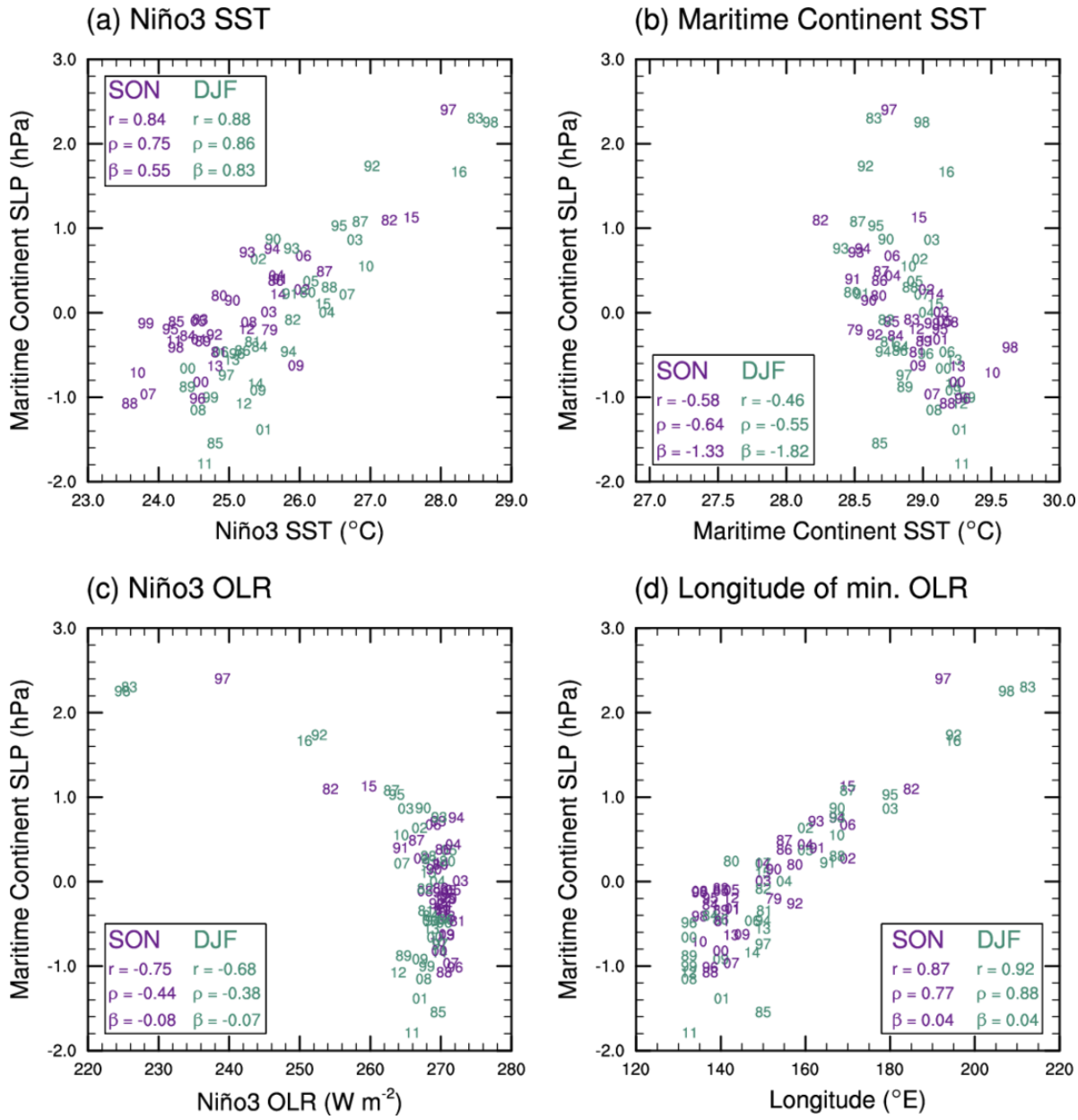

Fig. 4.5: Observed Maritime Continent SLP anomalies vs. (a) Niño3 SST, (b) Maritime Continent SST, (c) Niño3 OLR, and (d) longitude of maximum convection (minimum OLR). Purple and green show SON and DJF values, respectively, with the numbers indicating the last two digits of the year in which October or January falls. r, ρ and β are the Pearson correlation coefficients, Spearman's rank correlation coefficients and the linear regression coefficients, respectively.

The SLP in the Maritime Continent is more strongly linked to eastern Pacific SSTs than to SSTs local to the Maritime Continent. In SON of 1997, the SLP over the Maritime Continent was strongly positive, consistent with a linear relationship with Niño3 SSTs in both SON and DJF

(Fig. 4.5a). The relationship between SLP over the Maritime Continent and SSTs around the Maritime Continent shows a stronger linear relationship in SON than in DJF, consistent with seasonal changes experienced in the region (Hendon, 2003). However, in SON of 1997 the concurrent SLP and SSTs over the Maritime Continent deviated significantly from what was expected (Fig. 4.5b). Instead, the relationship was closer to that experienced during DJF in 1982-1983 and 1997-1998 (Fig. 4.5b). This suggests that during 1997 SON the local Maritime Continent SLP-SST relationship behaved in a manner like that seen in DJF, suggesting a process that is typically seasonally dependant occurred earlier.

The SSTs in the Niño3 region are likely associated with SLP over the Maritime Continent through atmospheric processes like the Walker Circulation. However, convection in the Niño3 region typically shows a relatively weak nonparametric relationship with SLP over the Maritime Continent [Spearman's rank correlation coefficients (ρ in Fig. 4.5c) of -0.44 and -0.38 in SON and DJF, respectively]. Only three or four strong events make the nonlinear relationship more prominent (Fig. 4.5c), likely due to Niño3 SSTs in those events becoming warm enough to initiate deep convection (Gadgil et al., 1984; Johnson and Kosaka, 2016). In comparison, the longitude of maximum convection in the equatorial Pacific shows a robust linear relationship with SLP over the Maritime Continent, with 1997 the furthest east SON value (Fig. 4.5d). The location of maximum convection can be interpreted as the main ascending region of the Walker Circulation. As SSTs warm in the eastern Pacific, this shifts the ascending region east, allowing SLP in the Maritime Continent region to increase due to the reduced convection and increased potential for subsidence in the region. This process is typical of a strong El Niño in DJF, but occurred earlier in 1997, suggesting this process caused the record high SLP over the Maritime Continent in SON.

4.5 The 1997-1998 El Niño in the Community Earth System Model

The observational analysis above showed the El Niño of 1997 matured earlier compared to other El Niño events. We propose this led to unseasonal repercussions on the atmospheric teleconnections to the Maritime Continent and, subsequently, eastern Australia (see previous Chapters). A key process to the early development was the early development in warm SSTs in the eastern Pacific. Exploring this process in general circulation models can aid in improving confidence in our hypothesis, and will assess the capability of models to simulate events like 1997. Section 3.5 showed that the ACCESS 1.3 atmosphere model was able to simulate positive SLP anomalies over the Maritime Continent in the SON of 1997 that were comparable to those observed, but not to the same magnitude. The model also simulated significantly high SLP anomalies over the Maritime Continent during SON for the 1982 and 2015 El Niño events, which was not observed. In this study we use the CESM, to firstly assess if there is an improvement in Maritime Continent SLP simulation over ACCESS detailed in the previous chapter, and to also assess if air-sea coupling shows improvements to the simulated relationships. As our results will show, CESM is not able to simulate the record features to the same magnitude as observed in SON 1997. However, the poor simulation of key features, such as the limited eastward shift in maximum convection, may still provide insights into understanding the important processes that were observed.

4.5.1 CESM atmosphere-only

The CESM model forced with observed SSTs simulated a Maritime Continent SLP anomaly mostly higher than that of 1982 and 2015, but the model could not simulate the observed magnitude of SLP anomaly in the last half of 1997 (Fig. 4.6a). The evolution of the 1997

Maritime Continent SLP was similar to that of 1982 and 2015 (Fig. 4.6a). This was despite being forced with SSTs from the three events that were identical to our observational analysis (Fig. 4.6b). The simulation of Maritime Continent SLP in 1982 and 2015 was similar to that observed, suggesting the model struggles to simulate the SLP in 1997 in particular. Above average convection in the Niño3 region was simulated during the 1997 and 1982 events, but the convection in 1997 was not obviously larger than 1982, as seen in the observations (Fig. 4.6c). The model simulated the shift of maximum tropical Pacific convection the furthest east in the second half of 1997 (Fig. 4.6d), however, the model did not shift as far east as observed (Fig. 4.4d). With the model not able to simulate a strong convection anomaly in the Niño3 region, and not able to shift its maximum convection far enough east, this may explain why the model was not able to simulate a Maritime Continent SLP anomaly similar to observed.

The simulated 1997 SON average Maritime Continent SLP anomaly was the record for SON in the atmosphere-only experiment and our analysis period (Fig. 4.7a). Only the magnitude of the SLP anomaly is reduced compared to observations, which is in line with reduced Niño3 SST-Maritime Continent SLP sensitivity in this experiment. The CESM model has a similar correlation between Niño3 SST and Maritime Continent SLP to that observed, but the simulated SLP is less sensitive to the SST forcing (i.e. linear relationships of 0.44 hPa $°C^{-1}$ and 0.63 hPa $°C^{-1}$ was simulated in SON and DJF, respectively, but the observations showed 0.55 hPa $°C^{-1}$ and 0.83 hPa $°C^{-1}$, Fig. 4.7a and Fig. 4.5a). The local SLP-SST correlations around the Maritime Continent are also similar to observed, but are 23 % and 42 % weaker in sensitivity in SON and DJF, respectively (c.f. Fig. 4.7b and Fig. 4.5b). These results indicate that SSTs in the Niño3 region drives the simulated Maritime Continent SLP, rather than SSTs around the Maritime Continent, a process that is seen in observations (e.g. Nicholls, 1984c; Hendon, 2003; Fig. 4.5 a and b).

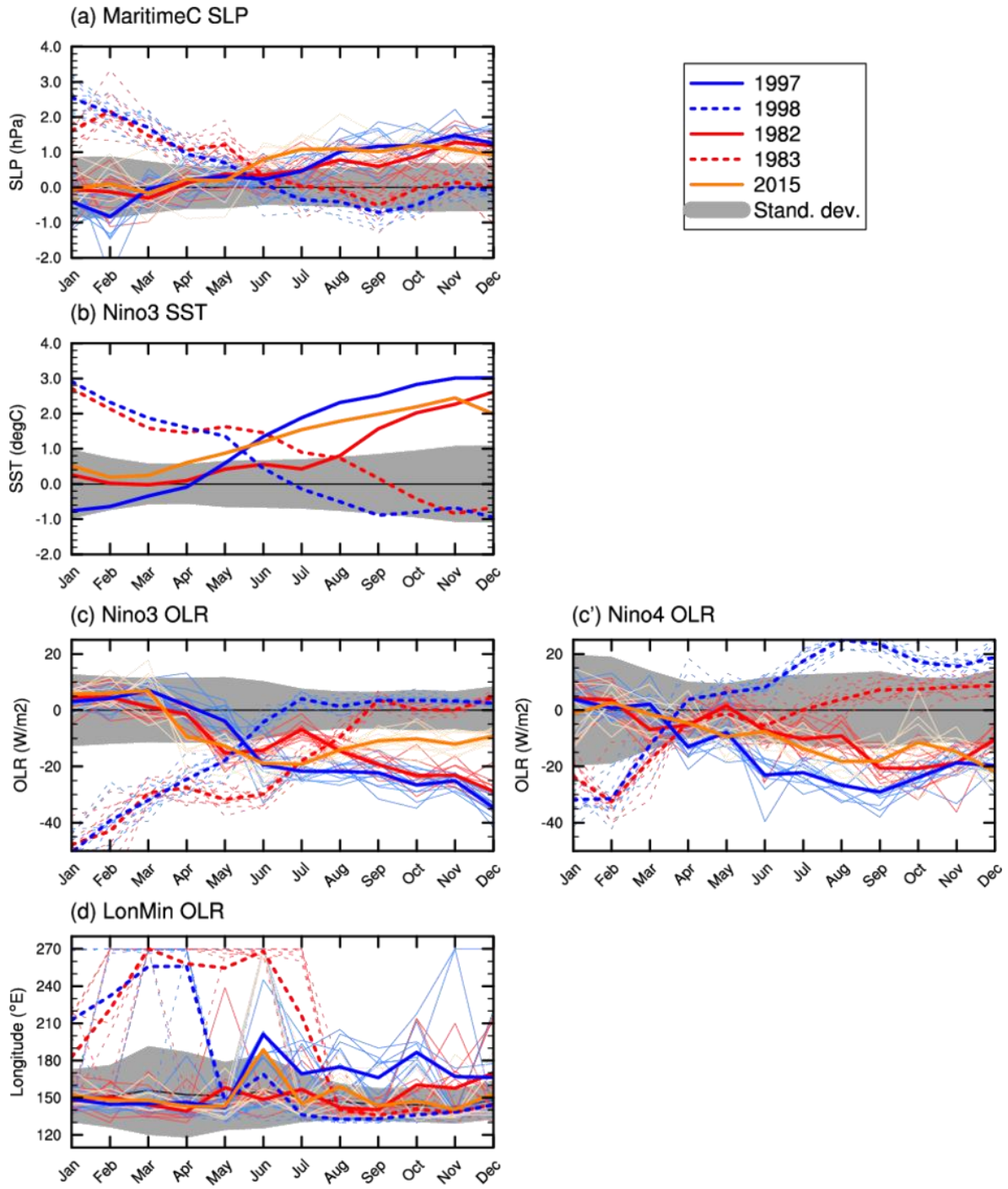

Fig. 4.6: As Fig. 4.4, but for CESM atmosphere-only experiment, and with individual model ensemble members (thin lines).

The CESM convective response to SST forcing shows greater disparity to the observations. In SON, there is a stronger Spearman correlation between Maritime Continent SLP and Niño3 convection in CESM compared to observations (Fig. 4.7c), but a weaker relationship than

observed was simulated in DJF. The stronger SON relationship could be due to the use of ensemble means reducing the influence of stochastic convection, especially for the cluster of events with very low convection centred around 280 W m^{-2} (Fig. 4.7c).

A potentially critical deficiency in the CESM model is its inability to shift tropical Pacific maximum convection eastwards. The maximum convection in the CESM model only shifts eastward for very high Maritime Continent SLP (Fig. 4.7d), whereas a linear relationship was observed (Fig. 4.5d). The relationship between SLP over the Maritime Continent and the longitude of maximum convection is better simulated in DJF than SON, with an insignificant Spearman rank correlation ($\rho = 0.11$) for SON (Fig. 4.7d). This suggests the model is deficient in its simulation of some aspects of the changes to the Walker Circulation with El Niño, which is likely to be important for simulating the magnitude of the observed link between Niño3 SSTs and SLP over the Maritime Continent.

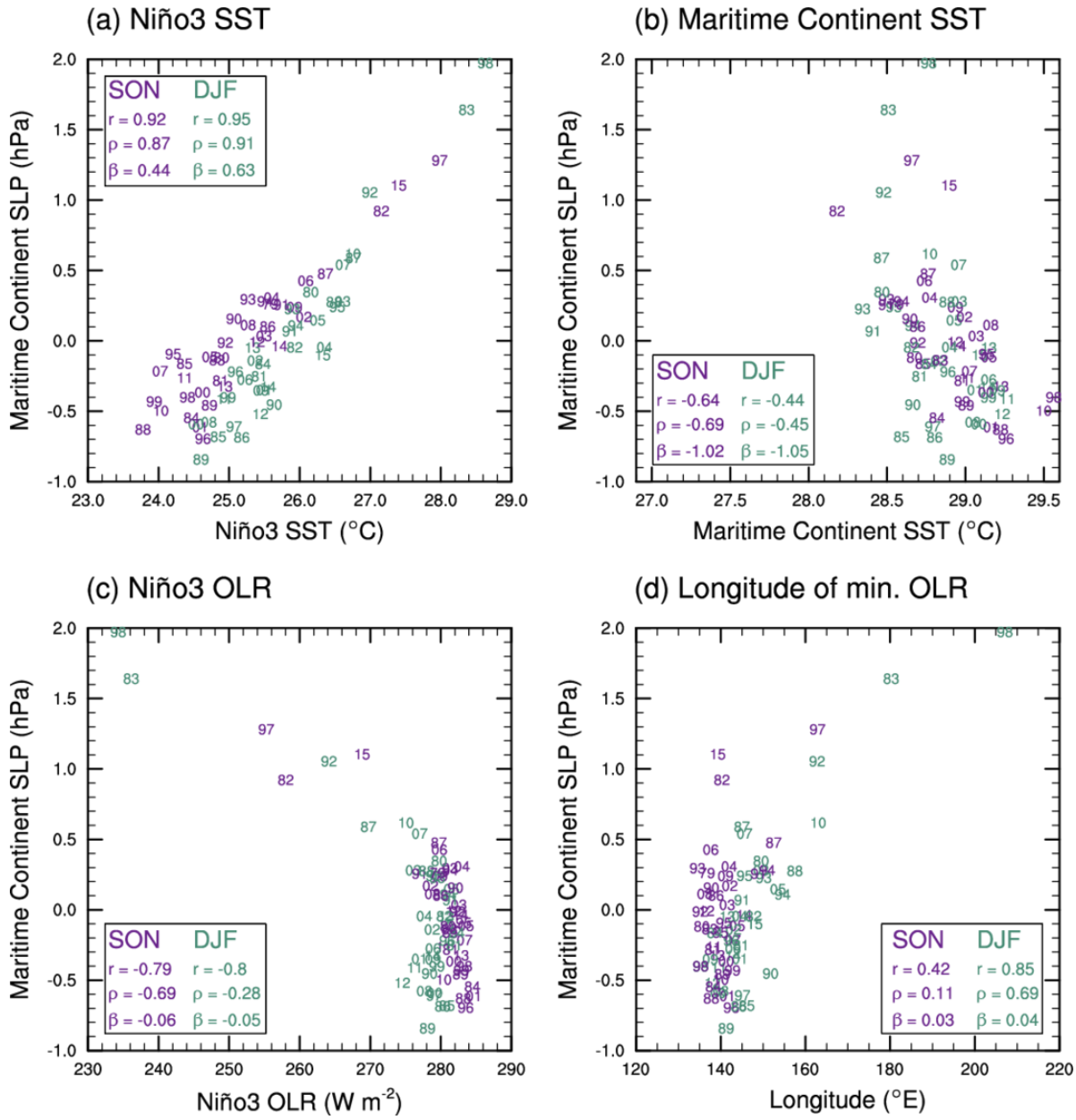

Fig. 4.7: As Fig. 4.5, but for CESM atmosphere-only. Different axis scales are used for clarity.

4.5.2 CESM Pacific pacemaker

Consistent with the observations, the CESM atmosphere-only model was able to simulate a record high Maritime Continent SLP anomaly during SON when forced with 1997 SSTs. This was true even despite the weaker simulation of its Maritime Continent SLP and convection

compared to that observed (Fig. 4.7). The statistical relationships in observations and the atmosphere-only experiment show that the SSTs in the Niño3 region have a stronger correlation to Maritime Continent SLP than the SSTs local to that region. The influence from SSTs outside the Niño3 and Maritime Continent regions cannot be ruled out in observations or the atmosphere-only experiment, which was forced by global SSTs. To assess the importance of the eastern tropical Pacific SSTs to SLP over the Maritime Continent, both historically and in the 1997 event, we used the tropical Pacific pacemaker experiment. In addition, with a more realistic air-sea interaction outside the tropical eastern Pacific, we assessed if there is an improvement in the representation of convection and the Walker Circulation over the atmosphere-only experiment.

The pacemaker experiment simulated a record high SLP anomaly over the Maritime Continent during the 1979-2013 analysis period, when the tropical eastern Pacific SSTs were nudged to observed SON 1997 anomalies (Fig. 4.8a). The result confirms that this region is a key contributor to the record high SLP over the Maritime Continent in the SON of 1997. However, the record high SLP in the model did not reach the same magnitude as observed. This was also simulated in the atmosphere-only experiment, but some key metrics performed worse in the pacemaker than the atmosphere-only experiment. The correlation between Maritime Continent SLP and Niño3 SST is similar to the atmosphere-only experiment, but has roughly half of the sensitivity during SON (Fig. 4.8a). In addition, allowing air-sea coupling in the pacemaker experiment introduced a stronger than observed local SST-SLP correlation over the Maritime Continent (Fig. 4.8b). This resulted in a cooler than observed Maritime Continent SST anomaly in the pacemaker experiment during SON 1997. The cooler local SSTs may have acted to increase the Maritime Continent SLP, leading to the simulation of a record SLP anomaly from a different process than was observed.

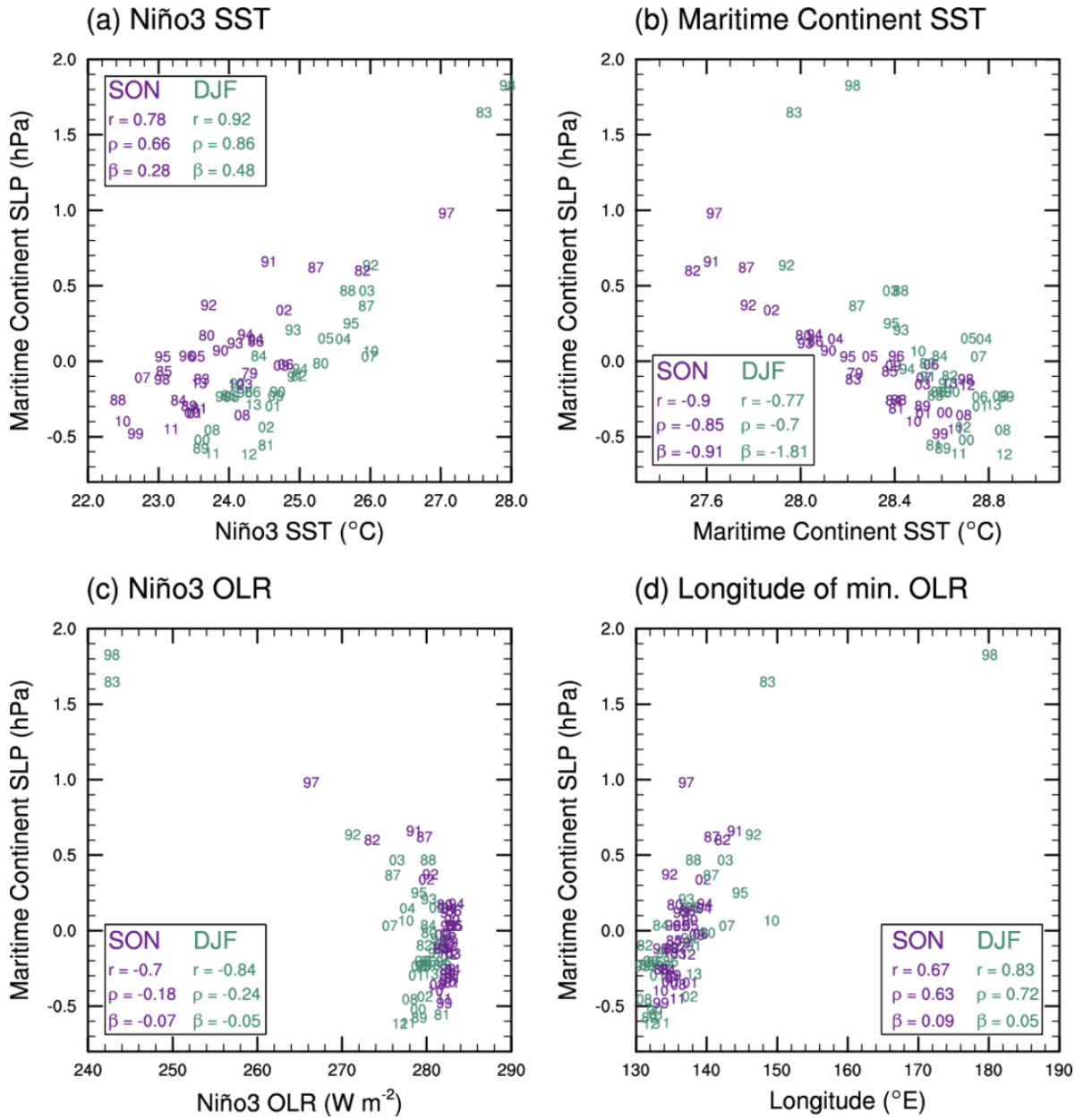

Fig. 4.8: As Fig. 4.5, but for CESM Tropical Pacific pacemaker experiment. Different axis scales are used for clarity.

The simulation of convection in the pacemaker experiment did not show any appreciable improvement over the atmosphere-only CESM experiment. The simulation of convection in the Niño3 region during SON of 1997 was generally weaker in the pacemaker experiment compared to observations (c.f. Fig. 4.8c and Fig. 4.5c), and even compared to the atmosphere-only experiment (Fig. 4.7c). This aligns with a weaker nonparametric relationship between

Maritime Continent SLP and Niño3 convection in the pacemaker compared to both observations, and the atmosphere-only experiment. In DJF, however, the pacemaker shows a Maritime Continent SLP-Niño3 convection relationship that was more like observations (Fig. 4.8c) , suggesting a seasonal dependency to a possible convection bias in this experiment. The weaker-than-observed SON convection that the pacemaker simulated in the Niño3 region, particularly for the 1997 event, may partly be explained by its simulation of the shift in maximum convection. The pacemaker experiment simulated the location of maximum convection in SON 1997 close to its mean location, not shifted eastwards as observed (c.f. Fig. 4.8c and Fig. 4.5c). The pacemaker experiment also showed a shorter eastward shift than the already deficient atmosphere-only experiment (c.f. Fig. 4.8c and Fig. 4.7c). In addition, the maximum convection in the pacemaker experiment was only able to reach Niño4 longitudes in DJF 1997-1998 (Fig. 4.8). The observations showed that a shift in maximum convection to the east is strongly related to the SLP over the Maritime Continent. With the model unable to simulate the observed shift in SON, this may partly explain why the model cannot simulate a Maritime Continent SLP anomaly in SON 1997 of a similar magnitude to that observed.

The pacemaker experiment also has climatological SSTs in the eastern Pacific roughly 1 °C cooler than the atmosphere-only experiment, due to the necessity for this region to have consistent SSTs with the coupled model (c.f. Fig. 4.9 a and c, see methods). This represents a key distinguishing factor between the two experiments. The cooler SSTs likely lead to a weaker convection response in the pacemaker experiment compared to the atmosphere-only experiment in the Niño3 region. In the observations, deep convection in the tropics tends to initiate when the underlying SSTs are at roughly 27 °C (Gadgil et al., 1984; Johnson and Kosaka, 2016), which is seasonally independent (Fig. 4.9a). In SON 1997 the Niño3 SST was observed to reach 28 °C; this allowed convection anomalies in the Niño3 region to approach DJF 1982-

1983 and 1997-1998 levels (Fig. 4.9a). The CESM atmosphere-only model forced with observed SSTs can simulate a similar convection response to the observed, with the initiation of deep convection at roughly 26.8 °C (Fig. 4.9b). The pacemaker experiment, however, initiated deep convection in the Niño3 region at roughly 25.8 °C, apparently accounting for the 1 °C cooler climatological SST. The convection response to SSTs in the Niño3 region during SON still appears weaker than the atmosphere-only experiment and the observations (c.f. Fig. 4.9 a, b, c). Weaker convection in the Niño3 region may mean a weaker Walker Circulation, which may also reduce the magnitude of the high SLP anomaly over the Maritime Continent during SON 1997.

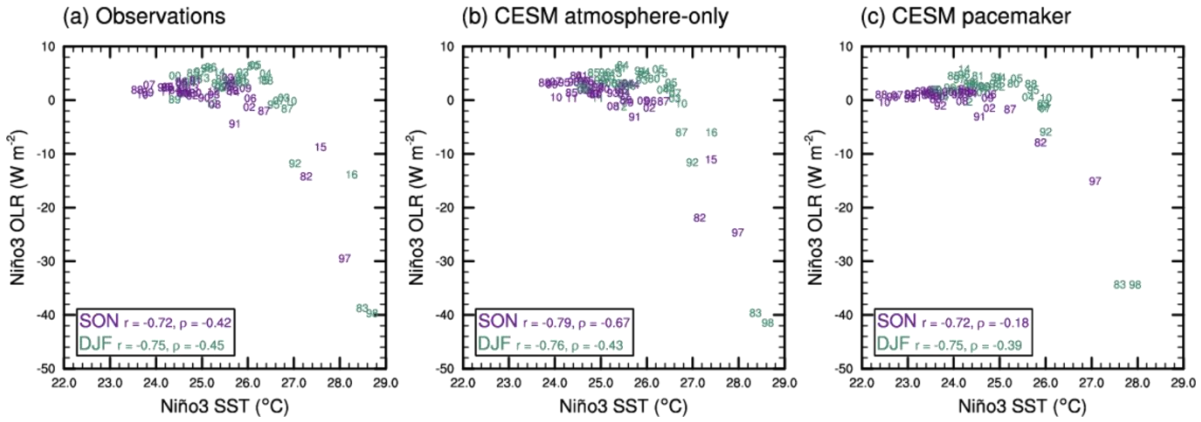

Fig. 4.9: Niño3 OLR anomalies vs. Niño3 SST in (a) observations, (b) CESM atmosphere-only, (c) CESM Tropical Pacific pacemaker experiment. Plotting conventions as in Fig. 4.5.

4.6 Summary and Discussion

The strong, positive SLP anomaly over the Maritime Continent that was observed in the SON of 1997 was the highest on record for that season. The anomaly covered a large area, appearing over the equatorial Indian Ocean and extending into the central equatorial Pacific. The zonal extension was so large that it influenced SLP at Tahiti longitudes. This extension

rendered the Troup Southern Oscillation Index largely ineffective as a metric for changes to the atmospheric circulation associated with El Niño for the 1997 event. From the evidence we have presented in this Chapter, the high SLP over the Maritime Continent was associated with an early maturation of the 1997 El Niño in SON, rather than DJF which is more typical for other strong El Niño events. The warm SSTs in the eastern Pacific in the SON of 1997 drew the location of maximum convection eastward and coincided with an increase in SLP over the Maritime Continent.

Deser and Wallace (1990) showed that the warmer the SSTs in the tropical east Pacific, the further east the location of maximum convection can traverse. In this study we attempted to link this shift to an increase in Maritime Continent SLP. This process is typically observed in strong eastern Pacific type El Niño events in DJF. However, in 1997, we showed that this process occurred in SON. This highlights that the timing of the warm eastern Pacific SSTs anomalies has important repercussions for the atmospheric teleconnections associated with El Niño, such as to east Australian rainfall (Chapter 2; Chapter 3; van Rensch et al., 2015, 2019). The 1997-1998 El Niño was well forecasted by assuming persistence of its early strong SST anomalies (Barnston et al., 1999). However, the impact on east Australian rainfall was not well forecast due to the reliance on statistical relationships at the time. This study shows that the impacts seen in SON 1997 were different to other El Niño events, but in a potentially predictable way. Based on this hypothesis, accurately forecasting the impacts of future El Niño events like that of 1997-1998 could be possible.

The CESM atmosphere-only model simulated a record high SLP over the Maritime Continent in SON of 1997. However, the magnitude of the anomaly was smaller than observed and it was not substantially higher than the simulations of other strong El Niño events in 1982-1983

and 2015-2016. The simulation of the SLP anomaly over the Maritime Continent did not improve in the pacemaker experiment, with the model simulating an air-sea relationship that was too strong over the Maritime Continent. In addition, both experiments could not simulate the eastward shift in maximum tropical Pacific convection to the same distance as observed during SON 1997. The shift in convection was significantly related to SLP over the Maritime Continent in the observations. The reduced simulated shift in convection compared to observations could be a key source of SLP bias in both experiments. The pacemaker experiment also suffers from a problem that is typical of coupled models. This is that the tongue of cold SSTs in the eastern tropical Pacific extends too far west (Bellenger et al., 2014; Taschetto et al., 2014), reducing the efficiency of the convective response to SSTs. In addition to the spatial biases, some coupled models also exhibit biases in the typical onset of El Niño events (Bellenger et al., 2014; Taschetto et al., 2014). Our study shows that the onset bias may then have implications on the teleconnections of strong El Niño events in the Maritime Continent and, subsequently, Australian regions.

The influence of stochastic processes in contributing to the record high Maritime Continent SLP in SON 1997 cannot be ruled out. However, proving this with the current model will be challenging due to the numerous biases already discussed. Based on observations, the SON 1997 SLP anomaly is largely consistent with the observed significant linear relationship between Maritime Continent SLP and both Niño3 SST and the longitude of maximum convection. This indicates a consistent dynamical process for the SON 1997 SLP anomaly, suggesting that if there is an influence from stochastic processes during this event it would likely be small.

Strong El Niño events like 1997-1998 have been projected to increase in frequency in the future due to increased greenhouse gas concentrations (Cai et al., 2014). Likewise, the spatial extent of ENSO teleconnections has also been projected to increase (Perry et al., 2017). Due to the unique features of the 1997-1998 El Niño teleconnection pattern, an assessment of the future strong El Niño teleconnections should be undertaken. However, that study would rely on assessment/improvements of the maximum tropical Pacific convection shift and a further reduction in cold tongue bias in coupled models. In addition, it is unknown how warming SSTs around the Maritime Continent region may influence the local Maritime Continent SLP during strong El Niño events, which may also have implications to the resulting teleconnections.

5 Discussion

This thesis describes how three strong El Niño events influenced east Australian rainfall via different processes, resulting in different rainfall responses in eastern Australia. In this section we will focus on three main findings that arose from this work and their implications for future studies:

1. How the atmosphere reacts, or does not react, to SST forcing is a key factor in determining how east Australian rainfall is modified by an El Niño. This incorporates not only the influence of stochastic forcing, but also how the overlying circulation of either zonal wind, meridional wind, or sea level pressure influences rainfall in different locations.
2. The timing, strength and structure of the SST forcing in the Pacific can have significant implications for the resulting circulation and therefore rainfall over east Australia in SON.
3. The finding that local SSTs can have an influence on the resulting rainfall in east Australia during strong El Niño events.
4. The implications of these results in the study of past and future climate.

Before discussing these main findings, we will discuss a limitation in this work regarding sample size. This study only focused on three strong El Niño events, due to these events being the strongest El Niño events during the satellite era – an era of good data coverage. This study is dependent on the features and processes that occurred during these events. Therefore, it is possible that future strong El Niño events may influence east Australian SON rainfall in a manner that has not yet been observed. We have attempted to mitigate this limitation by using the full observation record when determining typical relationships, such as in analysing

the most important circulation features for rainfall and in investigating the processes related to Maritime Continent SLP increases. Regarding the three El Niño events, we used ensembles of AGCM simulations to reduce any influence from processes unrelated to SSTs, with the important caveat that the models contain biases compared to the observations.

5.1 The role of the atmosphere in teleconnections from SSTs

Atmospheric processes are instrumental in teleconnecting the influence of SSTs to rainfall in east Australia. Additionally, variations within the atmosphere have the potential to produce large rainfall differences between similar El Niño events. Although differences in SSTs between El Niño events have been shown to be important, and will be discussed in following sections, the SST-forced atmosphere contains internal stochastic variability unrelated to SSTs (Sardeshmukh et al., 2000). Stochastic deviations range from the short timescale, from individual weather events (Pook et al., 2006), the influence of the MJO passing through the region (Wheeler et al., 2009), to monthly timescale, such as the SAM (Lim and Hendon, 2015). Based on our modelling, even the three strongest El Niño events of the satellite era could not guarantee a rainfall anomaly of a certain sign. The stochasticity of the atmosphere will always provide a limit to the seasonal forecasting of rainfall, and the circulation, as highlighted by the 2015 event.

Despite the apparent dominance of stochastic processes, this thesis brings a cautionary note on the assumption that any unusual teleconnections are due to stochasticity. There was an assumption that the near average east Australian SON rainfall associated with the 1997 El Niño event was due to stochastic processes (e.g. Walland, 1998), but this did not tell the full story. Our modelling results showed that the SON east Australian rainfall anomaly was SST forced. This highlights that the assumption of stochastic interference in historical

teleconnections should not be assumed. A proper analysis of individual events could result in the discovery of new important processes that have the potential to be applied to future events.

Analysing the east Australian rainfall anomalies during the three El Niño events could not have been possible without understanding how the local atmospheric circulation is related to rainfall on a seasonal timescale. Previous studies of the relationship between climate drivers and rainfall typically analysed the driver-circulation and driver-rainfall link and assumed the associated circulation-rainfall link (e.g. Cai et al., 2011b). However, this thesis has shown that understanding the circulation-rainfall link is crucial for a more complete understanding of the processes relating strong El Niño to rainfall. This is highlighted during the 1997 event, by showing that average east Australian rainfall could occur despite a widespread high SLP anomaly over the region, because the rainfall at this time of year was more closely related to wind direction rather than SLP. Incorporating the link between circulation and rainfall into the analysis of other climate drivers may also provide a greater understanding of processes relating that climate driver to rainfall, potentially improving forecasts. In addition, we showed the performance of GCMs could be assessed by comparing its circulation-rainfall relationship with that observed.

A deficiency of the circulation-rainfall analysis is that it has only been used on a seasonal timescale; further insights could be obtained by analysing sub-seasonal scale relationships. Analysis of large-scale circulation features have been related to synoptic scale systems, such as atmospheric blocking. Blocking in the Tasman has shown a strong relationship with the frequency of cut-off low events in southeast Australia which themselves show detectable decadal variations (Risbey et al., 2013). However, the literature contains limited analysis on

how El Niño events influence weather systems on synoptic or convective scales in Australia. Such analysis could potentially provide a deeper understanding of the underlying mechanisms than presented here.

5.2 Differences between El Niño events

The spatial structure of El Niño, i.e., whether the maximum anomaly is in the central or eastern Pacific, has been shown to have different teleconnections in Australia (Wang and Hendon, 2007; Taschetto and England, 2009; Frauen et al., 2014). Central Pacific El Niño events typically show a greater influence on Australian rainfall than eastern Pacific events (Wang and Hendon, 2007). We showed that other characteristics of El Niño can also cause differing teleconnections to east Australia during SON. Comparison of the strong eastern Pacific El Niño events of 1982 and 1997 highlight that the timing of when strong SSTs occur, and the resulting atmospheric response, are also important.

The 1982-1983 El Niño reached its peak strength during DJF, whereas the 1997 event reached similar magnitudes in SON – one season earlier. As a result, the typical eastward shift of the rising branch of the Walker Circulation seen in El Niño events occurred earlier in the 1997 El Niño event compared to the 1982-1983 event. This early eastward shift in 1997 influenced Maritime Continent SLP, and subsequently, east Australian rainfall. Previous studies have not focussed on the impact of the timing of strong SST anomalies during the 1997 event. However, our results show that the temporal evolution of the event, including the timing of the mature phase, could provide important information for forecasting the impact of future strong El Niño events on east Australian rainfall. A complicating factor is the poorly simulated phasing of the seasonal cycle to El Niño peak in many CMIP5 models (Taschetto et al., 2014; Roy et

al., 2019). This indicates that model improvements are required if we are to utilise this aspect of the El Niño teleconnection.

Model improvements are also required in simulating the shift in convection associated with the rising branch of the Walker Circulation. We found evidence that the eastward shift in convection is related to the increase in SLP anomalies over the Maritime Continent. However, due to the inability of the CESM atmosphere model to simulate an eastward shift similar to that observed, our hypothesis could not be explored robustly. The limited eastward shift appears to be a common feature in other CMIP5 models (Bayr et al., 2018). Whether this has implications on the accuracy of their Maritime Continent SLP requires further exploration.

The idea of pantropical interactions has emerged in the literature, where the interaction of all three tropical ocean basins are used to explain the behaviour of tropical climate variability (Cai et al., 2019). For instance, the IOD has been implicated in both the development (Izumo et al., 2010; Hameed et al., 2018), and termination of El Niño (Kug and Kang, 2006). Further analysis of the behaviour of the IOD during these events may reveal complex interactions with east Australian rainfall. In addition, models should be analysed with these interactions in mind with a view to improve the simulation of these processes.

5.3 SSTs adjacent to Australia influencing the El Niño – east Australian rainfall teleconnection

The SSTs adjacent to Australia have at times received less attention than remote SSTs, in terms of their influence on Australian rainfall during strong El Niño events. The influence of SSTs adjacent to Australia, particularly to the north, has not been unnoticed, with numerous studies finding a relationship between these SSTs and southern Australian rainfall (Nicholls, 1984a, 2010; Watterson, 2010; Timbal and Hendon, 2011). However, the influence of these

adjacent SSTs was typically analysed throughout the historical record, with limited analysis of their impact during ENSO events. This changed after the La Niña of 2010-2011, which showed warmer than normal SSTs surrounding the north of Australia. Evans and Boyer-Souchet (2012) showed these warm SSTs contributed roughly 25 % of the rainfall received in north Australia, a result that later corroborated with Ummenhofer et al. (2015). Whether Australian rainfall was influenced by these adjacent SSTs in other ENSO events was unknown.

In this thesis we have demonstrated that east Australian rainfall associated with strong El Niño events can be influenced by local SSTs. We found that roughly half of the 1982 SST forced east Australian SON rainfall anomaly could be attributed to northeast Australian SSTs, when our analysis in Fig. 3.8 was reframed relative to the 1979-2008 model climatology. The remote SST-forced circulation anomalies during the 1982 El Niño likely contributed the remainder of the rainfall anomaly. This was confirmed in the 1997NEAus1982 experiment which simulated a near average SST-forced circulation, but a SON rainfall deficit approaching that of 1982. This indicates that the SSTs to the northeast of Australia have potential to force an east Australian rainfall anomaly comparable to the remote SST-forced circulation, provided the concurrent seasonal-scale circulation anomalies are weak. These results show that SSTs local to Australia could be employed to provide a more accurate Australian rainfall forecast during strong ENSO events.

Our AGCM analysis indicated that the SSTs adjacent to Australia influence rainfall in east Australia by modifying the availability of moisture. The influence of moisture availability to east Australian rainfall has been explored previously during individual ENSO events. Increased moisture transport was shown to be a contributing factor during the 2010-2011 La Niña (Ummenhofer et al., 2015). In addition, parcel tracking showed less moisture was available

for cut-off low events over the Mallee region during the 1982 El Niño event (Brown et al., 2009). The importance of SSTs adjacent to Australia for moisture availability, and therefore rainfall, in east Australia has not been firmly established. An expansion of the parcel tracking analysis to all years may expose sub-seasonal processes and additional sources of rainfall predictability. This could be particularly useful in combination with the analysis of synoptic systems, e.g. the frequency of east coast lows have been shown to increase with warmer SST anomalies (Pepler et al., 2016b).

5.4 Past and future implications

Our analysis showed it is possible that large El Niño events may not necessarily exhibit a strong rainfall influence in east Australia during SON. Whether a weaker rainfall response similar to that in 1997 SON has occurred in the past during strong El Niño events is not known. Likewise, it is unknown whether an event like that of 1997 can distort the ENSO-Australian rainfall relationship. The relationship has exhibited a transient nature in the past, experiencing periods of strong and weak relationships (McBride and Nicholls, 1983; Gallant et al., 2013; Ashcroft et al., 2016), which has been linked to the Interdecadal Pacific Oscillation (Power et al., 1999; E.-P. Lim et al., 2017). The relationship also experiences an asymmetry, where La Niña events have a greater influence on rainfall than a similar magnitude El Niño (Power et al., 2006). Additionally, other events, such as the 2002 El Niño event, may have the opposite effect, i.e., of strengthening the apparent relationship. The relatively weak 2002 El Niño event was associated with significantly below average SON rainfall to east Australia, but evidence suggests that the below average rainfall was influenced by a concurrent SAM event, which highlights the influence of stochastic variability (Lim and Hendon, 2015). Whether features in

the ENSO-Australian rainfall relationship can be attributed to complexities of individual events remains unknown. If so, this could have implications for paleoclimate studies.

Climate change has the potential to influence El Niño and its teleconnection to east Australian rainfall. Studies using coupled models and future emission scenarios have found that the frequency of strong El Niño events may increase in the future (Cai et al., 2014, 2018), but this is still debated due to the current disconnect between the observed and modelled background SST trend (Lim et al., 2019). The background SST was found to be favourable for the strong El Niño of 1982-1983 and 1997-1998, indicating that this could be important for strong El Niño development (Zhao et al., 2016). There has also been a tendency for El Niño to have its maximum anomaly in the central Pacific since roughly the 1980s (Freund et al., 2019). Whether this is a result of climate change is unknown, but if this trend continues it may make events like 1982 and 1997 less likely.

Teleconnections associated with El Niño may change locations with increased greenhouse gases (Perry et al., 2017). Also, the rainfall received during an El Niño event in Australia has been projected to reduce (Power and Delage, 2018). The positive trend in the SAM could also have an impact on zonal winds, and therefore, ENSO teleconnection (Hendon et al., 2007; Lim et al., 2019), highlighting the tangled web of climate drivers that must be assessed when examining possible rainfall change in Australia. Incorporating the analysis from this thesis into that of future emission scenarios could also prove enlightening.

In addition to the possible changes in El Niño SST structure, our results show that warming trends in local SSTs are also likely to influence east Australian rainfall. Increasing SSTs to the north and northeast of Australia could make cool SSTs like that of SON 1982 less likely – reducing the chance of very low rainfall in east Australian associated with El Niño. The change

in temperature experienced in local Australian SSTs was highlighted in the SST swap experiments where the cold 1982 northeast Australian SSTs was inserted into 2015 global SSTs. Although the moisture response was as expected, there was a small region of significant circulation change compared to the 2015 control simulation. The circulation change was likely associated with an enhanced local SST gradient as a result of the large SST temperature differences between the two periods. This highlights the dramatic change in temperature experienced during our period of analysis, and may indicate that climate change could already be influencing the teleconnection between east Australian rainfall and El Niño, however this requires further research.

6 Conclusion

In this thesis, we investigated the mechanisms associated with the teleconnection of three strong El Niño events to east Australian SON rainfall. In doing so we covered the main aspects involved in connecting an El Niño SST anomaly in the Pacific with rainfall in east Australia. Firstly, the timing, spatial structure and magnitude of the El Niño SST pattern in the Pacific can modify the circulation in the Australian region. In addition, the SSTs local to Australia can also act to modify rainfall. Secondly, the circulation of the atmosphere can be modified by stochastic interference; and finally, the resulting rainfall is dependent on the most important localised circulation features for rainfall. The following summarises the thesis main results.

Using the atmosphere-only experiments from CMIP5, we showed that the rainfall received in both SON 1997 and 1982 were likely forced by sea surface temperatures rather than a stochastic atmosphere. The CMIP5 multi-model ensemble mean simulated near average rainfall in 1997, with less than average rainfall simulated in 1982, but not to the same magnitude as observed. We used ACCESS to include the 2015 event, by running a 60-member atmosphere-only experiment for each of the three strong El Niño events. The ACCESS model simulated consistent rainfall anomalies to observations for 1982, 1997, and 2015 events. In addition, the simulated SLP pattern associated with the 1982 and 1997 SSTs was consistent with observations, but weaker in magnitude. The simulated circulation pattern associated with 2015 SSTs was similar to the 1982 event, whereas the observations showed a more widespread and strongly positive SLP anomaly over southern Australia. This suggests either the atmosphere was highly influenced by stochastic processes in 2015, or the model was not able to simulate an SST-related process.

The SSTs adjacent to Australia were assessed for their importance to the east Australian SON rainfall anomalies during the 1982 and 1997 events. The SSTs were significantly cooler than average in the region off the northeast and northern coasts of Australia during 1982, whereas in 1997 the SSTs in these regions were near average. Partial correlations using observed data showed a relationship between the local SSTs and southeast Australian rainfall when ENSO is excluded. The region to the northeast of Australia showed the greater influence, particularly when the influence of a stochastic atmosphere is minimised using the CMIP5 ensemble mean rainfall. We performed targeted experiments using the ACCESS model where we swapped the SSTs in the northeast and north between the three strong El Niño events. The experiments showed that the northeast Australian SSTs during SON 1982 further reduced the rainfall by roughly 17-21%, whereas north Australian SSTs reduced rainfall by roughly 9%. The ACCESS results showed that local SSTs influenced rainfall through modifying moisture availability in the sub-seasonal flow, and the SSTs had no significant influence on the seasonal-scale circulation. Despite the strong influence of these SSTs, they could not fully explain the rainfall anomalies in these years, suggesting other factors were also important.

The atmospheric circulation during SON of 1982 and 1997 were SST-forced, but not from SSTs local to Australia. Both events were associated with a positive SLP anomaly off the southern coast of Australia, which is typical of El Niño events, yet they still resulted in different rainfall anomalies. To understand what aspect of the seasonal circulation was important for SON rainfall, we used localised multiple regression to determine whether SLP, zonal, or meridional wind is most important for rainfall. We found SLP was most important for rainfall in the southern regions of east Australia; zonal wind was most important for rainfall along the southern and central east Australian coast, following the Great Dividing Range; and meridional wind was most important in the remainder of eastern Australia. Applying this to

the circulation of 1982 showed the high pressure and the significantly strong southeasterly wind anomalies produced ideal conditions for significant rainfall deficits. Whereas the circulation associated with the 1997 saw a spatially uniform positive SLP anomaly throughout east Australia, but near average wind anomalies – leading to near average rainfall in most of the region. The positive SLP anomaly over eastern Australia in SON 1997 was the result of the El Niño-typical positive SLP to the south of Australia combining with a significantly positive SLP to the north of Australia centred over the Maritime Continent.

The 1997 SON Maritime Continent SLP was a record high for that season, with the anomaly extending to the eastern pole of the Southern Oscillation Index, rendering the index incapable of capturing this extreme event. A Maritime Continent SLP of similar magnitude was observed in the DJF seasons of 1982-1983 and 1997-1998. We deduce that this record high SON Maritime Continent SLP was due to the 1997 El Niño peaking stronger earlier than any other El Niño in the satellite era. SON SSTs in the eastern tropical Pacific were also record high, inducing convection and shifting the maximum tropical Pacific convection the furthest east during SON in the satellite era. With the maximum convection so far east, away from its typical location near the Maritime Continent, this allowed the SLP to increase in the Maritime Continent region. Confirming this process in general circulation models proved challenging. ACCESS simulated a stronger positive SON Maritime Continent SLP anomaly in 1997 than in 1982 and 2015, but not to the same magnitude as observed. CESM also struggled to simulate the magnitude of the Maritime Continent SON SLP anomaly when forced with 1997 SSTs. We show that the CESM atmosphere model was unable to shift the maximum convection anomaly far enough east in SON, possibly prohibiting the build-up of SLP in the Maritime Continent region. Introducing coupling between atmosphere and ocean in all regions but the tropical central and eastern Pacific did not improve the processes in the model. This suggests

a deficiency in the atmosphere model prevented the simulation of the record strong SON Maritime Continent SLP anomaly to the same extent as observed.

7 References

Adler, R.F., Huffman, G.J., Chang, A., Ferraro, R., Xie, P.-P., Janowiak, J., Rudolf, B., Schneider, U., Curtis, S., Bolvin, D., Gruber, A., Susskind, J., Arkin, P., Nelkin, E., 2003. The version-2 global precipitation climatology project (GPCP) monthly precipitation analysis (1979-present). J. Hydrometeorol. 4, 1147–1167.

Allan, R., Ansell, T., 2006. A New Globally Complete Monthly Historical Gridded Mean Sea Level Pressure Dataset (HadSLP2): 1850–2004. J. Clim. 19, 5816–5842. https://doi.org/10.1175/JCLI3937.1

Angell, J.K., 2000. Tropospheric temperature variations adjusted for El Niño, 1958-1998. J. Geophys. Res. Atmospheres 105, 11841–11849. https://doi.org/10.1029/2000JD900044

Ashcroft, L., Gergis, J., Karoly, D.J., 2016. Long-term stationarity of El Niño–Southern Oscillation teleconnections in southeastern Australia. Clim. Dyn. 46, 2991–3006. https://doi.org/10.1007/s00382-015-2746-3

Ashok, K., Behera, S.K., Rao, S.A., Weng, H., Yamagata, T., 2007. El Niño Modoki and its possible teleconnection. J. Geophys. Res. 112. https://doi.org/10.1029/2006JC003798

Barber, R.T., Chavez, F.P., 1983. Biological Consequences of El Niño. Science 222, 1203–1210. https://doi.org/10.1126/science.222.4629.1203

Barnston, A.G., Glantz, M.H., He, Y., 1999. Predictive Skill of Statistical and Dynamical Climate Models in SST Forecasts during the 1997-98 El Niño Episode and the 1998 La Niña Onset. Bull. Am. Meteorol. Soc. 80, 28.

Bayr, T., Latif, M., Dommenget, D., Wengel, C., Harlaß, J., Park, W., 2018. Mean-state dependence of ENSO atmospheric feedbacks in climate models. Clim. Dyn. 50, 3171–3194. https://doi.org/10.1007/s00382-017-3799-2

Bellenger, H., Guilyardi, E., Leloup, J., Lengaigne, M., Vialard, J., 2014. ENSO representation in climate models: from CMIP3 to CMIP5. Clim. Dyn. 42, 1999–2018. https://doi.org/10.1007/s00382-013-1783-z

Bi, D., Dix, M., Marsland, S., O'Farrell, S., Rashid, H., Uotila, P., Hirst, A., Kowalczyk, E., Golebiewski, M., Sullivan, A., Yan, H., Hannah, N., Franklin, C., Sun, Z., Vohralik, P., Watterson, I., Zhou, X., Fiedler, R., Collier, M., Ma, Y., Noonan, J., Stevens, L., Uhe, P., Zhu, H., Griffies, S., Hill, R., Harris, C., Puri, K., 2013. The ACCESS coupled model: description, control climate and evaluation. Aust. Meteorol. Oceanogr. J. 63, 41–64. https://doi.org/10.22499/2.6301.004

Bjerknes, J., 1966. A possible response of the atmospheric Hadley circulation to equatorial anomalies of ocean temperature. Tellus 18, 820–829. https://doi.org/10.1111/j.2153-3490.1966.tb00303.x

Bjerknes, J., 1969. Atmospheric Teleconnections from The Equatorial Pacific. Mon. Weather Rev. 97, 163–172.

Boer, G.J., Smith, D.M., Cassou, C., Doblas-Reyes, F., Danabasoglu, G., Kirtman, B., Kushnir, Y., Kimoto, M., Meehl, G.A., Msadek, R., Mueller, W.A., Taylor, K.E., Zwiers, F., Rixen, M., Ruprich-Robert, Y., Eade, R., 2016. The Decadal Climate Prediction Project (DCPP) contribution to CMIP6. Geosci. Model Dev. 9, 3751–3777. https://doi.org/10.5194/gmd-9-3751-2016

Boulanger, J.-P., Menkes, C., Lengaigne, M., 2004. Role of high- and low-frequency winds and wave reflection in the onset, growth and termination of the 1997-1998 El Niño. Clim. Dyn. 22, 267–280. https://doi.org/10.1007/s00382-003-0383-8

Brown, J.N., McIntosh, P.C., Pook, M.J., Risbey, J.S., 2009. An Investigation of the Links between ENSO Flavors and Rainfall Processes in Southeastern Australia. Mon. Weather Rev. 137, 3786–3795. https://doi.org/10.1175/2009MWR3066.1

Cai, W., Borlace, S., Lengaigne, M., van Rensch, P., Collins, M., Vecchi, G., Timmermann, A., Santoso, A., McPhaden, M.J., Wu, L., England, M.H., Wang, G., Guilyardi, E., Jin, F.-F., 2014. Increasing frequency of extreme El Niño events due to greenhouse warming. Nat. Clim. Change 4, 111–116. https://doi.org/10.1038/nclimate2100

Cai, W., Lengaigne, M., Borlace, S., Collins, M., Cowan, T., McPhaden, M.J., Timmermann, A., Power, S., Brown, J., Menkes, C., Ngari, A., Vincent, E.M., Widlansky, M.J., 2012. More extreme swings of the South Pacific convergence zone due to greenhouse warming. Nature 488, 365–369. https://doi.org/10.1038/nature11358

Cai, W., van Rensch, P., Cowan, T., 2011a. Influence of Global-Scale Variability on the Subtropical Ridge over Southeast Australia. J. Clim. 24, 6035–6053. https://doi.org/10.1175/2011JCLI4149.1

Cai, W., van Rensch, P., Cowan, T., Hendon, H.H., 2011b. Teleconnection Pathways of ENSO and the IOD and the Mechanisms for Impacts on Australian Rainfall. J. Clim. 24, 3910–3923. https://doi.org/10.1175/2011JCLI4129.1

Cai, W., van Rensch, P., Cowan, T., Sullivan, A., 2010. Asymmetry in ENSO Teleconnection with Regional Rainfall, Its Multidecadal Variability, and Impact. J. Clim. 23, 4944–4955. https://doi.org/10.1175/2010JCLI3501.1

Cai, W., Wang, G., Dewitte, B., Wu, L., Santoso, A., Takahashi, K., Yang, Y., Carréric, A., McPhaden, M.J., 2018. Increased variability of eastern Pacific El Niño under greenhouse warming. Nature 564, 201–206. https://doi.org/10.1038/s41586-018-0776-9

Cai, W., Wu, L., Lengaigne, M., Li, T., McGregor, S., Kug, J.-S., Yu, J.-Y., Stuecker, M.F., Santoso, A., Li, X., Ham, Y.-G., Chikamoto, Y., Ng, B., McPhaden, M.J., Du, Y., Dommenget, D., Jia, F., Kajtar, J.B., Keenlyside, N., Lin, X., Luo, J.-J., Martín-Rey, M., Ruprich-Robert, Y., Wang, G., Xie, S.-P., Yang, Y., Kang, S.M., Choi, J.-Y., Gan, B., Kim, G.-I., Kim, C.-E., Kim, S., Kim, J.-H., Chang, P., 2019. Pantropical climate interactions. Science 363, eaav4236. https://doi.org/10.1126/science.aav4236

Chen, H.-C., Jin, F.-F., 2019. Fundamental Behavior of ENSO phase-locking. J. Clim. JCLI-D-19-0264.1. https://doi.org/10.1175/JCLI-D-19-0264.1

Chung, C., Power, S., 2017. The non-linear impact of El Niño, La Niña and the Southern Oscillation on seasonal and regional Australian precipitation. J. South. Hemisphere Earth Syst. Sci. 67, 25–45. https://doi.org/10.22499/3.6701.003

Dee, D.P., Uppala, S.M., Simmons, A.J., Berrisford, P., Poli, P., Kobayashi, S., Andrae, U., Balmaseda, M.A., Balsamo, G., Bauer, P., Bechtold, P., Beljaars, A.C.M., van de Berg, L., Bidlot, J., Bormann, N., Delsol, C., Dragani, R., Fuentes, M., Geer, A.J., Haimberger, L., Healy, S.B., Hersbach, H., Hólm, E.V., Isaksen, L., Kållberg, P., Köhler, M., Matricardi, M., McNally, A.P., Monge-Sanz, B.M., Morcrette, J.-J., Park, B.-K., Peubey, C., de Rosnay, P., Tavolato, C., Thépaut, J.-N., Vitart, F., 2011. The ERA-Interim reanalysis: configuration and performance of the data assimilation system. Q. J. R. Meteorol. Soc. 137, 553–597. https://doi.org/10.1002/qj.828

Deser, C., Simpson, I.R., McKinnon, K.A., Phillips, A.S., 2017. The Northern Hemisphere Extratropical Atmospheric Circulation Response to ENSO: How Well Do We Know It and How Do We Evaluate Models Accordingly? J. Clim. 30, 5059–5082. https://doi.org/10.1175/JCLI-D-16-0844.1

Deser, C., Wallace, J.M., 1990. Large-Scale Atmospheric Circulation Features of Warm and Cold Episodes in the Tropical Pacific. J. Clim. 3, 1254–1281.

DiNezio, P.N., Deser, C., Karspeck, A., Yeager, S., Okumura, Y., Danabasoglu, G., Rosenbloom, N., Caron, J., Meehl, G.A., 2017. A 2 Year Forecast for a 60–80% Chance of La Niña in 2017–2018. Geophys. Res. Lett. 44, 11,624-11,635. https://doi.org/10.1002/2017GL074904

Dix, M.R., Hunt, B.G., 1995. Chaotic influences and the problem of deterministic seasonal predictions. Int. J. Climatol. 15, 729–752. https://doi.org/10.1002/joc.3370150703

Dommenget, D., Bayr, T., Frauen, C., 2013. Analysis of the non-linearity in the pattern and time evolution of El Niño southern oscillation. Clim. Dyn. 40, 2825–2847. https://doi.org/10.1007/s00382-012-1475-0

Durack, P.J., Taylor, K.E., 2018. PCMDI AMIP SST and sea-ice boundary conditions version 1.1.4. Version 1.1.0a. Earth Syst. Grid Fed. https://doi.org/10.22033/ESGF/input4MIPs.2204

Evans, J.P., Boyer-Souchet, I., 2012. Local sea surface temperatures add to extreme precipitation in northeast Australia during La Niña. Geophys. Res. Lett. 39. https://doi.org/10.1029/2012GL052014

Frauen, C., Dommenget, D., Tyrrell, N., Rezny, M., Wales, S., 2014. Analysis of the Nonlinearity of El Niño–Southern Oscillation Teleconnections. J. Clim. 27, 6225–6244.

Frederiksen, C.S., Zhang, H., Balgovind, R.C., Nicholls, N., Drosdowsky, W., Chambers, L., 2001. Dynamical Seasonal Forecasts during the 1997/98 ENSO Using Persisted SST Anomalies. J. Clim. 14, 21.

Freund, M.B., Henley, B.J., Karoly, D.J., McGregor, H.V., Abram, N.J., Dommenget, D., 2019. Higher frequency of Central Pacific El Niño events in recent decades relative to past centuries. Nat. Geosci. 12, 450–455. https://doi.org/10.1038/s41561-019-0353-3

Gadgil, S., Joseph, P.V., Joshi, N.V., 1984. Ocean–atmosphere coupling over monsoon regions. Nature 312, 141–143. https://doi.org/10.1038/312141a0

Gallant, A.J.E., Phipps, S.J., Karoly, D.J., Mullan, A.B., Lorrey, A.M., 2013. Nonstationary Australasian Teleconnections and Implications for Paleoclimate Reconstructions. J. Clim. 26, 8827–8849. https://doi.org/10.1175/JCLI-D-12-00338.1

Geng, X., Zhang, W., Stuecker, M.F., Jin, F.-F., 2017. Strong sub-seasonal wintertime cooling over East Asia and Northern Europe associated with super El Niño events. Sci. Rep. 7, 3770. https://doi.org/10.1038/s41598-017-03977-2

Grötzner, A., Latif, M., Dommenget, D., 2000. Atmospheric response to sea surface temperature anomalies during El Niño 1997/98 as simulated by ECHAM4. Q. J. R. Meteorol. Soc. 126, 2175–2198.

Hamada, J.-I., Mori, S., Kubota, H., Yamanaka, M.D., Haryoko, U., Lestari, S., Sulistyowati, R., Syamsudin, F., 2012. Interannual Rainfall Variability over Northwestern Jawa and its Relation to the Indian Ocean Dipole and El Niño-Southern Oscillation Events. SOLA 8, 69–72. https://doi.org/10.2151/sola.2012-018

Hameed, S.N., Jin, D., Thilakan, V., 2018. A model for super El Niños. Nat. Commun. 9, 2528. https://doi.org/10.1038/s41467-018-04803-7

Harris, S., Lucas, C., 2019. Understanding the variability of Australian fire weather between 1973 and 2017. PLOS ONE 14, e0222328. https://doi.org/10.1371/journal.pone.0222328

Harrison, D.E., Vecchi, G.A., 1999. On the termination of El Niño. Geophys. Res. Lett. 26, 1593–1596. https://doi.org/10.1029/1999GL900316

Hendon, H.H., 2003. Indonesian rainfall variability: Impacts of ENSO and local air-sea interaction. J. Clim. 16, 1775–1790.

Hendon, H.H., Thompson, D.W.J., Wheeler, M.C., 2007. Australian Rainfall and Surface Temperature Variations Associated with the Southern Hemisphere Annular Mode. J. Clim. 20, 2452–2467. https://doi.org/10.1175/JCLI4134.1

Hoerling, M.P., Kumar, A., Zhong, M., 1997. El Niño, La Niña, and the Nonlinearity of Their Teleconnections. J. Clim. 10, 18.

Horel, J.D., Wallace, J.M., 1981. Planetary-Scale Atmospheric Phenomena Associated with the Southern Oscillation. Mon. Weather Rev. 109, 813–829.

Hoskins, B.J., Karoly, D.J., 1981. The steady linear response of a spherical atmosphere to thermal and orographic forcing. J. Atmospheric Sci. 38, 1179–1196.

Huang, B., L'Heureux, M., Hu, Z.-Z., Zhang, H.-M., 2016. Ranking the strongest ENSO events while incorporating SST uncertainty. Geophys. Res. Lett. 43, 9165–9172. https://doi.org/10.1002/2016GL070888

Hurrell, J.W., Hack, J.J., Shea, D., Caron, J.M., Rosinski, J., 2008. A New Sea Surface Temperature and Sea Ice Boundary Dataset for the Community Atmosphere Model. J. Clim. 21, 5145–5153. https://doi.org/10.1175/2008JCLI2292.1

Hurrell, J.W., Holland, M.M., Gent, P.R., Ghan, S., Kay, J.E., Kushner, P.J., 2013. The Community Earth System Model 22.

Indeje, M., Semazzi, F.H.M., Ogallo, L.J., 2000. ENSO signals in East African rainfall seasons. Int J Clim. 28.

Izumo, T., Vialard, J., Lengaigne, M., de Boyer Montegut, C., Behera, S.K., Luo, J.-J., Cravatte, S., Masson, S., Yamagata, T., 2010. Influence of the state of the Indian Ocean Dipole on the following year's El Niño. Nat. Geosci. 3, 168–172. https://doi.org/10.1038/ngeo760

Jin, F.-F., 1997. An Equatorial Ocean Recharge Paradigm for ENSO. Part I: Conceptual Model. J. Atmospheric Sci. 54, 19.

Johnson, N.C., Kosaka, Y., 2016. The impact of eastern equatorial Pacific convection on the diversity of boreal winter El Niño teleconnection patterns. Clim. Dyn. 47, 3737–3765. https://doi.org/10.1007/s00382-016-3039-1

Jones, D., Wang, W., Fawcett, R., 2009. High-quality spatial climate data-sets for Australia. Aust. Meteorol. Oceanogr. J. 58, 233–248. https://doi.org/10.22499/2.5804.003

Kalnay, E., Kanamitsu, M., Kistler, R., Collins, W., Deaven, D., Gandin, L., Iredell, M., Saha, S., White, G., Woollen, J., Zhu, Y., Chelliah, M., Ebisuzaki, W., Higgins, W., Janowiak, J., Mo, K.C., Ropelewski, C., Wang, J., Leetmaa, A., Reynolds, R., Jenne, R., Joseph, D., 1996. The NCEP-NCAR 40-Year Reanalysis Project. Bull Amer Meteor Soc 77, 437–471.

Kang, I.-S., Jin, K., Lau, K.-M., Shukla, J., Krishnamurthy, V., Schubert, S.D., Waliser, D.E., Stern, W.F., Satyan, V., Kitoh, A., Meehl, G.A., Kanamitsu, M., Galin, V.Ya., Sumi, A., Wu, G., Liu, Y., Kim, J.-K., 2002. Intercomparison of Atmospheric GCM Simulated Anomalies Associated with the 1997-98 El Niño. J. Clim. 15, 2791–2805.

Kao, H.-Y., Yu, J.-Y., 2009. Contrasting Eastern-Pacific and Central-Pacific Types of ENSO. J. Clim. 22, 615–632. https://doi.org/10.1175/2008JCLI2309.1

Karoly, D.J., 1989. Southern hemisphere circulation features associated with El Niño-Southern Oscillation events. J. Clim. 2, 1239–1252.

Karoly, D.J., Black, M.T., Grose, M.R., King, A.D., 2016. The Roles of Climate Change and El Niño in the Record Low Rainfall in October 2015 in Tasmania, Australia [in "Explaining Extremes of 2015 from a Climate Perspective"]. Bull Amer Meteor Soc 97, S127–S130. https://doi.org/10.1175/BAMS-D-16-0139.1

Katsafados, P., Papadopoulos, A., Kallos, G., 2005. Regional atmospheric response to tropical Pacific SST perturbations. Geophys. Res. Lett. 32, n/a-n/a. https://doi.org/10.1029/2004GL021828

Kessler, W.S., 2002. Is ENSO a cycle or a series of events? Geophys. Res. Lett. 29, 40-1-40–4. https://doi.org/10.1029/2002GL015924

Kidson, J.W., Renwick, J.A., 2002. Patterns of convection in the tropical pacific and their influence on New Zealand weather. Int. J. Climatol. 22, 151–174. https://doi.org/10.1002/joc.737

Kiladis, G.N., Diaz, H.F., 1989. Global Climatic Anomalies Associated with Extremes in the Southern Oscillation. J. Clim. 2, 1069–1090.

King, A.D., Donat, M.G., Alexander, L.V., Karoly, D.J., 2015. The ENSO-Australian rainfall teleconnection in reanalysis and CMIP5. Clim. Dyn. 44, 2623–2635. https://doi.org/10.1007/s00382-014-2159-8

Kug, J.-S., Jin, F.-F., An, S.-I., 2009. Two Types of El Niño Events: Cold Tongue El Niño and Warm Pool El Niño. J. Clim. 22, 1499–1515. https://doi.org/10.1175/2008JCLI2624.1

Kug, J.-S., Kang, I.-S., 2006. Interactive Feedback between ENSO and the Indian Ocean. J. Clim. 19, 1784–1801. https://doi.org/10.1175/JCLI3660.1

Kumar, K.K., Rajagopalan, B., Hoerling, M.P., Bates, G., Cane, M., 2006. Unraveling the Mystery of Indian Monsoon Failure During El Niño. Science 314, 115–119.

Landsea, C.W., Knaff, J.A., 2000. How Much Skill Was There in Forecasting the Very Strong 1997–98 El Niño. Bull Amer Meteor Soc 81, 2107–2119.

Larsen, S.H., Nicholls, N., 2009. Southern Australian rainfall and the subtropical ridge: Variations, interrelationships, and trends. Geophys. Res. Lett. 36, L08708. https://doi.org/10.1029/2009GL037786

Lee, S., 2012. Testing of the Tropically Excited Arctic Warming Mechanism (TEAM) with Traditional El Niño and La Niña. J. Clim. 25, 4015–4022. https://doi.org/10.1175/JCLI-D-12-00055.1

Lengaigne, M., Guilyardi, E., Boulanger, J.-P., Menkes, C., Delecluse, P., Inness, P., Cole, J., Slingo, J., 2004. Triggering of El Niño by westerly wind events in a coupled general circulation model. Clim. Dyn. 23, 601–620. https://doi.org/10.1007/s00382-004-0457-2

Lestari, S., King, A., Vincent, C., Karoly, D., Protat, A., 2019. Seasonal dependence of rainfall extremes in and around Jakarta, Indonesia. Weather Clim. Extrem. 24, 100202. https://doi.org/10.1016/j.wace.2019.100202

L'Heureux, M.L., Thompson, D.W.J., 2006. Observed Relationships between the El Niño–Southern Oscillation and the Extratropical Zonal-Mean Circulation. J. Clim. 19, 276–287. https://doi.org/10.1175/JCLI3617.1

L'Heureux, M.L., Tippett, M.K., Barnston, A.G., 2015. Characterizing ENSO Coupled Variability and Its Impact on North American Seasonal Precipitation and Temperature. J. Clim. 28, 4231–4245. https://doi.org/10.1175/JCLI-D-14-00508.1

Liebmann, B., Smith, C.A., 1996. Description of a Complete (Interpolated) Outgoing Longwave Radiation Dataset. Bull Amer Meteor Soc 77, 1275–1277.

Lim, E.-P., Hendon, H.H., 2015. Understanding the Contrast of Australian Springtime Rainfall of 1997 and 2002 in the Frame of Two Flavors of El Niño. J. Clim. 28, 2804–2822. https://doi.org/10.1175/JCLI-D-14-00582.1

Lim, E.-P., Hendon, H.H., Hope, P., Chung, C., Delage, F., McPhaden, M.J., 2019. Continuation of tropical Pacific Ocean temperature trend may weaken extreme El Niño and its linkage to the Southern Annular Mode. Sci. Rep. 9, 17044. https://doi.org/10.1038/s41598-019-53371-3

Lim, E.-P., Hendon, H.H., Zhao, M., Yin, Y., 2017. Inter-decadal variations in the linkages between ENSO, the IOD and south-eastern Australian springtime rainfall in the past 30 years. Clim. Dyn. 49, 97–112. https://doi.org/10.1007/s00382-016-3328-8

Lim, Y.-K., Kovach, R.M., Pawson, S., Vernieres, G., 2017. The 2015/16 El Niño Event in Context of the MERRA-2 Reanalysis: A Comparison of the Tropical Pacific with 1982/83 and 1997/98. J. Clim. 30, 4819–4842. https://doi.org/10.1175/JCLI-D-16-0800.1

Marshall, G.J., 2003. Trends in the Southern Annular Mode from Observations and Reanalyses. J. Clim. 16, 4134–4143. https://doi.org/10.1175/1520-0442(2003)016<4134:TITSAM>2.0.CO;2

McBride, J.L., Nicholls, N., 1983. Seasonal Relationships between Australian Rainfall and the Southern Oscillation. Mon. Weather Rev. 111, 1998–2004.

McIntosh, P.C., Hendon, H.H., 2018. Understanding Rossby wave trains forced by the Indian Ocean Dipole. Clim. Dyn. 50, 2783–2798. https://doi.org/10.1007/s00382-017-3771-1

McPhaden, M.J., 1999. Genesis and Evolution of the 1997-98 El Niño. Science 283, 950–954. https://doi.org/10.1126/science.283.5404.950

Murphy, B.F., Power, S.B., McGree, S., 2014. The Varied Impacts of El Niño–Southern Oscillation on Pacific Island Climates. J. Clim. 27, 4015–4036. https://doi.org/10.1175/JCLI-D-13-00130.1

Nicholls, N., 1984a. Seasonal relationships between Australian rainfall and North Australian sea surface temperature, in: Extended Abstracts, Conference on Australian Rainfall Variability, 6-8 August 1984, Arkaroola, Part 2. Australian Academy of Science, Canberra, Australia, pp. 71–73.

Nicholls, N., 1984b. The Southern Oscillation, sea-surface-temperature, and interannual fluctuations in Australian tropical cyclone activity. J. Climatol. 4, 661–670.

Nicholls, N., 1984c. The Southern Oscillation and Indonesian sea surface temperature. Mon. Weather Rev. 112, 424–432.

Nicholls, N., 1989. Sea surface temperature and Australian winter rainfall. J. Clim. 2, 965–973.

Nicholls, N., 2010. Local and remote causes of the southern Australian autumn-winter rainfall decline, 1958–2007. Clim. Dyn. 34, 835–845. https://doi.org/10.1007/s00382-009-0527-6

Nicholls, N., Kariko, A., 1993. East Australian rainfall events, Interannual variations, trends, and relationships with the Southern Oscillation. J. Clim. 6, 1141–1152.

O'Kane, T.J., Monselesan, D.P., Risbey, J.S., 2017. A Multiscale Reexamination of the Pacific–South American Pattern. Mon. Weather Rev. 145, 379–402. https://doi.org/10.1175/MWR-D-16-0291.1

O'Kane, T.J., Squire, D.T., Sandery, P.A., Kitsios, V., Matear, R.J., Moore, T.S., Risbey, J.S., Watterson, I.G., 2020. Enhanced ENSO Prediction via Augmentation of Multimodel Ensembles with Initial Thermocline Perturbations. J. Clim. 33, 2281–2293. https://doi.org/10.1175/JCLI-D-19-0444.1

Okumura, Y.M., Deser, C., 2010. Asymmetry in the Duration of El Niño and La Niña. J. Clim. 23, 5826–5843. https://doi.org/10.1175/2010JCLI3592.1

Pan, X., Chin, M., Ichoku, C.M., Field, R.D., 2018. Connecting Indonesian Fires and Drought With the Type of El Niño and Phase of the Indian Ocean Dipole During 1979-2016. J. Geophys. Res. Atmospheres. https://doi.org/10.1029/2018JD028402

Pepler, A., Coutts-Smith, A., Bertrand Timbal, 2014. The role of East Coast Lows on rainfall patterns and inter-annual variability across the East Coast of Australia. Int J Clim. 34, 1011–1021.

Pepler, A.S., Alexander, L.V., Evans, J.P., Sherwood, S.C., 2016a. Zonal winds and southeast Australian rainfall in global and regional climate models. Clim. Dyn. 46, 123–133. https://doi.org/10.1007/s00382-015-2573-6

Pepler, A.S., Alexander, L.V., Evans, J.P., Sherwood, S.C., 2016b. The influence of local sea surface temperatures on Australian east coast cyclones: SSTS AND AUSTRALIAN EAST COAST CYCLONES. J. Geophys. Res. Atmospheres 121, 13,352-13,363. https://doi.org/10.1002/2016JD025495

Perry, S.J., McGregor, S., Gupta, A.S., England, M.H., 2017. Future Changes to El Niño-Southern Oscillation Temperature and Precipitation Teleconnections: Future Changes to Teleconnections. Geophys. Res. Lett. 44, 10,608-10,616. https://doi.org/10.1002/2017GL074509

Pook, M.J., McIntosh, P.C., Meyers, G.A., 2006. The Synoptic Decomposition of Cool-Season Rainfall in the Southeastern Australian Cropping Region. J. Appl. Meteorol. Climatol. 45, 1156–1170. https://doi.org/10.1175/JAM2394.1

Power, S., Casey, T., Folland, C., Colman, A., Mehta, V., 1999. Inter-decadal modulation of the impact of ENSO on Australia. Clim. Dyn. 15, 319–324. https://doi.org/10.1007/s003820050284

Power, S., Haylock, M., Colman, R., Wang, X., 2006. The Predictability of Interdecadal Changes in ENSO Activity and ENSO Teleconnections. J. Clim. 19, 4755–4771. https://doi.org/10.1175/JCLI3868.1

Power, S.B., Delage, F.P.D., 2018. El Niño–Southern Oscillation and Associated Climatic Conditions around the World during the Latter Half of the Twenty-First Century. J. Clim. 31, 6189–6207. https://doi.org/10.1175/JCLI-D-18-0138.1

Pui, A., Sharma, A., Santoso, A., Westra, S., 2012. Impact of the El Niño–Southern Oscillation, Indian Ocean Dipole, and Southern Annular Mode on Daily to Subdaily Rainfall Characteristics in East Australia. Mon. Weather Rev. 140, 1665–1682. https://doi.org/10.1175/MWR-D-11-00238.1

Quayle, E.T., 1929. Long-range rainfall forecasting from tropical (Darwin) air pressure. Proc Roy Soc Vic. 41, 160–164.

Rakich, C.S., Holbrook, N.J., Timbal, B., 2008. A pressure gradient metric capturing planetary-scale influences on eastern Australian rainfall. Geophys. Res. Lett. 35. https://doi.org/10.1029/2007GL032970

Rasmusson, E.M., Carpenter, T.H., 1982. Variations in Tropical Sea Surface Temperature and Surface Wind Fields Associated with the Southern Oscillation El Niño. Mon. Weather Rev. 110, 354–384.

Rasmusson, E.M., Wallace, J.M., 1983. Meteorological aspects of the El Niño-Southern Oscillation. Science 222, 1195–1202.

Renwick, J.A., 2002. Southern Hemisphere Circulation and Relations with Sea Ice and Sea Surface Temperature. J. Clim. 15, 11.

Risbey, J.S., McIntosh, P.C., Pook, M.J., 2013. Synoptic components of rainfall variability and trends in southeast Australia: SYNOPTIC COMPONENTS OF RAINFALL VARIABILITY. Int. J. Climatol. 33, 2459–2472. https://doi.org/10.1002/joc.3597

Risbey, J.S., Pook, M.J., McIntosh, P.C., Ummenhofer, C.C., Meyers, G., 2009a. Characteristics and variability of synoptic features associated with cool season rainfall in southeastern Australia. Int. J. Climatol. 29, 1595–1613. https://doi.org/10.1002/joc.1775

Risbey, J.S., Pook, M.J., McIntosh, P.C., Wheeler, M.C., Hendon, H.H., 2009b. On the Remote Drivers of Rainfall Variability in Australia. Mon. Weather Rev. 137, 3233–3253. https://doi.org/10.1175/2009MWR2861.1

Ropelewski, C.F., Halpert, M.S., 1987. Global and Regional Scale Precipitation Patterns Associated with the El Niño/Southern Oscillation. Mon. Weather Rev. 115, 1606–1626.

Roy, I., Gagnon, A.S., Siingh, D., 2019. Evaluating ENSO teleconnections using observations and CMIP5 models. Theor. Appl. Climatol. 136, 1085–1098. https://doi.org/10.1007/s00704-018-2536-z

Saji, N.H., Goswami, B.N., Vinayachandran, P.N., Yamagata, T., 1999. A dipole mode in the tropical Indian Ocean. Nature 401, 360–363. https://doi.org/10.1038/43854

Sanabria, J., Bourrel, L., Dewitte, B., Frappart, F., Rau, P., Solis, O., Labat, D., 2018. Rainfall along the coast of Peru during strong El Niño events. Int. J. Climatol. 38, 1737–1747. https://doi.org/10.1002/joc.5292

Santoso, A., Hendon, H., Watkins, A., Power, S., Dommenget, D., England, M.H., Frankcombe, L., Holbrook, N.J., Holmes, R., Hope, P., Lim, E.-P., Luo, J.-J., McGregor, S., Neske, S., Nguyen, H., Pepler, A., Rashid, H., Gupta, A.S., Taschetto, A.S., Wang, G., Abellán, E.,

Sullivan, A., Huguenin, M.F., Gamble, F., Delage, F., 2019. Dynamics and Predictability of El Niño–Southern Oscillation: An Australian Perspective on Progress and Challenges. Bull. Am. Meteorol. Soc. 100, 403–420. https://doi.org/10.1175/BAMS-D-18-0057.1

Santoso, A., Mcphaden, M.J., Cai, W., 2017. The Defining Characteristics of ENSO Extremes and the Strong 2015/2016 El Niño. Rev. Geophys. 55, 1079–1129. https://doi.org/10.1002/2017RG000560

Sardeshmukh, P.D., Compo, G.P., Penland, C., 2000. Changes of probability associated with El Niño. J. Clim. 13, 4268–4286.

Sardeshmukh, P.D., Hoskins, B.J., 1988. The Generation of Global Rotational Flow by Steady Idealized Tropical Divergence. J. Atmospheric Sci. 45, 1228–1251.

Shi, L., Hendon, H.H., Alves, O., Wheeler, M.C., Anderson, D., Wang, G., 2011. On the importance of initializing the stochastic part of the atmosphere for forecasting the 1997/1998 El Niño. Clim. Dyn. 37, 313–324. https://doi.org/10.1007/s00382-010-0933-9

Smith, T.M., Reynolds, R.W., Peterson, T.C., Lawrimore, J., 2008. Improvements to NOAA's Historical Merged Land–Ocean Surface Temperature Analysis (1880–2006). J. Clim. 21, 2283–2296. https://doi.org/10.1175/2007JCLI2100.1

Stephens, G.L., L'Ecuyer, T., Forbes, R., Gettelmen, A., Golaz, J.-C., Bodas-Salcedo, A., Suzuki, K., Gabriel, P., Haynes, J., 2010. Dreary state of precipitation in global models. J. Geophys. Res. Atmospheres 115. https://doi.org/10.1029/2010JD014532

Sulca, J., Takahashi, K., Espinoza, J.-C., Vuille, M., Lavado-Casimiro, W., 2018. Impacts of different ENSO flavors and tropical Pacific convection variability (ITCZ, SPCZ) on austral summer rainfall in South America, with a focus on Peru. Int. J. Climatol. 38, 420–435. https://doi.org/10.1002/joc.5185

Taschetto, A.S., England, M.H., 2009. El Niño Modoki Impacts on Australian Rainfall. J. Clim. 22, 3167–3174. https://doi.org/10.1175/2008JCLI2589.1

Taschetto, A.S., Gupta, A.S., Jourdain, N.C., Santoso, A., Ummenhofer, C.C., England, M.H., 2014. Cold Tongue and Warm Pool ENSO Events in CMIP5: Mean State and Future Projections. J. Clim. 27, 2861–2885. https://doi.org/10.1175/JCLI-D-13-00437.1

Taschetto, A.S., Gupta, A.S., Ummenhofer, C.C., England, M.H., 2016. Can Australian Multiyear Droughts and Wet Spells Be Generated in the Absence of Oceanic Variability? J. Clim. 29, 6201–6221. https://doi.org/10.1175/JCLI-D-15-0694.1

Taylor, K.E., Stouffer, R.J., Meehl, G.A., 2012. An Overview of CMIP5 and the Experiment Design. Bull. Am. Meteorol. Soc. 93, 485–498. https://doi.org/10.1175/BAMS-D-11-00094.1

Theobald, A., McGowan, H., Speirs, J., Callow, N., 2015. A Synoptic Classification of Inflow-Generating Precipitation in the Snowy Mountains, Australia. J. Appl. Meteorol. Climatol. 54, 1713–1732. https://doi.org/10.1175/JAMC-D-14-0278.1

Timbal, B., Drosdowsky, W., 2013. The relationship between the decline of Southeastern Australian rainfall and the strengthening of the subtropical ridge. Int. J. Climatol. 33, 1021–1034. https://doi.org/10.1002/joc.3492

Timbal, B., Hendon, H.H., 2011. The role of tropical modes of variability in recent rainfall deficits across the Murray-Darling Basin. Water Resour. Res. 47, W00G09. https://doi.org/10.1029/2010WR009834

Timmermann, A., An, S.-I., Kug, J.-S., Jin, F.-F., Cai, W., Capotondi, A., Cobb, K.M., Lengaigne, M., McPhaden, M.J., Stuecker, M.F., Stein, K., Wittenberg, A.T., Yun, K.-S., Bayr, T., Chen, H.-C., Chikamoto, Y., Dewitte, B., Dommenget, D., Grothe, P., Guilyardi, E., Ham, Y.-G., Hayashi, M., Ineson, S., Kang, D., Kim, S., Kim, W., Lee, J.-Y., Li, T., Luo, J.-J.,

McGregor, S., Planton, Y., Power, S., Rashid, H., Ren, H.-L., Santoso, A., Takahashi, K., Todd, A., Wang, Guomin, Wang, Guojian, Xie, R., Yang, W.-H., Yeh, S.-W., Yoon, J., Zeller, E., Zhang, X., 2018. El Niño–Southern Oscillation complexity. Nature 559, 535–545. https://doi.org/10.1038/s41586-018-0252-6

Turner, J., 2004. The El Niño–southern oscillation and Antarctica. Int. J. Climatol. 24, 1–31. https://doi.org/10.1002/joc.965

Ummenhofer, C.C., England, M.H., 2007. Interannual Extremes in New Zealand Precipitation Linked to Modes of Southern Hemisphere Climate Variability. J. Clim. 20, 5418–5440. https://doi.org/10.1175/2007JCLI1430.1

Ummenhofer, C.C., Sen Gupta, A., England, M.H., Taschetto, A.S., Briggs, P.R., Raupach, M.R., 2015. How did ocean warming affect Australian rainfall extremes during the 2010/2011 La Niña event? Geophys. Res. Lett. 42, 9942–9951. https://doi.org/10.1002/2015GL065948

van Rensch, P., Arblaster, J., Gallant, A.J.E., Cai, W., Nicholls, N., Durack, P.J., 2019. Mechanisms causing east Australian spring rainfall differences between three strong El Niño events. Clim. Dyn. 53, 3641–3659. https://doi.org/10.1007/s00382-019-04732-1

van Rensch, P., Gallant, A.J.E., Cai, W., Nicholls, N., 2015. Evidence of local sea surface temperatures overriding the southeast Australian rainfall response to the 1997-1998 El Niño. Geophys. Res. Lett. 42, 9449–9456. https://doi.org/10.1002/2015GL066319

Vecchi, G.A., Harrison, D.E., 2000. Tropical Pacific Sea Surface Temperature Anomalies, El Niño, and Equatorial Westerly Wind Events. J. Clim. 13, 17.

Walker, G.T., 1923. Correlation in seasonal variations of weather, VIII. A preliminary study of world weather. Mem. India Meteorol. Dep. XXIV, 75–131.

Walker, G.T., 1924. Correlation in seasonal variations of weather, IX. A further study of world weather. Mem. India Meteorol. Dep. XXIV, 275–332.

Walland, D.J., 1998. Seasonal climate summary southern hemisphere (spring 1997) a strong Pacific warm episode (El Niño) near maturity. Aust. Meteorol. Mag. 47, 159–166.

Wang, C., Weisberg, R.H., 2000. The 1997–98 El Niño Evolution Relative to Previous El Niño Events. J. Clim. 13, 14.

Wang, G., Cai, W., Bolan, G., Wu, L., Santoso, A., Lin, X., Chen, Z., McPhaden, M.J., 2017. Continued increase of extreme El Niño frequency long after 1.5 °C warming stabilization. Nat. Clim. Change 7, 568–572.

Wang, G., Hendon, H.H., 2007. Sensitivity of Australian Rainfall to Inter–El Niño Variations. J. Clim. 20, 4211–4226. https://doi.org/10.1175/JCLI4228.1

Watterson, I.G., 2010. Relationships between southeastern Australian rainfall and sea surface temperatures examined using a climate model. J. Geophys. Res. 115, D10108. https://doi.org/10.1029/2009JD012120

Webster, P.J., Moore, A.M., Loschnigg, J.P., Leben, R.R., 1999. Coupled ocean–atmosphere dynamics in the Indian Ocean during 1997–98. Nature 401, 356–360. https://doi.org/10.1038/43848

Wheeler, M.C., Hendon, H.H., Cleland, S., Meinke, H., Donald, A., 2009. Impacts of the Madden–Julian Oscillation on Australian Rainfall and Circulation. J. Clim. 22, 1482–1498. https://doi.org/10.1175/2008JCLI2595.1

Whetton, P., 1988. A synoptic climatological analysis of rainfall variability in south-eastern Australia. J. Climatol. 8, 155–177.

Williams, A.A.J., Karoly, D.J., 1999. Extreme fire weather in Australia and the impact of the El Niño Southern Oscillation. Aust. Meteorol. Mag. 48, 15–22.

Wyrtki, K., 1985. Water displacements in the Pacific and the genesis of El Niño cycles. J. Geophys. Res. 90, 7129. https://doi.org/10.1029/JC090iC04p07129

Zhao, M., Hendon, H.H., Alves, O., Liu, G., Wang, G., 2016. Weakened Eastern Pacific El Niño Predictability in the Early Twenty-First Century. J. Clim. 29, 6805–6822. https://doi.org/10.1175/JCLI-D-15-0876.1

Zhu, J., Shukla, J., 2013. The Role of Air–Sea Coupling in Seasonal Prediction of Asia–Pacific Summer Monsoon Rainfall. J. Clim. 26, 5689–5697. https://doi.org/10.1175/JCLI-D-13-00190.1